Editorial

The field of nano science and technology is one of the most exciting frontiers of science in the 21st century. Nanoscience is the study of phenomena and manipulation of materials at atomic, molecular and macromolecular scale, where the properties differ from those at larger scale. The main difference being (i) the increased surface area, which in turn results in increased chemical reactivity, and (ii) dominance of quantum effects, which can significantly change the optical, magnetic or electrical properties of the material. Nanoscience is currently one of the most exciting and promising new fields of study. One of the most important cornerstones in the development of nanoscience is the discovery of a new form of carbon (C60) by Dr. Kroto and his colleagues, Richard Smalley and Robert Curl Jr., for which they received the Nobel Prize for chemistry in 1996. The intense research in nanoscience during the last decade or so has led to the development of nanotechnology which deals with the design, production, characterization and application of nanostructures, devices and systems by controlling the shape and size at nanometer scale. Owing to the great potential of nanoscience and nanotechnology in bringing benefits to mankind, substantial funding of research and development activities have been made in this field during the last few years all over the world.

The present bulletin is aimed at bringing the current developments in nanoscience and nanotechnology to our young researchers. I thank Dr. S.K.Gupta for readily agreeing to our request to be the guest editor of this bulletin. My sincere thanks are due to Dr. V.C.Sahni for giving the FOCUS of the bulletin. All the authors sent their articles well in time which helped us publish this bulletin in time. I thank all the authors for their cooperation. I hope this bulletin will ignite the young minds and inspire them to take up research in this exciting field.

CONTENTS

From the Secretary's Desk

Greetings from Mumbai,

The Silver Jubilee year of IANCAS provided a wonderful opportunity for the resource persons of the association to emphasize their commitment to the cause of promoting science. The association has commemorated the occasion as auspicious in its novel way that IANCAS is known for, by conducting 11 one-day school/college workshops in Mumbai in a span of 3 months. It has also organized a Project/poster contest for the graduate/postgraduate students of Mumbai University as a boost to the creativity and a wide participation from various institutes in the city. The popularity of school workshops could be gauged from the large number of invitations that IANCAS received. Many institutes take pride in organizing this workshop as a regular facet in their curriculum and these workshops helped in encouraging the young minds to appreciate the relevance of nuclear energy in a country like India. No doubt the recent reports in the media on the Indo-US deal and the subsequent debate and discussions at the National political level has given the much needed alertness to the public about the Energy scenario in India and the need for the external support at this stage to sustain our long drawn indigenous fast reactor programme.

Encouraging young scientists is an essential feature these days. One of the most popular techniques is the institution of awards. While the new spate of awards is meant to encourage those who are already committed to a career in science, there are new inducements provided to the young to join science. The announcement of the awards to young students for the best presentation during the NUCAR-2007 symposium at M.S. University, Baroda is expected to prove attractive enough to entice 'bright young students' to research careers in nuclear science. IANCAS is far more optimistic in its ability to locate young scientists worthy of such recognition. As has been the wont, IANCAS has honoured five renowned persons in their chosen fields with Dr.M.V.Ramaniah memorial, Dr.Tarun Datta Memorial and Prof. H.J. Arnikar's Best thesis awards on the occasion and the credentials of the recipients are presented in this bulletin. The response for the awards is very heartening.

Prof. B.C. Haldar is a well known and a legendary in establishing schools of nuclear science and IANCAS has established awards on his name with the active support and initiative from his students and admirers. These awards will be announced during every NUCAR symposia among the best research contributions.

IANCAS has so far conducted 64 National Workshops with the support of BRNS. The next two workshops for this year are scheduled at Kurukshetra (December, 07) and Vanasthali (February, 08). Information about all these workshops and the bulletins is regularly updated in our website www.iancas.org. Members are encouraged to write to us their feedback on the bulletins with suggestions about any contemporary topics that could be a theme of the bulletin.

IANCAS compliments the authors of this bulletin on 'Nanoscience', a promising field of science of this era for taking their time off to contribute the articles on the topic.

G.A. Rama Rao

IANCAS Dr. M.V. Ramaniah Memorial Award to

Prof. S.F. Patil

**INDIAN ASSOCIATION OF NUCLEAR CHEMISTS
AND ALLIED SCIENTISTS (IANCAS)**
is happy to confer
IANCAS Dr. M.V. Ramaniah Memorial Award
on
Prof. S.F. Patil
Pune, India

For his outstanding and lifetime achievements in teaching and research in the field of radiochemistry. He made stupendous contributions in the area of diffusion studies using radiotracers and radiation effects in alkali halide crystals. He was responsible for the sustained research work in nuclear analytical chemistry and the discipline of nuclear and radiochemistry in Pune University got a radical face-lift during his long and inspiring academic career. An environmentalist at heart, Prof. Patil has served as a Vice-Chancellor at Marathwada University, Jalgaon and Bharatiya Vidyapeeth at Pune. He has plentiful number of publications in reputed journals and has guided several students in their M.Phil and Ph.D pursuits. He is a member of several scientific committees and is a former vice-president of IANCAS.
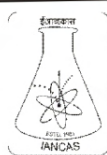
February 15, 2007

(V.K. Manchanda)
President, IANCAS

IANCAS Dr. Tarun Datta Memorial Award to

Dr. A.K. Tyagi

INDIAN ASSOCIATION OF NUCLEAR CHEMISTS AND ALLIED SCIENTISTS (IANCAS)

is happy to bestow

IANCAS Dr. Tarun Datta Memorial Award

on

Dr. A.K. Tyagi

Chemistry Division
Bhabha Atomic Research Centre
Mumbai, India

For his important contributions in the field of Solid State Chemistry related to Nuclear Materials. He has contributed extensively on the study of thermophysical properties of thoria based fuels. His recent work on the development of glasses for the immobilization of AHWR high level waste has shown promise. His work has helped in unraveling the structural aspects of thorium and uranium containing Barium borosilicate glasses. He has made significant contributions in the preparation of designer materials with tailored thermal expansion behaviour. Dr. Tyagi's work on mixed fluoride system is aimed at rare-earth utilization, a thrust area in DAE. A recipient of several awards, author of more than 180 research publications, Dr. Tyagi is currently engaged in the sysnthesis of many nano-crystalline materials like zirconia, ceria, barium polytitanate and yttria-doped-thoria etc.
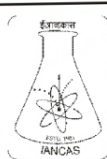
February 14, 2007

(V.K. Manchanda)
President, IANCAS

IANCAS Dr. Tarun Datta Memorial Award to

Dr. B.N. Murty

INDIAN ASSOCIATION OF NUCLEAR CHEMISTS AND ALLIED SCIENTISTS (IANCAS)

is happy to bestow

IANCAS Dr. Tarun Datta Memorial Award

on

Dr. B.N. Murty

Control Lab
Nuclear Fuel Complex
Hyderabad, India

For his significant contributions in the field of Analytical Chemistry related to fabrication of AHWR fuels. Innovative approaches adopted by Dr. Murty have helped in understanding the Chemistry involved in optimization of process parameters in the production of uranium dioxide, a pivotal material in nuclear fuel cycle, from its precursor ammonium diuranate. The novel analytical methodologies developed and applied by Dr. Murty for quality control measurements are characterized by their simplicity and ruggedness. The benefits accrued in terms of savings in time, economy and manpower have resulted in increased throughput. The outcome of research of Dr. Murty is not only useful in nuclear industry but also in other industries engaged in ceramic and powder material processing.

February 14, 2007

(V.K. Manchanda)
President, IANCAS

IANCAS Prof. H.J. Arnikar Best Thesis Award to

Dr. Dhanadeep Dutta

INDIAN ASSOCIATION OF NUCLEAR CHEMISTS AND ALLIED SCIENTISTS (IANCAS)

is happy to bestow

IANCAS Prof. H.J. Arnikar Best Thesis Award

on

Dr. Dhanadeep Dutta

Radiochemistry Division
Bhabha Atomic Research Centre
Trombay, Mumbai, India

For his work in the field of Positron Annihilation Spectroscopy by proposing a new model to study the porous nature of molecular substances. He has developed the basic notion of ortho-positronium annihilation characteristics in meso-pores with a simple description of the underlying process. His study also helped in explaining the annihilation rates on the basis of thermal vibration of surface atoms of the pores. The proposed model was employed to explain the porous nature of zeolites elegantly. Dr. Dutta has impeccably exposed the merits and fineness of the technique in its ability to characterize pores smaller than those investigated by other techniques.

February 2007

(V.K. Manchanda)
President, IANCAS

IANCAS Prof. H.J. Arnikar Best Thesis Award to

Dr. J. Mary Gladis
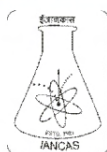
INDIAN ASSOCIATION OF NUCLEAR CHEMISTS AND ALLIED SCIENTISTS (IANCAS)

is happy to bestow

IANCAS Prof. H.J. Arnikar Best Thesis Award

on

Dr. J. Mary Gladis

RRL
CSIR
Thiruvananthapuram, India

For her work in the field of Solid Phase Extraction as a pre-concentration and separation technique with multifold application. She has developed and characterized several quinoline based reagents as extractants which have immense applications to investigate complex environmental and geological samples. Dr. Gladis has synthesized a new ion recognition polymer and has studied the effect of various cations and anions on the pre-concentration of uranium(VI). The selectivity of the reagent has been evaluated on the marine sediment reference materials. She has also synthesized an imprinted polymer which has been successfully used to enrich uranium ion selectively from sea water and soil materials.

February 2007

(V.K. Manchanda)
President, IANCAS

Dr. Tarun Datta Memorial Award

Indian Association of Nuclear Chemists and Allied Scientists (IANCAS) invites nominations for the annual Tarun Datta Memorial Young Scientist Award from eligible scientists for their outstanding contributions to the field of Nuclear and Radiochemistry. The Award, carrying a cash prize of Rs.5000/-, a citation and a medal, will be presented to the selected candidate during the Annual General Body Meeting(AGM) of IANCAS.

Eligibility

Citizens of Indian nationality below 45 years of age as on 31st December of the calender year of the Award. The candidate must have made significant contributions in the field of Nuclear and Radiochemistry, or Applications of Radioisotopes for the basic research in any branch of sciences.

It may be noted that the award would be given for research work carried out in India.

How to apply ?

The application should be as per the proforma given on the reverse side of this announcement. Photocopies of the proforma may also be used or downloaded from the web site (www.iancas.org). Applicants should submit the proforma along with a summary (not exceeding 500 words) highlighting the significant research contributions & achievements especially during the last five years. In addition, they should enclose two passport size photographs, proof of age, and reprints of ten best published papers in support of the application and a declaration by the applicant ratified by the Head of the Department, Research Guide or Head of the Institution. The declaration should also bring out clearly the contributions of the co-workers. The application, complete in all respects should reach the General Secretary, IANCAS on or before 30th November of the calender year.

Selection

An expert panel will scrutinise the applications and judge the best research contribution for the award. The awardee has to present her/his work by giving a lecture during the AGM of IANCAS. The awardee will be provided with DA & first class/AC III tier return railway fare, if the awardee cannot get the same from any other source.

It may please be noted that the decision of the expert panel is FINAL and canvassing in any form is a disqualification.

Completed application may please be forwarded to   *General Secretary, IANCAS*
C/o Radiochemistry Division
BARC, Trombay, Mumbai 400 085

Dr. Tarun Datta Memorial Award

(PROFORMA FOR APPLICATION)

1.	Name in full	
2.	Present office address with telephone, e-mail and FAX	
3.	Date of Birth (attach proof)	
4.	Academic Qualifications (attach certificates)	
5.	Details of employment	
6.	Awards / Recognitions	
7.	Field of specialisation	
8.	Research experience	
9.	Number of publications (Journals only) Attach list	
10.	Invited talks / Session Chairperson in National / International Symposia / Conferences, if any	
11.	Reviews / Books / Chapter contributed to books / Technical Reports, if any	
12.	Popular Science articles, if any	
13.	Citation Index of 10 best papers published (if any)	
14.	Any other contribution(s), academic or otherwise, supporting your candidature	
15.	Signature of the Applicant	
16.	Signature, Name, Designation and full address of the proposer of the nomination with Telephone, e-mail and FAX	

(Please include (i) two passport size photographs, (ii) brief write-up not exceeding 500 words, clearly bringing out significant research contributions, (iii) reprints of ten best published papers, (iv) list of publications and (v) a declaration stating that the work was carried out in India)

DECLARATION

(By Head of the Institute or Head of the Department or Research Guide)

I certify that the research work mentioned by Dr. / Mr. / Ms .... of .... (Name of the Institute) was carried out by him / her. The candidate is mainly responsible for the outcome of this work. I request the Committee to consider the nomination for Dr. Tarun Datta Memorial Award.

Signature and Seal

IANCAS - Prof. H.J. Arnikar - Best Thesis Award

The Indian Association of Nuclear Chemists and Allied Scientists invites applications for the Prof. H.J. Arnikar Best Thesis Award in the field of Radiochemistry and Allied Sciences. The award carries a medal, a citation and Rs.5,000/- in cash. The awardee will be provided return I class/AC III tier fare to attend the award function, which will be held during the Annual General Body meeting of IANCAS, the date and venue of which will be intimated to the selected candidate.

Eligibility

1. Ph.D. Degree awarded by any of the Indian Universities preceding two years from June of the calender year of the Award e.g. for the calender year 2007, the Ph. D. degree should have been awarded to the candidate between July 2005 to June 2007.

2. The work reported in the thesis should be in any one of the following fields
   - Radiochemistry
   - Nuclear Chemistry
   - Nuclear Materials
   - Radioanalytical Chemistry
   - Isotope Production
   - Radiotracer Studies
   - Radioactivity Measurement or
   - Any Allied Fields wherein Radioisotopes are Used

3. Age limit : There is no age limit for this award

How to Apply?

The nomination should be sent by the Ph.D. Guide along with

(a) 3 copies of the synopsis as submitted to the University,

(b) a write up not exceeding 500 words highlighting the significant achievements of the work carried out leading to the award of the degree,

(c) list of publications (journals only) & reprints/preprints of five best papers. It is essential that the list of publications & reprints cover only those papers that are included in the thesis,

(d) A copy of the Ph.D. Degree /provisional certificate from the University.

Last Date : on or before November 30, of the calender year

The application, complete in all respects, should reach the General Secretary, IANCAS, C/o Radiochemistry Division, Bhabha Atomic Research Centre, Mumbai - 400 085.

Selection

A panel of experts nominated by the Executive Committee of IANCAS comprising members from the Department of Atomic Energy and the Universities will select the best thesis. It may please be noted that the decision of the panel is FINAL and canvassing in any form will be a disqualification. The awardee will be given an opportunity to present his/her work during the Annual General Body Meeting of IANCAS.

Prof. H.J. Arnikar Best Thesis Award

(PROFORMA FOR APPLICATION)

1.	Name and address of the Candidate	
2.	Name and affiliation of the Guide(s)	
3.	Institute where the work was carried out	
4.	Name of the University awarding the degree	
5.	Title of the Thesis	
6.	Year and month of the award	

CERTIFICATE

I hereby confirm that the work pertaining to the Ph.D. Thesis mentioned above of ....

.... was carried out under my supervision

(Signature of Guide)

Nanoscience and Nanotechnology

Guest Editor

S.K. Gupta

Technical Physics and Prototype Engineering Division
Bhabha Atomic Research Centre
Mumbai 400 085

FOCUS

Dr. V.C. Sahni
Director, RRCAT, Indore and
Director, Physics Group, BARC

An overview of Nanoscience and Nanotechnology

*The word nanoscience has been derived from the Greek "nanos" (or Latin "nanus") meaning Dwarf. Thus literally this subject pertains to the study of tiny objects in the size range of 1-100 nanometers. Nanotechnology entails the manipulation of matter at nanoscale, paving the way to finding new properties, phenomena and their applications. In a way, nanometer-sized objects are some times encountered in chemical reactions of large molecules. However, in a typical reaction, only macroscopic control variables, such as heat, pressure etc. are used and one does not **directly manipulate** matter on nanometer scale. Biochemists and biologists too work with large-sized molecules ranging from proteins, enzymes and DNA in living objects, but again their techniques involve only gross and not any microscopic control. But in recent times, rapid advances in new synthetic techniques have made manipulation of matter at nanometer scale a reality. Indeed recent effort in nanoscience and technology has seen the development of a host of techniques for the preparation and study of materials in 1-100 nm size. Nanotechnology by its very nature is an interdisciplinary area and chemists, physicists, biologists and engineers all have a role to play in its development.*

Presently, nanoscience/nanotechnology is a field of frontline research and is being driven by a number of developments, ideas and technical advances. Primary drivers behind nanotechnology revolution are the following:

(i) *Construction of instruments to see and manipulate individual atoms and molecules: A good example is Scanning Tunneling Microscope with which one can "see" a single atom on a surface. Prior to its development, x-ray diffraction was used to find positions of atoms in a crystalline solid using Bragg reflection data. But x-rays did not "see" single atoms, whereas a tunneling electron microscopes (TEM) can directly image atoms in a lattice.*

(ii) *The drive to make smaller computer chips and higher density information storage devices. Gordon Moore the co-founder of Intel, had projected in the 1960s and 1970s that every 24 months the number of transistors on a chip increases by roughly factor of two. This relationship has been representing advances in the world of microelectronics fairly well for almost thirty years. However, will this prediction hold when the size of devices becomes less than 100 nanometers? One does not know but effort is on to discover new approaches to make such devices. Likewise, for information handling, an essential element of modern civilization, there is an ever-increasing need for compactor memory devices and faster data transmission techniques. Today information is stored digitally and transmitted electronically, with dimensions of individual memory elements (stored on magnetic disks and compact discs) being sub-micron.*

(iii) *Emerging belief that it is possible to mimic the mechanisms of biology: Over the past few decades, scientists have shown that many life forms operate through mechanisms that can be characterized as "micro-machines", involving absorption of energy and causing biological events to occur in a systematic way. For example, during the process of digestion, body acids and enzymes break down the food into small digestible pieces which are then ingested through cells. During viral fever, a virus can permeate body cells, integrate with genetic material and produce agents that harm the body. Presently, we can observe such processes, but do not fully understand how they work. Evidently, any insight or*

understanding of such processes will help us "better control" such "bio machines" that operate in biological systems.

(iv) <u>*Nanotechnology: A tool for improving the quality of human life*</u>: *At this point it appears that very soon many nanotechnology applications will be with us which include improved materials (for industrial applications), faster and smaller communication devices, efficient and compact devices for environmental monitoring, tiny targeted drug delivery systems etc. Perhaps an exciting nanoscience applications is the treatment (and even elimination) of disease through nanosystems, like, colloidal gold nanoparticles, iron oxide nanocrystals etc., to be used for drug delivery or diagnostic applications. Nanocapsules that are able to resist being rejected by the immune system and nanoporous materials that enable targeted delivery of medication have been envisioned. Nanovehicles, involving the use of "therapeutic and diagnostic" agents that can be encapsulated, covalently attached or absorbed on such nanocarriers and administrated by injection have been visualized. Far out into the future people are predicting development of computers and sensing systems that fit in a pack of the size of a pill and warning us of danger ahead. Life extension through systems and modules that replicate the body functions is the ultimate target.*

The development of nanotechnology is largely dependent on the availability of cost-effective and accessible methods to manufacture nanostructures. Scientists are utilizing both top-down and bottom-up approaches. Top-down methods involve creating a structure and then carving out or adding aggregates of molecules to a surface. Bottom-up methods involve building nanostructures atom by atom largely through self-assembly processes. Successful development of bottom-up methods appears to be most promising route to nanofabrication; however, such developments have yet a long way to go, largely because a full understanding of how self-assembly methods work in nature is not yet fully known. Understanding nature's nanofabrication methods is of importance not just to biologists working at the nanoscale, but also to scientists working in many disciplines that include materials science and cover a range from chemical engineering to aerospace industry. Interdisciplinary nature of nanoscience/nanotechnology requires close partnership among the different disciplines ranging from biology to electronics.

Guest Editorial

Dr. S.K. Gupta

Technical Physics and Prototype Engineering Division, BARC

One hundred years after the discovery of quantum physics, which revolutionized our view of the microworld, we are beginning to realize the dream of the eminent physicist Richard Feynman who foresaw that the most powerful machines of the future would be of nanometer size. During the recent years, efforts have been made by many research groups to comprehend the physical phenomena appearing in nano-materials and prepare nano-structures for future nano-sized devices. The revolution in this interdisciplinary field has been promoted by the development of new measuring techniques and refinement of synthesis methods. In nanomaterials, microscopic structure has a notable influence on macroscopic properties and this yields a wide variety of new phenomena. Nano-science and technology is an interdisciplinary field with developments occurring along different directions. Therefore, it is not possible to cover every aspect of the field in a small volume and few review articles in this issue cover some of the important areas of research.

In this special issue of IANCAS Bulletin we have seven review articles that cover techniques for nanomaterials preparation and fabrication of small structures. The first two articles deal with the synthesis of the nanocrystalline materials. It has been demonstrated that functional nanocrystalline oxide ceramics can be synthesized by solution combustion technique, which can be readily sintered to high density at a comparatively lower temperature. The nanoparticles of semiconducting metal chalcogenides can be synthesized using single source molecular precursors. Third article describes deposition of nanowires and nanotubes of various semiconductor materials and their application in detection of toxic gases at room temperatures. Fourth article discusses the methods of synthesis of carbon nanotubes and their hydrogen uptake behavior for hydrogen storage application. The fifth article demonstrates fabrication of passive and active molecular devices (dielectric, diodes, resonant tunnel diodes and memory) compatible to Si-microelectronics using self-assembly and electrografting. The sixth article describes tailoring of nanostructures with energetic ion beams and emphasizes on understanding of ion-solid interactions at nanoscale regime with possible applications. The seventh article overviews the current trends in Micro Electro Mechanical Systems (MEMS) and Nano Electro Mechanical Systems (NEMS). The processes described in this article are used in top down approach of fabrication of nano-structures.

I am indeed very grateful to all the authors who readily agreed to contribute articles covering various facets of the nanoscience and nanotechnology in a very short time. Editing this special IANCAS bulletin was an enjoyable experience and I personally thank Dr. B.S. Tomar for entrusting me with this opportunity.

Single Source Molecular Precursors for Semiconducting Metal Chalcogenide Nanoparticles

Shri G. Kedarnath *obtained his M. Sc (General Chemistry) from University of Hyderabad in 1999. After graduating from 43rd batch of Training School he joined BARC. He has been actively involved in the design, synthesis and characterization of molecular precursors for II-VI and IV-VI nano-materials, and has 6 research publications in international referred journals. He has been conferred with 'Prof. B.C. Halder Memorial' award for the year 2006 in 'Inorganic Chemistry' section of the Indian Chemical Society.*

Dr. V.K. Jain *is currently working at Bhabha Atomic Research Centre, Mumbai as a Scientific Officer (H) and Head, Synthesis and Pure Materials Section. He is an honorary Professor of Chemistry at Homi Bhabha National Institute (deemed University). He obtained his M.Sc. degree in organic chemistry from Agra University (1976) and Ph.D. from Rajasthan University in 1981 under the supervision of Prof. R.C. Mehrotra. After his Ph.D. he moved to Canada in 1981 where he was a post-doctoral fellow at the University of Guelph, Ontario with Prof. H.C. Clark. He joined Chemistry Division, BARC in 1984 as SO'SD'. His research interests include: organometallic and metallo-organic chemistry of platinum group metals and main group elements, synthesis and molecular design of molecular precursors for advanced inorganic materials. He is author/ co-author of more than 220 research papers and review articles published in international referred journals. He has supervised doctoral work of more than a dozen Ph.D. students. He is the recipient of several awards including "Homi Bhabha Science and Technology Award (1996)". In 1995 he was elected Fellow of the National Academy of Sciences, India.*

Introduction

The materials spectrum has always been in a dynamic state. There has been an insatiable quest to discover new materials or to modify properties of already known materials so as to exploit their properties for the benefit of the mankind. Properties of a material can be modified at least in three possible ways, viz. by changing purity level, by altering phase/morphology and by modifying the size. While referring to size, one thinks about the modern nanotechnology mania which is sweeping almost all the sub disciplines of science and engineering, making the subject area rather inter-disciplinary in nature. Although colloidal metals were in use to dye glass articles and fabric from the Roman period, the first systematic study was made by Michel Faraday in 1857 who prepared colloidal gold exhibiting different colors in aqueous solution [1]. However, the past two decades have witnessed a dramatic progress in experimental and theoretical methods and applications of nanoparticles encompassing their utility in opto-electronics and photovoltaic [2], biological imaging agents [3], enhanced hydrophobicity (Lotus effect) [4], biomedicine [5], catalysis [6], cosmetics [7]. Great advances have been made in recent years to prepare and study nanoparticles of metals, semiconductors and various other substances.

In the nano-meter size regime, new mesoscopic phenomena develop which are neither found in molecular systems (e.g., molecular chemistry) nor in bulk materials (e.g., solid state physics), but are characteristic of this intermediate state of matter. In this size regime (1-100 nm) intrinsic properties, like

Shri G. Kedarnath and Dr. Vimal K. Jain, Chemistry Division, Bhabha Atomic Research Centre, Mumbai 400085:
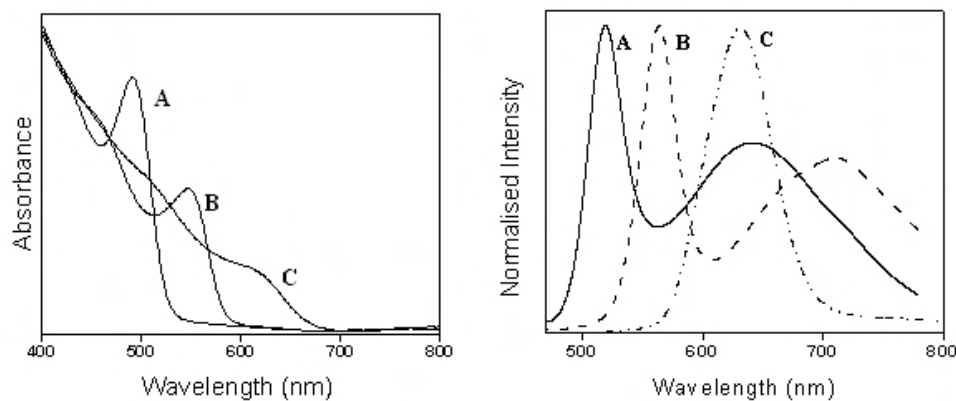E-mail: jainvk@barc.gov.in

Fig. 1   Absorption and emission spectra of CdSe nanoparticles obtained by pyrolysis of [Cd(SeCH₂CH₂NMe₂)₂] at 187°C in HDA/TOPO, that are recorded at (A) 4 (B) 6 (C) 30 minutes of preparation.

electronic, optical, magnetic, melting points, specific heat, surface energies, etc., are changed which can be further fine tuned by controlling the size [8]. Total fraction of atoms on the surface of a nanoparticle increases with decreasing the size of a particle and can be estimated by a relationship: $P_s = 4N^{-1/3} \times 100$ (where P_s is percentage of atoms and N is the total number of atoms in the particle) [9]. For example, a 3 nm iron particle has 50% of its atoms on the surface, whereas 10 and 30 nm particles have just 20 and 5% atoms, respectively on the surface. These surface properties can be and have been exploited for a variety of chemical reactions such as catalysis [10]. Size dependent electronic and optical properties of metals and semiconductor materials are of considerable interest. For instance, the absorption and fluorescence wavelengths of nanoparticles show size dependence. Depending on the size of the particle (Fig. 1) and dielectric constant of the medium, characteristic colors are observed.

Over a period, a wide range of synthetic routes involving physical (top-down or fabrication approach, *e.g.* ion sputtering), chemical (bottom-up or synthesis strategy, *e.g.* reduction of metal salts, solvothermal synthesis) or hybrid methods have been developed for the preparation of nanoparticles of various materials. Biological methods, employing yeasts and bacteria, have also been used in some cases [11]. No matter how nanoparticles are prepared, they are never monodispersed in terms of size, shape, internal structure and surface chemistry. However, samples with standard deviation of $\sigma \le 5\%$ are usually considered as monodispersed. Due to large surface energy, nanoparticles tend to aggregate leading to precipitation. Thus to prevent aggregation, stabilizing agents are employed during the growth process. When the stabilizing molecules, often coordinating solvents like trialkylphosphines, trialkylphosphine oxides, alkylamines, thiols, esters, etc., are attached to the nanoparticle surface as a mono-layer through covalent, dative or ionic bonds, they are referred as capping agents. These capping agents serve to mediate growth of nanoparticles and also stabilize them sterically in solution.

Being an interdisciplinary subject area, many scientists and engineers, who are interested in properties and applications of nanoparticles, but are not experts in synthetic chemistry, may like to adopt user-friendly synthetic approaches rather than developing their own synthetic methods. For nanoparticles of unitary materials like Cu, Ag, Au, Pd, Pt, chemical reduction of their metal salts, which are commercially available, is quite versatile and is used routinely. However, for nanoparticles of binary, ternary and quaternary systems, stoichiometry requirements, both in the product as well as in the reactants, pose numerous synthetic challenges. For such materials a single source precursors route seems to be easily adoptable synthetic scheme due to obvious reasons [12]. Some
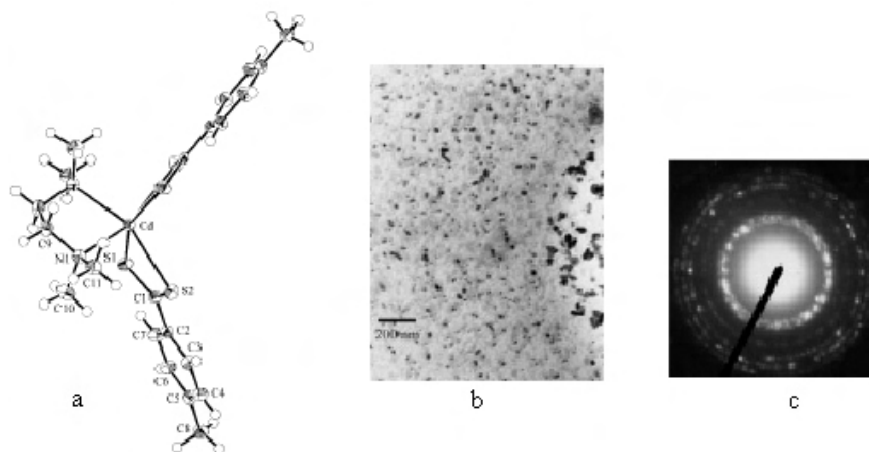
Fig. 2   (a) Molecular structure of [Cd(S$_2$CTol)$_2$(tmeda)], b) TEM image and c) SAED pattern of CdS nanoparticles

representative examples of this strategy are described here.

Molecular Precursors for II-VI Nanoparticles

Synthesis and properties of II-VI semiconductor nanoparticles have been extensively investigated and reviewed recently [13]. Although a wide range of routes have been developed, single source route is quite promising. Single source precursor method is earlier reported by Brennan, *et.al.* [14] for the preparation of CdSe nanoclusters from [Cd(SeC$_2$H$_5$)$_2$] and later on extensively investigated by O'Brien and coworkers [15]. The synthesis of nanoaprticles involves dissolution of the precursor in trioctylphosphine (TOP) followed by decomposition in a suitable high-boiling coordinating solvent (trioctyl phospine oxide (TOPO) or 4-ethylpyridine) at high temperatures.

Several dithiolate complexes of these elements have proved versatile precursors for metal sulfide nanoparticles. Recently, synthesis of phase pure metal sulfide nanoparticles by decomposition of [M(S$_2$CPh)$_2$(tmeda)] (M = Zn, Cd, Hg) (Fig. 2) both in the solid-state (furnace heating) and in solvents like ethylenediamine and hexa decyl amine (HAD) [16] is reported. In case of mercury, nanoparticles of HgS could be isolated at a temperature as low as 57ºC. Different phases (cubic/hexagonal) can be obtained under different experimental conditions.

For metal selenide nanoparticles a number of precursors have been developed. Few representative examples are described here. The MSe (M = Zn or Cd) nanoparticles are conveniently isolated by decomposing air stable monomeric selenocarboxylates of group II with the general formula [M(SeCOPh)$_2$(tmeda)] (M = Zn, Cd; tmeda = Me$_2$NCH$_2$CH$_2$NMe$_2$; Me = Methyl) either in hot HDA as coordinating solvent or in a furnace without any capping agent. The facile cleavage of the C-Se linkage in selenocarboxylates has been successfully exploited in these preparations [17]. The analogous mercury complexes, being unstable at room temperature, readily afford HgSe nanoparticles in good yields (Fig. 3). Other precursors employing internally functionalized selenolate ligands, such as N, N-dimethylaminoethylchalcogenolates, are another family of promising single source precursors for metal selenides as these ligands assist in suppressing polymerization [18, 19]. Accordingly chemistry of group II complexes of the type, [M(Se(CH$_2$)$_n$NMe$_2$)$_2$] (M = Zn or Cd for n =2; M = Zn, Cd and Hg for n =3) has been developed. Although these complexes give metal selenide nanoparticles on thermolysis, the preparation of HgSe nanoparticles from [Hg(SeCH$_2$CH$_2$CH$_2$NMe$_2$)$_2$] is rather intriguing. The mercury selenolate complexes in general yield metallic mercury rather HgSe [20].
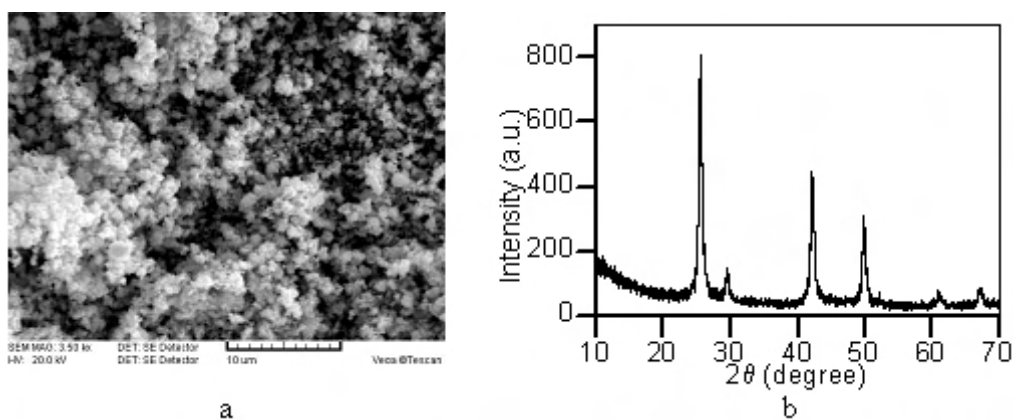
Fig. 3   a) SEM image and b) XRD pattern of HgSe obtained by the reaction of Hg(OAc)$_2$ with PhCOSeK at room temperature

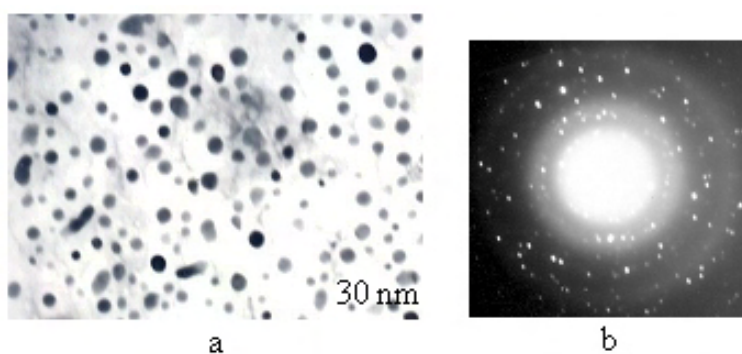*Fig. 4   a) TEM image and b) SAED pattern of Hg$_{0.973}$Mn$_{0.027}$Te quantum dots prepared at 90°C*

In contrast to extensive literature on group II sufide and selenide nanoparticles, group II tellurides are relatively unexplored [21]. Recently, we have prepared photoluminescent HgTe quantum dots by pyrolysis of [Hg(TeCH$_2$CH$_2$NMe$_2$)$_2$] in HDA at temperatures below 100°C in the size range of 5-10 nm (Figure 4) [22].

Molecular precursors for III-VI nanoparticles

Group III elements form several metal chalcogenides differing in composition and phases [23]. They have potential applications in opto-electronics, non-linear optics, and photovoltaic devices and as passivating agent for III-V films (e.g., GaAs). Among III-VI materials, indium sulfide and selenide have received considerable attention due to their photovoltaic properties.

Both gallium and indium form a variety of dithiolate (S$^\frown$S = xanthate, dithiocarbamate, dithiocarboxylate, dithiophosphate) complexes. These complexes are discrete monomeric molecules (Scheme 1) and are promising candidates as single source molecular precursors. These molecules in general have distorted geometries due to restricted bite of the dithio ligands with the S-M-S angles of the chelating dithio ligands varying between 66.6 and 81.7^o [24].

Diorganoindium dithiocarbamates and xanthates, [R$_2$In(S$^\frown$S)] [25] and indium tris xanthates, [In(S$_2$COR)$_3$] [26] have been successfully used as precursors for indium sulfide nanoparticles. Pyrolysis of [In(S$_2$COR)$_3$] (R = Me, Et, Pr^n, Bu^n) in refluxing ethylene glycol affords yellow-orange

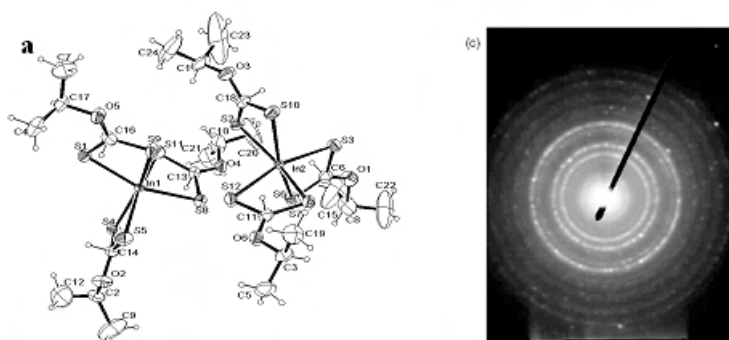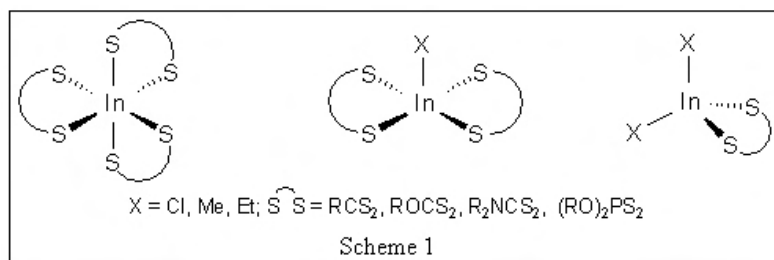$X = Cl, Me, Et; S S = RCS_2, ROCS_2, R_2NCS_2, (RO)_2PS_2$

Scheme 1

Fig. 5   a) Molecular structure of [In(S_2COPr^i)_3] b) SAED pattern of β-In_2S_3 nanoparticles

cubic β-In_2S_3 nanoparticles (Figure 5) of 13-30 nm as revealed by XRD and TEM [26]. Highly blue shifted emission (440 nm) in the PL spectra of these nanoparticles relative to the bulk material (620 nm) has been attributed to quantum confinement of the particles.

Molecular Precursors for IV-VI Nanoparticles

In contrast to the multitude of synthesis of II-VI nanoparticles, there are a fewer synthetic routes for IV-VI semiconductor nanoparticles. The IV-VI compounds show unique properties which distinguish them from II-VI nanoparticles [27]. The IV-VI materials such as SnSe, SnTe, PbE (E = S, Se, Te) are widely used as IR detectors and as thermoelectric materials [27, 28]. Although various methods which have been used to prepare different geometries of PbE (E = S, Se, Te) nanoparticles [28-31], single source precursor route has yet to receive a momentum. O'Brien, *et.al.* [32] reported the preparation of PbE nanoparticles by thermolysis of [Pb(E_2CNEtPr^i)_2] in TOPO with a size of 6-16 nm. The complexes [Pb(S_2CAr)_2] (Ar = Ph or Tol),

[Pb(SeCH_2CH_2NMe_2)_2], [Pb(SeCH_2 CH_2COOMe)_2], in refluxing HDA yield PbE nanoparticles at moderately low temperatures [33]. The pyrolysis of [Pb(SeCH_2CH_2NMe_2)_2] afforded PbSe nanoparticles with an average diameter of 10 nm.

Molecular Precursors for V-VI Nanoparticles

The group V-VI compounds, M_2E_3 (M = Sb or Bi, E = S, Se, Te), are highly anisotropic semiconductors with a layered structure in which metal can adopt either trigonal prismatic or octahedral coordination within a layered matrix of chalcogens. These compounds are attractive due to their photovoltaic properties and high thermoelectric power which allows their applications in opto-electronic and thermoelectric cooling devices [34]. Recently polymer coated Bi_2S_3 nano-particles have been used as imaging agent in X-ray computed tomography [35]. Several approaches have been employed to prepare different shapes and morphologies of these materials. Single source precursors, such as [Bi(S_2COR)_3] [36],
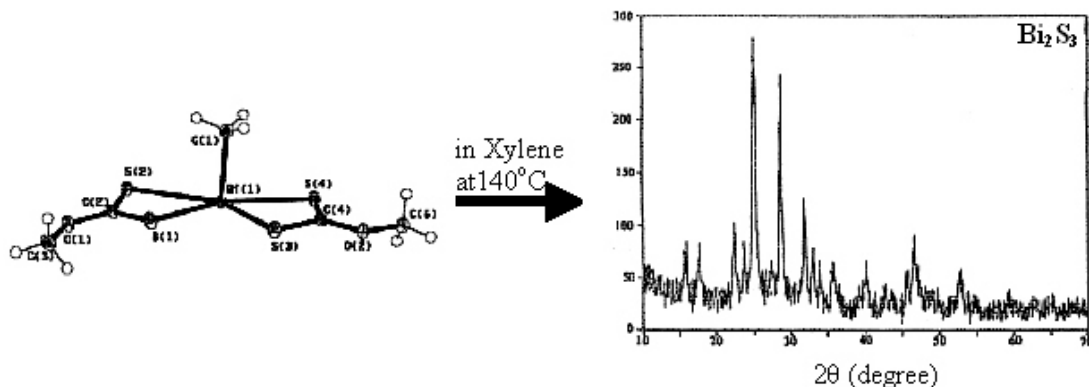
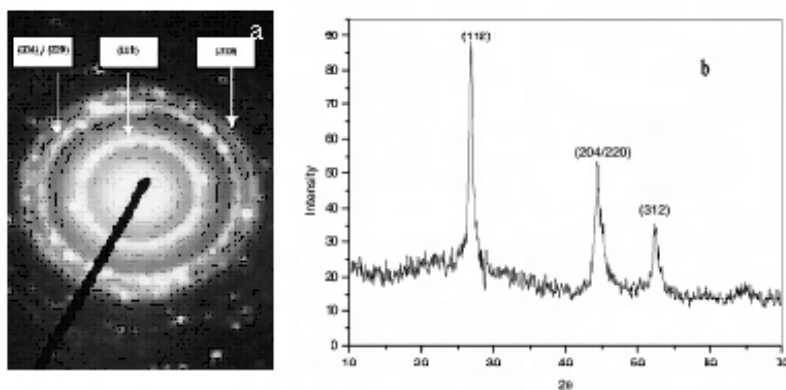*Fig. 6   ORTEP plot of [MeBi(S₂COMe)₂] and XRD pattern of the Bi₂S₃ nanoparticles*

Fig. 7   a) SAED and b) XRD patterns of the CuInSe₂ nanoparticles obtained by pyrolysis of [(Ph₃P)₂CuIn(SeCOTol)₄] in ethylene glycol

[Bi(Se₂CNR₂)₃] [37], have been used to deposit thin films of M₂E₃.

Although group V complexes with dithio ligands have been extensively studied [38], their role as single source precursors for the preparation M₂E₃ nanoparticles is evolving [39, 40]. Pyrolysis of [M{S₂P(OC₈H₁₇)₂}₃] (M = Sb or Bi) in oleylamine at 160°C yields nanorods of orthorhombic M₂E₃ phase [39]. The TEM images show the formation of Bi₂S₃ nanorods with a diameter of 7-21 nm and several hundred nanometers in length. Organobismuth xanthates, [MeBi(S₂COR)₂] (Figure 6) in refluxing xylene readily afford Bi₂S₃ nanoparticles [40].

Molecular Precursors for Nnanoparticles of Ternary Chalcogenide Materials

MM'E (M = Cu, Ag, Zn, Cd, *etc.*; M' = Al, Ga, In; E = S, Se, Te) have attracted much attention recently due to their tunable electronic and optical properties. The ternary materials, CuInS₂ and CuInSe₂ have been studied extensively for solar cell applications. Although single source precursors like, [(Ph₃P)₂CuIn(EPh)₄] (E = S or Se) [41] and [(Ph₃P)ₙMIn(ECOPh)₄] (M =Ag or Cu) [42] have been used to prepare thin films of MInE₂ (M = Ag, Cu; E = S or Se); the use of the latter for the preparation of nanoparticles has been demonstrated by Vittal, *et.al.* [43] and Jain, *et.al.* [44]. Pyrolysis of [(Ph₃P)₂MIn(SeCOAr)₄] (M = Ag, Cu Ar = Ph or

Tolyl) in boiling ethylene glycol gave black MInSe$_2$ nanoparticles, which were isolated in tetragonal phases (from XRD) [44]. The particle sizes estimated from the Scherrer's formula for CuInSe$_2$ and AgInSe$_2$ are 12 nm and 35 nm, respectively.

References

1. M. Faraday, *Philos. Trans. R. Soc. London*, **147** (1857) 145.

2. W. Huynch, X. G. Peng and A. P. Alivisatos, *Adv. Mater.*, 11 (1999) 923; M. Nirmal and L. Brus, *Acc. Chem. Res.,* **32** (1999) 407; X. Chen and S. S. Mao, *Chem. Rev.*, **107** (2007) 2891.

3. W. C. W. Chen and S. Nie, Science, 281 (1998) 2016; D. R. Larson, W. R. Zipfel, R. M. Williams, S. W. Clark, M. P. Bruchez, F. W. Wise, W. W. Webb, *Science,* **300** (2003) 1434; M. Green, Angew. Chem. Int. Ed., **43** (2004) 4129.

4. Z. Gu, H. Uetsuka, K. Takahashi, R. Nakajima, H. Onishi, A. Fujishima, O. Sato, *Angew. Chem. Int. Ed.*, **42** (2003) 894.

5. Q A Pankhurst, J Connolly, S K Jones and J Dobson, *J. Physics D. Applied Physics,* **36** (2003) R 167.

6. T. S. Ahmadi, *Science,* **272** (1996) 1924.

7. N. Serpone, D. Dondi and A. Albini, *Inorg. Chim. Acta*, **360** (2007) 794; P. Walter, et. al., *Nano Letters*, **6** (2006) 2215.

8. E. Roduner, *Chem. Soc. Rev.,* **35** (2006) 583.

9. C. N. R. Rao, P. J. Thomas and G. U. Kulkarni, "Nanocrystals, Synthesis, properties and Applications", Springer Verlag, Heidelberg (2007).

10. A. Zecchina, E. Groppo and S. Bordiga, *Chem. Eur. J.*, 13 (2007) 2440; M. Haruta, *Catal. Today*, 36 (1997) 153; S. Eustis and M. A. El. Sayed, *Chem. Soc. Rev.*, 35 (2006) 209.

11. C. T. Dameron, R. N. Resse, R. K. Mehra, A. R. Kortan, P. J. Carroll, M. L. Steigerwald, L. E. Brus and D. R. Winge, *Nature*, **338** (1989) 596; A. Bharde, A. Wani, Y. Shouche, P. A. Joy, B. L. V. Prasad and M. Sastry, *J. Am. Chem. Soc.,* **127** (2005) 9326.

12. P. O'Brien and S. Haggata, *Adav. Materials Optics Electronics*, **5** (1995) 117.

13. X. Peng, *Chem. Eur. J.,* 8 (2002) 335; T. Trindade, P. O'Brien and N. L. Pickett, *Chem. Mater.*, **13** (2001) 3843.

14. J. G. Brennan, T. Siegrist, P. J. Carroll, S. M. Stuczynski, L. E. Brus and M. L. Steigerwald, *J. Am. Chem. Soc.,* 117 (1989) 4141.

15. N. L. Pickett and P. O'Brien, *Chem. Rec.*, **1** (2001) 467.

16. G. Kedarnath, V. K. Jain, S. Ghoshal, G. K. Dey, C. A. Ellis and E. R. T. Tiekink, *Eur. J. Inorg. Chem.*, (2007) 1556.

17. G. Kedarnath, L. B. Kumbhare, V. K. Jain, P. P. Phadnis and M. Nethaji, *Dalton Trans.,* (2006) 2714.

18. S. Dey, V. K. Jain, S. Chaudhury, A. Knoedler and W. Kaim, *Polyhedron*, **22** (2003) 489.

19. G. Kedarnath, S. Dey, V. K. Jain, G. K. Dey and B. Varghese, *Polyhedron*, **25** (2006) 2383.

20. G. Kedarnath, S. Dey, V. K. Jain and G. K. Dey, *J. Nanosci. Nanotechnol*, **6** (2006) 1031.

21. Y. W. Jun, C. S. Choi and J. Cheon, *Chem. Commun.,* (2001) 101.

22. G. Kedarnath, S. Dey, V. K. Jain, R. M. Kadam and G. K. Dey, unpublished results.

23. A. R. Barron, *Adv. Materials for Optics & Electronics*, **5** (1995) 245.

24. S. Ghoshal and V. K. Jain, *J. Chem. Res*. (in press).

25. S. Ghoshal, N. P. Kushwah, D. P. Dutta and V. K. Jain, *Appl. Organomet. Chem.,* **19** (2005) 1257.

26. D. P. Dutta, G. Sharma, S. Ghoshal, N. Kushwah and V. K. Jain, *J. Nanosci. Nanotechnol.,* **6** (2006) 235.

27. R. Venkatasubramanian, E. Siivola, T. Colpitts and B. O. Quinn, *Nature*, **413** (2001) 597.

28. A. J. Houtepen, R. Koole, D. Vanmaekelbergh, J. Meeldijk and S. G. Hickey, *J. Am. Chem. Soc.*, **128** (2006) 6792.

29. J. S. Steckel, B. K. H. Yen, D. C. Oertel and M. G. Bawendi, *J. Am. Chem. Soc.,* **128** (2006) 13032.

30. J. E. Murphy, *et. al., J. Am. Chem. Soc.*, **128** (2006) 3241.

31. G. A. Ozin, *et. al., J. Am. Chem. Soc.,* **128** (2006) 10337.

32. P. O'Brien, *et. al., J. Mater. Chem*., **7** (1997) 1011.

33. G. Kedarnath, V. K. Jain, S. Dey and L. B. Kumbahre, unpublished results.

34. W. Wang, X. Lu, T. Zhang , G. Zhang , W. Jiang and X. Li, *J. Am. Chem. Soc.,* **129** (2007) 6702; W. Wang, B. Poudel, J. Yang, D. Z. Wang and Z. F. Ren, *J. Am. Chem. Soc*., **127** (2005) 13792.

35. O. Rabin, J. M. Perez, J. Grimm, G. Wojtkiewicz and R. Weissleder*, Nature Materials*, **5** (2006) 118.

36. Y. W. Koh, C. S. Lai, A. Y. Du, E. R. T. Tieknik and K. P. Loh, *Chem. Mater*., **15** (2003) 4544.

37. O. C. Monteiro, T. Trindade, F. A. A. Paz, J. Klinowski, J. Waters and P. O'Brien, *J. Mater. Chem*., **13** (2003) 3006.

38. S. S. Garje and V. K. Jain, *Coord. Chem. Rev.,* **236** (2003) 35.

39. W. Lou, M. Chen, X. Wang and W. Liu, *Chem. Mater*., **19** (2007) 872.

40. V. K. Jain, *et. al., J. Organomet. Chem*., **678** (2003) 122.

41. W. Hirpo, S. Dhingra, A. C. Sutorik and M. G. Kanatzidis, *J. Am. Chem. Soc,* **115** (1993) 1597; S. L. Castro, S. G. Bailey, R. P. Raffaelle, K. K. Banger and A. F. Hepp, *Chem. Mater.,* **15** (2003) 3142.

42. T. C. Deivaraj, J. H. Park, M. Afzaal, P. O'Brien and J. J. Vittal, *Chem. Mater.,* **15** (2003) 2383.

43. M. T. Ng, C. B. Boothroyd, J. J. Vittal, *J. Am. Chem. Soc.,* **128** (2006) 7118.

44. S. Ghoshal, L. B. Kumbhare, V. K. Jain and G. K. Dey, *Bull. Mater. Sci.,* **30** (2007) 173.

Functional Nano-Ceramics Through Solution Combustion

Dr. A. K. Tyagi *joined BARC in 1986 after completing one year orientation course from 29th batch of BARC-Training school. He has done extensive work in the field of nuclear materials, nano-materials and functional materials. He was a postdoctoral fellow at Max-Planck Institute, Stuttgart, Germany (1995-96). He has to his credit large number of publications in internationally reputed journals, a number of invited talks and several review articles. He is a recipient of several prestigious awards like Max-Planck Fellowship, Gold Medal of Indian Nuclear Society, MRSI Medal, CRSI Medal, Rheometric Scientific ITAS Award, Dr. Laxmi Award of ISCAS and IANCAS-Dr. Tarun Dutta Memorial Award. He is a Fellow of National Academy of Sciences, India, and a also Fellow of Maharashtra Academy of Sciences. He has been a visiting scientist at Germany, Canada, France, Japan, Russia, Portugal and Malaysia. He is a recognized PhD guide of Mumbai University and HBNI. Presently, he is heading the Solid State Chemistry Section of Chemistry Division, BARC.*

Dr. R.D. Purohit *is a material chemist working in Energy Conversion Materials Section, BARC, Vashi Complex. After completing his post graduation in chemistry from Jodhpur University in 1992, he has joined BARC through 37th batch of Training School. He has completed his doctorate from Mumbai University in 2003. He was awarded post-doctoral fellowship by Jean Rouxel Institute for Materials, Nantes, France in 2004. His field of research is the synthesis, characterization and densification of nano-crystalline oxide ceramics for various technological applications. He has two patents and about twenty international publications (including the publications in American Chemical Society, American Ceramic Society and Royal Society of Chemistry) in his account. He is currently working in the development of Ceramic Fuel Cells and Thermo-electric materials and devices.*

Abstract

Nano-crystalline oxide ceramics are functional materials as they have great potentials for many advanced applications. Most of the applications require sintered products having desired shape, size and microstructure. Hence, the synthesis of powder with controlled and required characteristics is of utmost importance. Wet-chemical routes play an important role in the preparation of nano-crystalline oxide ceramics. In recent years, solution combustion technique has attracted a considerable attention because of its capability to produce phase-pure, nano-crystalline powders at low calcination temperatures, which can be readily sintered to high density at a comparatively lower temperature. In this review article, the versatility and capability of the solution combustion technique as a preparative method for a variety of nano-crystalline oxide ceramics will be discussed.

Introduction

The synthesis and characterization of nano-particles, nano-tubes and other nano-units at a length scale of 1-100 nm (at least in one direction) is a subject of intense research. In view of this, material chemists play a crucial role in the preparation, structural elucidation and property measurements of the materials, which are important ingredients in the discovery and commercialization of nanotechnologies and devices. In general most of the properties of micro-crystalline ceramics are significantly modified upon reducing the size to

Dr. A.K. Tyagi, Chemistry Division, Bhabha Atomic Research Centre, Mumbai 400 085
Dr. R. D. Purohit, Energy Conversion Materials Section, Bhabha Atomic Research Centre, Vashi Complex, Navi Mumbai-400 705;
E-mail: aktyagi@barc.gov.in

nano-meter scale. Nano-ceramics exhibit unusual properties (chemical, physical and biological) as shown in the following examples:

(a) Abrasives: Al_2O_3, Fe_2O_3, CeO_2 – Significant reduction in the surface defects [1].

(b) Catalysts: TiO_2, ZnO, Fe_2O_3, Pd – Enhanced catalytic activitiy due to highly stressed surface atoms, which are very reactive [2].

(c) Structural materials: Al_2O_3, ZrO_2 – Near net shaping of ceramic parts via super plastic deformation and in turn no need for costly post-forming machining. The mechanical properties are improved because of fine grain microstructure [3].

(d) New and unique electric and magnetic properties [4, 5].

Synthesis routes play a major role in improving/enhancing the physicochemical properties of most of the materials. The characteristics of nano-sized powders are influenced by shape, size, size distribution and nature of agglomeration of the constituting particles, which in turn depend on the nature of synthesis. The processes such as co-precipitation, sol-gel etc. are not suitable to produce the final product directly as they involve a number of tedious and time consuming intermediate steps e.g. repeated grindings and calcination in solid-state process; washing, drying and calcination of the precursors in co-precipitation and Pechini processes etc. Hence, exploring a novel direct conversion process, which can produce ultrafine powders of oxide ceramics in a simple and economic way with improved powder characteristics, is of utmost importance. The solution combustion technique is one of such processes. In general, the powder obtained by this process has the high degree of phase purity with improved powder characteristics such as narrow distribution of nano-particles, higher surface area and better sinter-ability [6-9].

Solution Combustion Process

Steps Involved

Preparation of Fuel-Oxidant Precursor

In this step, the nitrate salts of the metals of interest, in a required molar ratio, are mixed together in an aqueous media to produce the transparent mixed metal-nitrate solution. An organic compound capable of binding the metal ions and acting as a fuel in combustion reaction is added in an appropriate amount to this mixed metal-nitrate solution. The common examples of the fuels are citric acid, glycine and urea. The transparent aqueous solution containing metal nitrates and a suitable fuel is converted to a viscous liquid (hereafter termed as gel or precursor) by thermal dehydration (to remove the excess solvent) at about 80-100°C.

Combustion of the Fuel-Oxidant Precursor

The precursor is subjected to an external temperature of about 150-250°C, which triggers the combustion reaction. At this stage, exothermic decomposition of the fuel-oxidant precursor associated with evolution of large volume of gases results in the voluminous powder. If the fuel-to-oxidant molar ratio is properly adjusted, the very high exothermicity generated during combustion reflects in the form of flame or fire and the process are termed as auto-ignition.

Merits of Gel Combustion Process

(i) The process is capable to deliver phase pure, nano-crystalline powders with higher surface area and better sinterability.

(ii) The formation of homogeneous gel precursor prevents the random redox reaction between a fuel and an oxidizer. Thus, the possibility of local variations in the characteristics of the combustion-synthesized powder is very low.

(iii) The process is versatile leading to synthesis of single phase, solid-solutions and composites [10, 11]. In addition, it is possible to obtain metal and their oxides with variable valencies by the proper selection of process parameters [10].

(iv) The combustion-synthesized powders can be sintered to high densities at lower temperature in a short time.

(v) The combustion technique enables scale-up of the materials with high production rate.

(vi) The process does not require any elaborate experimental setup.

(vii) The process is capable to stabilize metastable phases [12].

Effect of Process Parameters on Powder Characteristics and Batch Size

The powder characteristics and batch size are the two important issues to be considered while performing any solution combustion process. Nature and amount of fuel used in a combustion process affect the following three competitive parameters, as given below, which subsequently affect the powder characteristics and batch size:

(i). Flame temperature, (ii). Volume of evolved gases and (iii). Nature of decomposition of precursor

In general, for a stoichiometric reaction, the amount of fuel (or fuel-to-oxidant ratio) is fixed on the basis of principle of propellant chemistry [13]. A general nature of combustion reaction and trend for variation in flame temperature as a function of fuel-to-oxidant ratio is shown in Fig. 1. The values presented in the X and Y axes are general and highly sensitive to the system under investigation. The heat of combustion (ΔH^0) and the adiabatic (theoretical) flame temperatures (T) can be calculated using the thermodynamic data [14] for the various reactants and products involved in the combustion reaction. It may be noted that the theoretical flame temperature increases as a function of fuel-to-oxidant ratio as shown in the Fig. 1. The theoretical situation may reach close to the actual situation over a wide range of fuel-to-oxidant ratio provided precursor decomposes in a single step in that range during auto-ignition phenomena. This type of situation has been observed by various researchers in case of single component systems, where phase formation temperature is very low [8, 9]. Fig. 1 also shows that the actual flame temperature values are always lower than the theoretically calculated values due to radiative losses, heating of air, water content in the precursor, incomplete combustion etc. The actual flame temperature increases up to certain value of fuel-to-oxidant ratio near stoichiometric region and then its value decreases [15]. The difference in the trend for the theoretical and actual flame temperature is due to the significant role of nature of decomposition of precursor (or kinetics of combustion reaction).
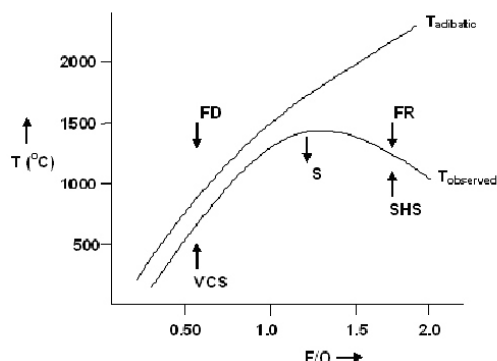
T – Flame temperature, F/O – Fuel-to-oxidant ratio, S – Stoichiometric,
FD – Fuel-deficient, FR – Fuel-rich, VCS – Volume combustion synthesis,
SHS – Self-propagating high temperature synthesis

Fig. 1   A general trend in variation in flame temperature as a function of fuel-to-oxidant ratio

In general, for a particular fuel, the rate of decomposition of precursor decreases as fuel-to-oxidant ratio increases. In spite of low flame temperature associated with the combustion of fuel-deficient ratio, the overall reaction looks very violent in nature due to very fast reaction kinetics. Most of the time, it is difficult to control such kind of reactions due to very fast reaction kinetics along with sudden release of gaseous products. In addition, a considerable amount of material is lost to the surrounding and hence, it is practically impossible to scale up the batch size in this case [7]. The low flame temperature and very short residence time of flame temperature in the case of combustion reaction involving fuel-deficient precursor may result in very small primary particles in the form of soft agglomerates without an appreciable local partial sintering [8,9]. The flame temperature generated during combustion and high surface energy associated with primary nano-particles are responsible for the formation of agglomerates among them. Strength of the agglomerates increases with flame temperature generated during combustion [9]. High resolution transmission electron micrograph (HRTEM) of an agglomerated ceria powder produced through combustion of fuel-deficient citrate-nitrate precursor is shown in Fig. 2(a). The very high flame temperature associated with stoichiometric reaction may results
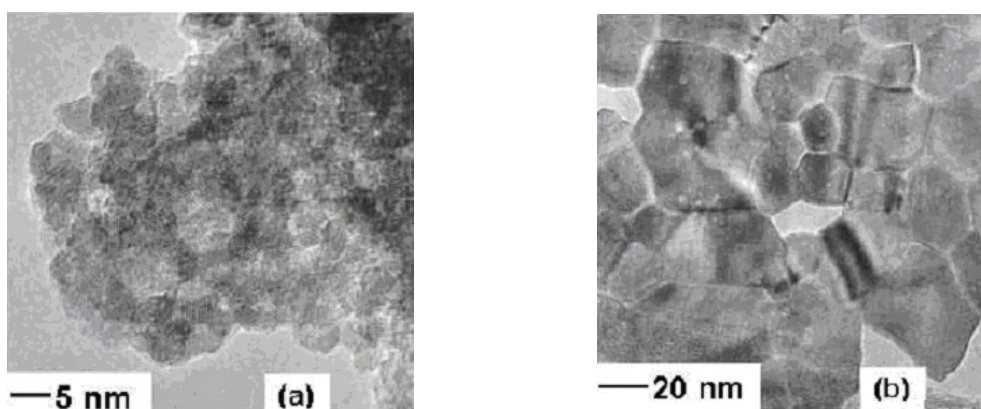
Fig. 2   HRTEM of ceria powder prepared using (a) fuel-deficient citrate-nitrate precursor, (b) stoichiometric citrate-nitrate precursor

in the local partial sintering among primary particles. HRTEM of ceria powder composed of hard agglomerates (aggregates) produced through stoichiometric citrate-nitrate combustion reaction is shown in Fig. 2(b).

Controlling the combustion reaction is an important issue for producing the powder in a significant amount. In general, it is quite difficult to scale up the fuel-deficient and stoichiometric combustion reactions due to their fast kinetics. One way of controlling the combustion reaction is to make it sluggish by using a fuel rich precursor in a range where auto-ignition phenomenon occurs [7]. This is possible due to comparatively lower flame temperature and slow reaction kinetics. It may be noted that total number of moles of evolved gases during auto-ignition and calcinations step also increases as fuel-to-oxidant ratio increases, which can results in the improved powder characteristics e.g. minimum agglomeration with high surface area [9]. The transmission electron micrograph (TEM) of $La(Ca)CrO_3$ powders produced through the glycine-nitrate combustion reactions involving stoichiometric and fuel-rich precursors are shown in Figs. 3(a) and 3(b), respectively.

Densification of Nano Powders

In general, densification of nano-crystalline powders takes place at much lower temperature as compared to larger grained powders due to predominant surface and grain boundary diffusion.
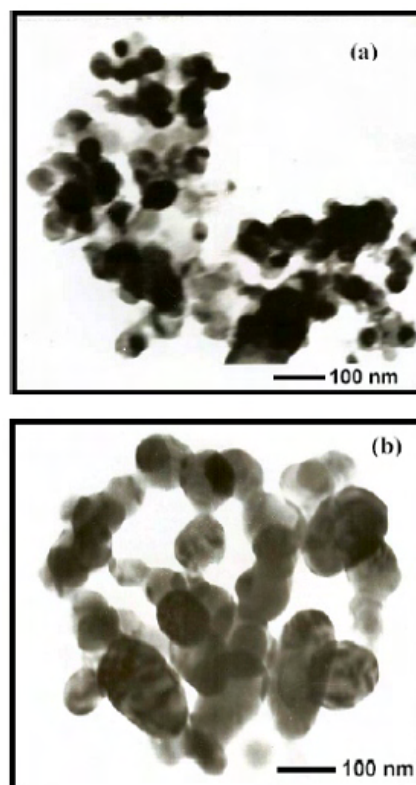

Fig. 3   HRTEM of La(Ca)CrO₃ powder prepared using (a) stoichiometric glycine-nitrate precursor, (b) fuel-rich glycine-nitrate precursor
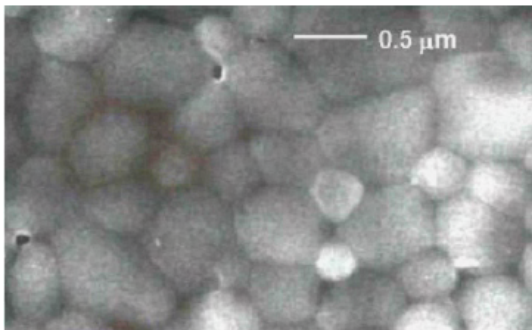
Fig. 4   SEM micrograph of sintered ceria

Fig. 5   SEM micrograph of sintered Nd_3GaO_6

There are numerous benefits associated with lower sintering temperature viz. faster densification, a small grain size of the end product, avoidance of undesirable phase transformation or interfacial reactions, elimination of sintering aids and less expensive sintering equipment. A full densification retaining the nano-grain size in the sintered product is required to achieve improved physical and mechanical properties. A narrow size distribution of non (or soft) agglomerated nano-powder is preferred for achieving this goal. Such kind of powders can produce a high green density with small pore size and uniform pore structure, which is an essential requirement for achieving the improved sintering characteristics.

Consolidation of combustion-synthesized nano-crystalline powders is an important issue to generate engineering components for novel applications. The challenges of sintering the combustion-synthesized powders are related to their high tendency to agglomerate, significant inter-particle friction and rapid sintering and grain coarsening. In general, combustion synthesis is capable to produce nano-crystalline powder for a wide range of fuel-to-oxidant ratio as described earlier. However, sintering characteristics of such powders predominantly depend on nature and extent of agglomeration rather than size of primary particles. The nature and extent of agglomeration in the combustion-synthesized powder is highly sensitive to the nature of fuel and fuel-to-oxidant ratio. Generally, the stoichiometric combustion reactions produce powders with hard agglomerates due to the generation of very high flame temperature,
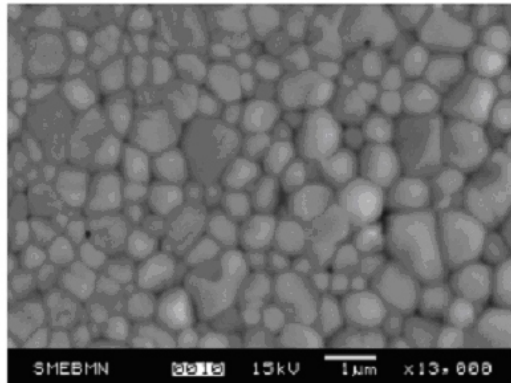
which in turn results in poor densification. However, it may be possible to break these agglomerates to some extent through ball milling. In spite of small volume of evolved gases, the powders derived through fuel-deficient precursors can produce soft agglomerates due to low flame temperature and its short residence time, which can be densified at comparatively lower temperature. A highly dense, fine grain microstructure of the sintered ceria derived using the powder produced through the fuel-deficient citrate-nitrate combustion is shown in Fig. 4 [9]. The fuel-rich combustion reactions are also capable to produce soft agglomerates due to low flame temperature and high volume of evolved gases, which in turn results in the high sintered density. An almost fully dense microstructure of the sintered Nd_3GaO_6 based material produced through the EDTA-nitrate combustion synthesis of fuel-rich precursor is shown in Fig. 5.

Apart from achieving full densification, retaining nano-grain size in the sintered product is also an important advantage for the combustion-synthesized powders. In general, it is quite difficult to retain nano-grain size in the sintered product due to limited heating rate and more exposure time for temperature, which facilitate grain growth. This can be best achieved using fast firing process such as hot press, microwave or spark plasma sintering.

Applications of Solution Combustion Technique

Structural Ceramics

Generally, ceramics are very hard and brittle, which pose difficulty in fabrication and machinability. However, for almost two decade now, it has been observed that many fine-grained ceramics can deform plastically [16]. As the nano-crystalline materials contain a very large fraction of atoms at the grain boundaries, the numerous interfaces provide a high density of short-circuit diffusion paths. The enhanced diffusivity can have a significant effect on mechanical properties such as creep and super-plasticity. There have been extensive efforts to fabricate nano-structured ceramics through fast firing or activated sintering processes. Methods such as hot isostatic pressing, spark plasma sintering, microwave sintering etc. have been employed to avoid an excessive grain growth [17]. The fully dense and fine grained yttria-stablized-zirconia (YSZ) ceramics were prepared through fast firing process using the powders produced by oxalic dihydrazide-nitrate combustion [18]. The authors have studied the effect of Y_2O_3 content and firing conditions on the sintered density and final grain size of YSZ. Lamas et al. [19] produced dense, fine grained CaO stabilized tetragonal zirconia polycrystals (TZP) ceramics through fast firing technique using the citrate-nitrate combustion-synthesized powder. The microwave sintering of urea-nitrate combustion synthesized powders was capable to yield dense, nano-structured CaO stabilized tetragonal ZrO_2 polycrystal (TZP) ceramics [20]. Nano-composites are believed to undergo enhanced creep, which is helpful in super-plastic deformation. Bhaduri and group [21] have synthesized almost fully dense Al_2O_3-ZrO_2 nano/nano composites through hot isostatic pressing of nano powders produced by urea-nitrate combustion. They observed the enhanced toughness or ductility at room temperature compared to that produced through conventional solid state route.

The magnesium aluminate spinel $MgAl_2O_4$ and related materials were synthesized by the combustion method using corresponding nitrates and urea as the fuel [22]. The nano powders were then sintered through hot isostatic pressing to yield dense, nano-structured bodies. They have shown an increase in the fracture toughness and reduction in hardness compared to that of coarse grained materials. Quenard et al. [23] produced nano-structured $MgAl_2O_4$ and ZrO_2-$MgAl_2O_4$ composite through hot pressing using urea-nitrate combustion synthesized powders. They have observed an increase in fracture strength, fracture toughness and Vickers micro-hardness for the composites compared to that of $MgAl_2O_4$. Synthesizing the nano-particles of calcium hydroxyapatite $Ca_{10}(PO_4)_6(OH)_2$ (HAP) and their coating on metal implant is of great significance in the medical field. A bio-active coating of HAP on Ti substrates was deposited through solution combustion process [24]. The nano-crystalline HAP powders were also synthesized through citric-acid sol-gel process [25]. These powders could be sintered into micro-porous ceramic in air at 1200°C and a flexural strength of 37 MPa could be achieved. Tas et al. [26] developed a new chemical recipe for the preparation of synthetic body fluid (SBF). These SBF solutions along with urea as a fuel have been used for the synthesis of calcium phosphate bio-ceramics. The combustion synthesized non-agglomerated, submicron size (0.45 μm) powders were found to contain Mg, Cl, Na, K, Fe, Zn and Cu, all being at the ppm levels similar to the chemical composition of natural bones.

Ceramic Based Catalysts

Ideally speaking, a catalyst should possess high purity, small average particle size and large surface area. The chemical activity of a conventional catalyst is proportional to the overall surface area per unit volume. Pervoskite type materials scores over conventional metal based catalysts due to their low cost and much more resistance to deactivation. Civera et al. [27] have prepared perovskite- type catalyst, $LaMnO_3$, used in natural gas combustion. They have adopted urea-nitrate combustion process and obtained a surface area value of about 5 m^2/g. The increase in the surface area value to ~ 18 m^2/g was observed by using NH_4NO_3 as an extra oxidant. Campagnoli et al. [28] investigated the effect of preparation method on the activity and stability of $LaMnO_3$ and $LaCoO_3$ catalysts for the flameless combustion of methane. They have used citric acid and ethylene diamine tetra acetic acid (EDTA) as

complexing agents. About 80 % conversion of CH_4 could be achieved at a temperature as low as $600^{\circ}C$. Generally, it has been observed that the doped perovskites have better catalytic activity due to a high lattice oxygen mobility, which facilitates the intra-facial catalytic activity. Richardson et al. [29] prepared $La_{0.6}Sr_{0.4}Co_{0.2}Fe_{0.8}O_{3-\delta}$ (LSCF) starting from a nitrate-citrate gel, which resulted in a product with high surface area (17.4 m^2/g). This value was higher than that obtained for same sample prepared by a mixed oxide route, mixed nitrate route, oxalic acid decomposition, drip pyrolysis etc. These LSCF membrane reactors were used for the oxidation of methane. As the temperature rises, the oxygen permeates across the membrane and methane is consumed, which leads to the formation of synthetic gas at about 1173 K.

Titania photo-catalysts have attracted a considerable attention ever since the discovery of photochemical dissociation of water by Fujishima and Honda [30]. A solution combustion process was developed for the preparation of porous ceramic materials with an open cellular structure [31]. The photochemical activity of the titania foam was found to be much better than that of powdered titania. Sivalingam et al. [32] synthesized nano-sized titania by glycine-nitrate combustion reaction. The nano-sized, porous and high surface area titania prepared by this combustion method showed excellent photo-chemical degradation of poly (bispheol-A-carbonate) under UV irradiation. The higher photo-activity of combustion-synthesized TiO_2 compared to that of commercial Degussa catalyst (P-25) for photodegradation of polycarbonate was attributed to reduced band gap and higher surface area.

The gas phase catalytic reactions have gained tremendous importance in view of the environmental concerns and production of useful gases. This conversion of carbon monoxide with steam leading to carbon dioxide and hydrogen reaction is called as water gas shift (WGS) reaction. A low temperature water gas shift reaction was developed by Bera et al. [33] using nanocrystalline $Ce_{1-x}Pt_xO_{2-\delta}$ catalyst, which was prepared by a combustion process. About 90% CO was converted to CO_2 at $200^{\circ}C$.

Electro-Ceramics

The electrical properties of various materials are greatly modified by parameters like grain size, stoichiometry, homogeneity etc. Ni-substituted $LiCoO_2$ is a cathode material used in rechargeable lithium batteries due to its high reversibility and higher voltage in $Li/LiCoO_2$ cell. Suresh et al. [34] successfully synthesized submicron $LiCo_{1-x}Ni_xO_2$ ($0 < x < 0.4$) powder at a calcination temperature of $850^{\circ}C$ using diformyl hydrazine as a fuel. Maximum discharge capacity of about 110 $mAhg^{-1}$ was obtained for the compositions $x = 0.1$ and 0.2. $LiNi_{0.3}Co_{0.7}O_2$ was synthesized through glycine-nitrate combustion as well as through sol-gel method [35]. Investigation of the cathode performances revealed that the sol–gel synthesized cathode yields inferior capacities (125 $mAhg^{-1}$) compared to that of combustion synthesized cathode (140 $mAhg^{-1}$) when discharged to a cut-off voltage of 2.8 V.

Recently, solid oxide fuel cells (SOFC) have received worldwide attention as they are environment-friendly, direct energy conversion devices with very high conversion efficiency (~70%). The characteristics of starting oxide ceramic powders have to be suitably modified to fabricate the SOFC components with required performance. The electrolyte for SOFC should be impervious for its better performance. Nanocrystalline, sinter-active powders of yttria stabilized zirconia (YSZ) elelctrolyte has been prepared by glycin-nitrate combustion process [36]. It was observed that a G/N ratio of 0.23 and calcination in the temperature range of $650-900^{\circ}C$ in oxygen flow gave high quality powder with crystallite size less than 10 nm. Singh et al. [37] prepared nano-crystalline YSZ powders through citrate-nitrate combustion process. Doped ceria (CeO_2) is an attractive electrolyte material for intermediate temperature SOFC ($< 800^{\circ}C$), which would allow greater flexibility in the design of electrode and inter-connectors. A study on the preparation of 20 mol % Gd and Sm-doped ceria by the combustion route by Mokkelbost et al. [38] showed that these powders could attain high sintered densities (92-95% of theoretical density) at $1300-1400^{\circ}C$. Peng et al. [39] have successfully prepared a series of compositions in the

$Ce_{1-x}Sm_xO_{2-x/2}$ system (0.0 < x < 0.60) by the combustion process using citric acid as a fuel. The powders could be densified > 95% theoretical density even at a sintering temperature of 1300^oC. The composition $Ce_{0.80}Sm_{0.20}O_{1.90}$ showed the highest conductivity of 5.4×10^{-3} S/cm at 600^oC. Purohit et al. [40] developed new oxygen ion conductors based on Nd_4GeO_8 and Nd_3GaO_6 using EDTA-nitrate combustion process. The powders could be sintered to ~ 98% at 1250^oC. The authors have successfully solved the problem related to the phase formation, densification and decomposition.

Unlike the electrolyte material, the cathode material for SOFC should be highly porous (porosity ~ 35-40%) and conducting. Sr-doped $LaMnO_3$ (LSM) cathode material was synthesized by the combustion route using citric acid as a fuel [41]. It was demonstrated that conductivity enhanced with citrate-to-nitrate ratio. It was found that optimum citrate-to-nitrate ratio of 1:1.5 resulted in the sintered product with maximum conductivity (150 S cm^{-1}) at about 800^oC. The major problem encountered in sintering the $LaCrO_3$ based SOFC interconnect materials is the losses due to chromium evaporation at higher temperature, which inhibit the sintering due to evaporation-condensation mechanism. The nano-crystalline Ca-doped $LaCrO_3$ have been prepared through glycine-nitrate combustion process by S. Nair et al. [42]. The near theoretical density could be achieved at a sintering temperature as low as 1200^oC. The improved conductivity of 57 Scm^{-1} could be achieved at 1000^oC.

Magnetic Ceramics

Nano-crystalline magnetic materials are unique in exhibiting unusual properties including Hopkinson effect, magnetization anomaly and spin glass-like behavior. Lithium and substituted lithium ferrites have found lots of applications in microwave devices due to their low cost, high resistivity and low eddy current losses. The preparation strategy for these materials assumes a great significance due the loss of lithium during heating. Yue et al. [43] prepared titanium-substituted LiZn ferrtites with composition $Li_{0.5(0.4+x)}Zn_{0.6}Ti_xFe_{(2.2-1.5x)}O_4$ (x = 0.05 to 0.2) through citrate-nitrate combustion process. It was observed that the Curie temperature decreases as a function of Ti concentration, which is a non-magnetic ion. The nano-crystalline

$Ni_{0.25}Cu_{0.25}Zn_{0.50}Fe_2O_4$ ferrite powders were prepared by sol-gel auto-ignition process starting from a citrate- nitrate gel. It was observed that the densification starts at 700^oC and the sintering rate is maximum at 800^oC. Yu et al. [44] reported the preparation of $Ni_{0.35}Cu_{0.11}Zn_{0.57}Fe_{1.97}O_4$ by a combustion process. The complete spinel structure was formed at a temperature as low as 480^oC. Denzanneau et al. [45] prepared $La_{1-x}Sr_{1-y}MnO_3$ by a gel combustion process based on a cation solution soaking by acrylamide polymerization. For the samples with La/Mn > 0.9, the presence of vacancies at Mn-sites was observed, which leads to the destruction of long-range ferromagnetic order. The glycine-nitrate solution combustion process was used to prepare $La_{0.70}Ca_{0.3}MnO_3$ (LCM) powders [46]. The surface area of solid state synthesized powder was 3.48 m^2/g as compared to 92 m^2/g for the combustion synthesized powder. In order to study the CMR behavior, thin films of LCM were made, which showed 96 % of maximum MR ratio at 97 K.

Barium hexaferrite, ($BaFe_{12}O_{19}$) as it is used as a permanent magnet. It has relatively high coercivity along with an excellent chemical stability and corrosion resistance. Nano-crystalline $BaFe_{12}O_{19}$ was synthesized by citrate-nitrate combustion process. [47]. The maximum saturation magnetization of 59.36 emu/g and a coercivity of 5540 Oe was achieved in $BaFe_{12}O_{19}$ sample prepared by this route. Qiu et al. [48] prepared $BaFe_{12}O_{19}$ using glycine as a fuel in three different glycine-to-nitrate (G/N) ratios. It was found that the specific saturation magnetization, specific remnant magnetization and coercivity of $BaFe_{12}O_{19}$ particulates were high in case of higher G/N ratios.

Optical Ceramics

Rare earth activated oxide phosphors have application in high energy photoluminescent plasma panel and cathodoluminescent flat panel displays. Fabrication of complex host compositions Y_2SiO_5, $Y_3Al_5O_{12}$ and Y_2O_3 along with controlled amounts of the activators (Cr^{3+}, Mn^{2+}, Eu^{2+}, Er^{3+}, Tb^{3+}, Tm^{3+}) pose a challenge to the materials synthesis community. High purity, compositionally uniform, single phase, small and uniform particle size powders are required for high resolution and high luminous efficiency in the new flat panel display

developments. Nano-crystalline Y_2O_3: Eu phosphors have been prepared by glycine-nitrate solution combustion process [49]. Due to surface effects, the peak of excitation spectra was found to be shifted towards red and becomes narrower with decreasing particle size. The reflection spectra also showed particle size dependence: the smaller the particle size, the stronger is the absorption. The glycine-nitrate gel combustion synthesis of $(Y_{0.95}Eu_{0.05})_2O_3$ phosphor was performed in presence of several kinds of lithium salt flux [50]. Luminescence enhancement was observed in both lower and higher concentration of Li salts addition. The Li doping into $(Y_{0.95}Eu_{0.05})_2O_3$ lattice and the crystal growth by using Li salt flux contributed to the respective luminescence enhancements.

Metal vanadates, MVO_4, (M = Fe, Al, Cr, Y, Gd etc.) are potential materials as laser hosts, phosphors etc. The $GdVO_4$ powder was synthesized by the combustion of aqueous solutions containing $Gd(NO_3)_3$, ammonium nitrate, ammonium metavanadate and 3-methyl-5-pyrazole-5-one (3MP5O) [51]. Similarly, $(Bi^{3+} - Eu^{3+})$ double-doped samples of $GdVO_4$ with Bi^{3+} varying from 0.1 to 1 mol % and Eu^{3+} from 1 to 7 mol % were synthesized. It was observed that the emission intensity of $GdVO_4$: Eu^{3+} varied slowly from 1 to 5 mol % of Eu^{3+} ions and thereafter decreased rapidly. Eu^{3+} is a routinely employed activator for the red emission. In an interesting study, solution combustion synthesis has been extended to two perovskite-based red phosphors; $(La_{0.96}Eu_{0.04})AlO_3$ and $(Y_{0.96}Eu_{0.04})AlO_3$ [52]. Here, both, the electric dipole transition and magnetic dipole transition were found to contribute equally to the color rendering index (CRI) and lumen output. Thus, these materials form a special red phosphor due to greater CRI and higher lumen output in a single phosphor.

There is a great deal of interest in upconversion phosphors using Er^{3+} as an activator oxide materials because of their stability, inexpensiveness, and ease of preparation. Nano-crystalline Er-doped ceria phosphors were prepared through glycine-nitrate combustion process [53]. The photo-acoustic spectra (PAS) showed the particle-size dependence of the optical properties. A blue shift of the PAS absorption peak and an enhancement of the exciton absorption were observed with decrease of the particle size. It was found that the luminescence of 18 nm CeO_2:Er has the largest red-to-green ratio of the emission bands.

Nuclear Ceramics

Oxide ceramics such as thoria, urania and their solid-solutions are widely used in nuclear industry. These materials are used in the form of dense products to realize high power density. In general, it is difficult to densify these materials due to large difference in diffusion rates of the constituent elements. One way to overcome this problem is to start with nano-crystalline powder, which can be sintered at comparatively lower temperature due to enhanced surface and grain boundary diffusion. Thorium has attracted a considerable attention in the recent past as it is expected to play an important role in the third stage of the Indian nuclear power generation program [54]. Thoria in the form of dense pellets is used as a blanket material in nuclear reactors. Thoria powders prepared by conventional routes [55] require sintering temperatures higher than 1600°C to get dense pellets. The feasibility of the solution combustion synthesis to prepare a thoria powder feed that can be compacted and sintered at lower temperatures was studied. Nano-crystalline thoria powders were prepared using thorium nitrate as oxidant and urea and citric acid as the fuels [56]. The citrate-nitrate derived powders could be sintered to 94% of the theoretical density at 1573 K. Purohit et al. [57] prepared nano-crystalline thoria powders by the glycine-nitrate combustion process. The specific surface areas as high as 90 m^2/g could be obtained. Thoria powders prepared by this process could be sintered to highly dense pellets (> 93% of the theoretical density) at a relatively low sintering temperature of 1300°C. It was observed that the fuel-deficient ratio yielded a product with desired powder characteristics. Chandramouli et al. [58] used polyvinyl alcohol aided microwave synthesis for the preparation of nano-crystalline thoria powders.

Thorium itself is not a fissile material by thermal neutrons, hence, it is proposed to use about 4-6% of fissile uranium and plutonium dioxides in ThO_2 matrix. Homogeneous solid solutions containing uranium and thorium oxides with U/(U + Th) < 0.3 are being developed as fuels for thermal

breeder reactors and advanced gas-cooled reactors. High density (U,Th) mixed oxide pellets can be prepared by various methods which use very high temperatures (> 2000 K) for sintering. Hence, studies were carried out by Anthonysamy et al. to examine the suitability of citric acid as the combustion fuel for the preparation of $(U,Th)O_2$ powder feed. [59]. Various process parameters like fuel-to-oxidant mole ratio, method of heating and calcination temperature were optimized to prepare a powder feed that could be sintered to high densities. It was observed that the powders obtained through the combustion route were nano-crystalline, highly free flowing and porous; that were found to be suitable as the feed material for making high density compacts.

Concluding Remarks

Based on the foregoing discussion, it can be conclusively said that the solution combustion synthesis route successfully caters to the preparation of oxide ceramics in the nano-regime. It covers a wide variety of subjects ranging from the chemistry of the catalysis to the modified mechanical, optical, magnetic and electrical properties. The tailoring of the particle sizes can allow one to engineer these different properties. The solution combustion technique is capable to meet the demands of material science engineering in tailor-making materials with desired composition, structure and property. The main feature of the solution combustion process is that the powder characteristics and batch size are highly dependent of the process parameters such as nature of fuel and fuel-to-oxidant ratio and one can tune the same using these parameters. This simple, versatile and cost-effective method of preparation of nano-crystalline oxide ceramics is an impetus to the study of powder property-functionality correlation.

Acknowledgements

References

1. Abrasive particles, abrasive articles, and methods of making and using the same US Patent No. 6802878, (2004)

2. S. Sato, K. Koizumi and F. Nozaki, J. Catal. 178, 264 (1998)

3. R. W. Seigel, Mater. Sci. Forum. 851, 235 (1997)

4. V. M. Ferreira, F. Azough J. L. Baptista and R. Freer, Ferroelectrics 133, 127 (1992)

5. D.-H. Chen and X.-R. He, Mater. Res. Bull. 36, 1369 (2001)

6. K. C. Patil , S.T. Aruna and T. Mimani, Curr. Opin. Solid State Mater. Sci. 6, 507 (2002)

7. L. A. Chick, L. R. Pederson, G. D. Maupin, J. L. Bates, L. E. Thomas and G. J. Exarhos, Mater. Lett. 10, 6 (1990)

8. J. Schafer, W. Sigmund, S. Roy, F. Aldinger, J. Mater Res. 12, 2518 (1997)

9. R. D. Purohit, S. Saha and A. K. Tyagi, J. Nanosci. Nanotechnol. 6, 209 (2006)

10. L.A. Chick, G.D. Maupin and L.R. Pederson, Nanostruc. Mater. 4, 603 (1994)

11. O. Que ard, C. Laurent, M. Brieu and A. Rousset, Nanostru. Mater. 7, 497 (1996)

12. O. Ozuna, G. A. Hirata and J. McKittrick, J. Phy.: Cond. Matt., 16, 2585 (2004)

13. S. R. Jain, K. C. Adiga and V. R. Pai Verneker, Combust. Flame 40, 71 (1981)

14. R.H. Perry, D. W. Green, Chemical engineers handbook, 7th ed., McGraw-Hill, (1997)

15. A. S. Mukasyan, C. Costello, K. P. Sherlock, D. Lafarga and A. Verma, Sep. Purif. Tech. 25, 117 (2001)

16. T.G. Langdon, JOM 42, 8 (1990)

17. Randall M German, Sintering Technology, Marcel Dekker Inc., New York USA (1996)

18. K. R. Venkatachari, D. Huang, S. P. Ostrander, W. A. Schulze and G. C. Stangle, J. Mater. Res. 10, 756 (1995)

19. D. G. Lamas, R. E. Juarez, A. Caneiro and N. E. W. De Reca, Nanostruc. Mater. 10, 1199 (1999)

20. S. B. Bhaduri, S. Bhaduri and J. G. Huang, Ceram. Eng. Sci. Proc. 20, 227 (1999)

21. S. Bhaduri and S. B. Bhaduri, Nanostruc. Mater. 8, 755 (1997)

22. S. Bhaduri, S. B. Bhaduri and K. A. Prisbrey, J. Mater. Res., 14, 3571 (1999)

23. O. Que ard, C. Laurent, A. Peigney and A. Rousset, Mater. Res. Bull. 35, 1979 (2000)

24. Y. Liu, X. Dan, Y. Du and F. Liu, J. Mater. Sci. 39, 4031 (2004)

25. Y. Han, S. Li, X. Wang and X. Chen, Mater. Res. Bull. 9, 25 (2004)

26. A. C. Tas, J. Europ. Ceram.Soc. 20, 2389 (2000)

27. A. Civera, M. Pavese, G. Sarcco, V. Spechhia, Catal. Today 83, 99 (2003)

28. E. Campagnoli, A. Tavares, L. Fabbrini, I. Rossetti, Yu. A. Dubitsky, A. Zaopo, L. Forni, Appl. Catal. B: Environ. 55, 133 (2005)

29. R. A. Richardson, J. W. Cotton and R. M. Ormerod, Dalton Trans. 3110 (2004)

30. A. Fujishima and K. Honda, Nature 238, 37 (1972)

31. A. Yamamoto and H. Imai, J. Catal. 226, 462 (2004)

32. G. Sivalingam and G. Madras, Appl. Catal. A: General 269, 81 (2004)

33. P. Bera, S Malwadkar, A. Gayen, C. V. V. Satyanarayana, B. S. Rao and M. S. Hegde, Catal. Lett. 96, 213 (2004)

34. P. Suresh, S. Rodrigues, A.K. Shukla, S.A. Shivashankar, N. Munichandraiah, J. Power Sources 112, 665 (2002)

35. C. Julien, S. S. Michael, S. Ziolkiewicz, Int. J. Inorg. Mater. 1, 29 (1999)

36. Ingeborg Kaus, Paul Inge Dahl, Johann Mastin, Tor Grande, and Mari-Ann Einarsrud, Journal of Nanomaterials Volume 2006 (2006), Article ID 49283, 7 pages

37. K. A. Singh, L. C. Pathak, S. K. Roy, Ceram. Int. (2006) (in Press)

38. T. Mokkelbost, I. Kaus, T. Grande and M.-A. Einassrud, Chem. Mater. 16, 5489 (2004)

39. C. Peng, Y. Zang, Z. W. Cheng, X. Cheng and J. Meng, J. Mater. Sci: Materials in electronics 13, 757 (2002)

40. R. D. Purohit, A. Chesnaud, A. Lachgar, M.T. Caldes, Y. Piffard, L. Brohan, Chem. Mater. 17, 4479 (2005)

41. R. S. Guo, Q. T. Wei, H. L. Li, F. H. Wang, Mater. Lett. 60, 261 (2006)

42. Sathi R. Nair, R. D. Purohit, A. K. Tyagi, P. K. Sinha and A. K. Tyagi, J. Amer. Ceram. Soc., July 2007 (accepted)

43. Z. Yue, Ji Zhou, X. Wang, Z. Gui, L. Li, J. Eur. Ceram. Soc. 23, 189 (2003)

44. L. Yu, S. Cao, Y. Liu, J. Wang, C. Jing, J. Zhang, J. Mag Mag. Mater. 301, 100 (2006)

45. G. Dezanneau, A. Sin, H. Roussel, M. Audier and H. Vincent, J. Solid State Chem. 173, 216 (2003)

46. K. R. Lee, J. Y. Chong, J. H. Lee, J. S. Song and S. Park, J. Mater. Synth. Procss. 10, 47 (2002)

47. J. Huang, H. Zhuang, W. Li, Mater. Res. Bull. 38, 149 (2003)

48. J. Qiu, L. Liang, M. Gu, Mater. Sci. & Eng. A 393, 361 (2005)

49. Tao Ye, Zhao Guiwen, Zhang Weipeng and Xia Shangda, Mater. Res. Bull. 32, 501 (1997)

50. T. Takeda, D. Koshiba, S. Kikkawa, J. Alloys Comp. 408-412, 879 (2006)

51. B.N. Mahalley, R.B. Pode, P.K. Gupta, Phys. Stat. Sol. (a) 177, 293 (1999)

52. S. Ekambarm, J. Alloys Comp. 390, L7 (2005)

53. Y. Xijuan, X. Pingbo and S. Qingde, Phys. Chem. Chem. Phys. 3, 5266 (2001)

54. R. Chidambaram, Proceedings of the Indo-Japan Seminar on Thoria Utilization, M. Srinivasan, I. Kimura Eds., India (1990), p. 7.

55. J.M. Pope, K.C. Redford, J. Nucl. Mater. 52, 241 (1974)

56. V. Chandramouli, S. Anthonysamy, P.R. Vasudeva Rao, J. Nucl. Mater. 265, 255 (1999)

57. R. D. Purohit, S. Saha, A.K. Tyagi, J. Nucl. Mater. 288, 7 (2001)

58. V. Chandramouli, S. Anthonysamy, P.R. Vasudeva Rao, R. Divakar, D. Sundaraman, J. Nucl. Mater. 231, 213 (1996)

59. S. Anthonysamy, K. Ananthsivan, V. Chandramouli, I. Kaliappan, P.R. Vasudeva Rao, J. Nucl. Mater. 278, 346 (2000)

Ion Beam Modification at Nanoscale

Dr. P. V. Satyam is at present working as an Assistant Professor in Institute of Physics (IOP), Sachivalaya Marg, Bhubaneswar. His areas of interest include nanosciene and nanotechnology (particularly materials science aspects of it), ion – nanostructure interactions, polymer nanocomposites, etc. His group has expertise in analytical experimental methods that include: high resolution TEM, X-ray methods (reflectometry, standing waves and XRD) and ion – scattering methods (RBS and Channeling). Dr. Satyam completed his Ph.D in 1996 (from Institute of Physics/Utkal University, Bhubaneswar) and did his post doctoral work from 1996 – 1999 at advanced photon source, Argonne National Lab., IL, USA. He was JSPS fellow in 2004. Dr. Satyam has about 70 publications in referred journals.

Dr. B. Satpati is at present visiting scientist at IOP. He completed his Ph.D. work in 2005 from IOP. Dr. Satpati has worked in Paul Drude Institute for Solid State Electronics, Berlin, Germany for his postdoctoral work (2005 – 2007). He has about 50 publications in referred journals. He is specialized in electron microscopy.
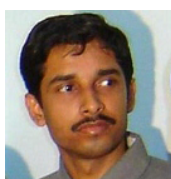
Shri J. Ghatak is Ph. D student working with Dr. P. V. Satyam. His specialization is on ion – nanostructure interactions, particularly with high flux irradiations. He has specialization is TEM, ion-implanters, ion scattering methods.

Shri M. Umananda is Ph. D student working with Dr. P. V. Satyam. His specialization is on soft-matter related work. He is working on ion – softmatter interactions, embedding nanostructures in polymers and Langmuir – Boldgett films. He is specialized in TEM (soft matter) and x-ray and ion scattering methods.

Abstract

Tailoring of nanostructures with energetic ion beams has become an active area of research leading to the fundamental understanding of ion-solid interactions at nanoscale regime and with possible applications in the near future. In this work, we review our recent work on ion – solid interaction, in particular, ion interaction with nanostructures. The fabrication of nanostructures using energetic ion beams involves ion implantation followed by annealing and ion irradiation of uniform and non-uniform films. The sputtered nanoparticles size and their size distribution due to ion irradiation are studied by varying the incident ion beam parameters. The possibility of surface and sub-surface/interface alloying at nano-scale regime, ion-beam induced embedding, and crater formation in semi-continuous and continuous films of noble metals (Au, Ag) deposited on single crystalline silicon are reviewed. In the case of low energy (32 keV) ions, where the

Dr. P.V. Satyam, Dr. B. Satpati, Shri J. Ghatak and Shri Umananda M. Bhatta, Institute of Physics, Sachivalaya Marg, Bhubaneswar 751005; E-mail: satyam@iopb.res.in

nuclear energy loss is dominant, sputtering is less as compared to medium energy (1.5 MeV). In the high-energy regime (100 MeV), where the electronic energy loss is dominant, sputtering is found to be maximum for non-uniform films.

Introduction

Understanding structure – property relationship of nanostructures can facilitate many important applications in various fields of advanced technology. Semiconductors, particularly Si, thin films on Si, doping and modifications of properties of Si with energetic ions, have been extensively studied. Nanostructures of variety of semiconductors, prepared by chemical methods are also being studied by large groups and have been finding enormous applications in various fields of industry due to their unique properties. Understanding the structure of these nanomaterials has become an interesting area of research activity as the structural properties get modified due to its low-dimensionality and due to the quantum confinement effects. Energetic ions have been used from doping to change the electrical properties semiconductors, synthesizing new structures, coating thin films, mixing immiscible layers and for characterizing the materials [1]. The process of ion-irradiation is an athermal or non-equilibrium thermal process and hence the properties of nanostructures could be tailored, which are otherwise difficult or not feasible by conventional methods. For example, ion induced shape changes have been reported [2]. For these ion induced modificational studies, the ion energies ranging from hundreds of eV to MeV, with various projectile ions have been used.

When an energetic ion impinges on a solid material, many interesting phenomena can occur, like sputtering of target material, surface and interface morphological changes, etc [1]. Until now, not much effort has been given on involved mechanisms to understand various processes during an energetic ion interaction with nanoparticles or embedded nanostructures. All the spike models involve a confined region where the energy or pressure or temperature arising because of ion impact is confined to nanometer zones. It requires a systematic study on ion irradiation with a control on separating nuclear regime and electronic energy loss

regimes and under various irradiation parameters like fluence, dose-rate, substrate temperature, and geometry. While the phenomena at surface and interfaces are yet to be properly understood, the ion-solid interaction for the case isolated nanoislands has become an important topic [3-5]. For example, in the case of ion-nanosolid interaction, sputtering, burrowing and wetting are competitive mechanisms for nanoparticles that are immiscible with the substrate to undergo smoothing reactions [3].

In this paper, we review the effects of ion implantation to form buried nanostructures, and ion irradiation to modify the nanostructures that are deposited on the surfaces. The gold ions of energy 32 keV, 1.5 MeV and 100 MeV have been used on Au, Ag and Ag nanostructures grown on silicon substrate. Our result show (i) higher probability of crater formation, (ii) larger particle size and its coverage, and (iii) enhanced sputtering yield when compared with continuous films of Au on Si substrate [6-8] . The average sputtered particle size and areal coverage was determined from transmission electron microscopy (TEM) measurements where as the amount of gold on the substrate has been found by Rutherford backscattering spectrometry (RBS). Two other important aspects of ion-induced effects on nanostructures: (i) effect of energy/thermal spike confinement causing nano-scale ion beam mixing and formation of nanoscale gold silicide structures (this might provide a route to fabricate embedded nanostructures) (ii) absence of this behavior in case of continuous Au film on silicon for low flux irradiation [9-12]. In these studies, the possibility of having sub-surface nano-alloy-mixing is demonstrated with nano Au_xSi_y formation. It is to be noted that the projected range of 1.5 MeV gold ions in silicon is very large compared to the thickness of the nano-islands and the substrate is found to be amorphized at a fluence of $1x10^{14}$ ions cm^{-2} when the irradiation is carried out using a low flux (corresponding to a current density of 20 nA cm^{-2}). But mixing is found for higher flux irradiations (corresponding to a current density of 2.0 μA cm^{-2}) [13]. We have also shown about the possibility of surface alloying for nano Au-Ge systems [14].

Experimental

For the work reported here, Au films of about 1.95 nm and 4.7 nm thickness, Ag films of 2.3 nm thickness were deposited at room temperature by thermal evaporation under high-vacuum conditions ($\approx 5 \times 10^{-5}$ mbar) onto Si(100) substrates. For the case of nanomixing of AuGe nanoalloy, a 1.0 nm thick Ge and subsequently 1.0 nm thick Au was deposited on silicon substrate. A ≈ 2.1 nm thick native oxide layer was present on the substrate surface prior to these depositions. The irradiation has been carried out with 1.5 MeV Au^{2+} ions (at Ion Beam Laboratory, Institute of Physics, Bhubaneswar) at various impact angles and a raster scanning has been used for uniform irradiation. High flux irradiations were carried out using the 1.7 MV accelerator at IGCAR, Kalpakkam. The Rutherford backscattering spectrometry measurements were carried out with 2.0 He^{2+} ions using the 3.0 MV tandem accelerator facility and TEM measurements were carried out with JEOL 2010 (UHR) electron microscope, both available at Institute of Physics, Bhubaneswar.

Results and Discussions

Fabrication of Nanostructures

Energetic ion beams have been in use for variety of nanostructures (particles, clusters). One among them is the use of ion implantation, known as ion beam synthesis. Figure 1 (a) and (b) schematically depicts the use of ion implantation process for nanostructure fabrication. In Figure 1(a), ion beams of energy, typically few tens to hundreds of keV, are used to implant in the materials of interest. The projected range of the ions (or where majority of implanted ions stay) varies with energy (sub-nanometers to thousands of nanometers) and depends on the mass of the projectile and mass and crystalline quality of the target. At high fluence, the implanted region is transferred into a highly supersaturated, far-from-equilibrium state. The nanostructure formation happens by phase separation, where self-organization may occur [4]. After annealing at high enough temperature (implantation followed by annealing – a process known as ion beam synthesis), depending on the system, can obtain buried nanostructured thin films. For examples, cobalt ions of 200 keV ions implanted
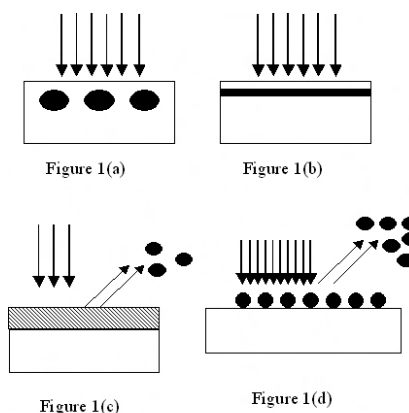

Fig. 1   *Schematic representation of nanostructure fabrication using energetic ion beams: (a) Use of ion implantation to form nanostructures at their projected ranges (b) Ion beam synthesis – making buried epitaxial layer by two step process: implantation followed by annealing (c) Nano-particles (clusters) ejected from continuous, uniform thin films (d) Sputter particles ejection from nano-disperse (non – uniform) films on a substrate.*

into silicon at a fluence of $\approx 1 \times 10^{17}$ ions cm^{-2}, followed by two step annealing process yield few tens of nm thick epitaxial $CoSi_2$ buried layer [5].

Another method of fabricating the nanostructures is by sputtering process. Sputtering phenomena is basically particle ejection from a target due to an energetic ion/atom bombardment. The sputtering yield is defined as the number atoms ejected per one impinging ion. Figure.1(c) and (d) show schematic representation of the sputtering from uniform and non-uniform thin films. Sputtering from isolated islands corresponds to non-uniform thin film case and continuous and thick film case corresponds to uniform film case. The particle size, size distribution, areal coverage and other structural aspects are determined using transmission electron microscopy measurements (high resolution TEM). The sputtering yield is determined by using the Rutherford backscattering spectrometry method. Figure 2(a) and (b) shows bright field planar TEM micrographs for (a) as-deposited 1.95 nm thick Au film on silicon

Figure 2 (a)

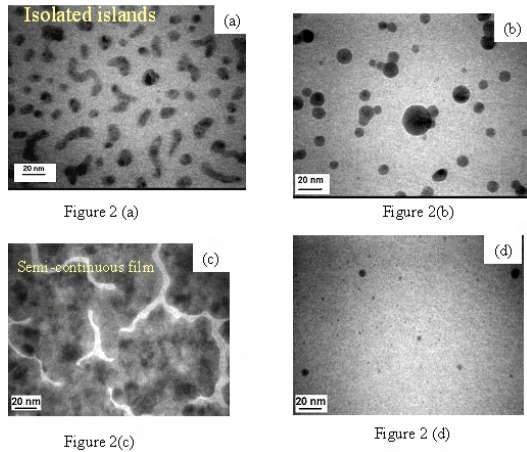Figure 2(b)

Figure 2(c)

Figure 2 (d)

Fig. 2   TEM micrographs for (a) as-deposited 1.95 nm thick Au film on silicon substrate (sample A) (b) as-deposited 4.5 nm thick Au film on silicon substrate (sample B) (c) sputtered particles collected from sample A, irradiated with 1.5 MeV Au ions to a fluence of 1×10^{14} ions cm^{-2} (d) sputtered particles collected from sample B, irradiated with 1.5 MeV Au ions to a fluence of 1×10^{14} ions cm^{-2} [8].

Figure 3 (a)
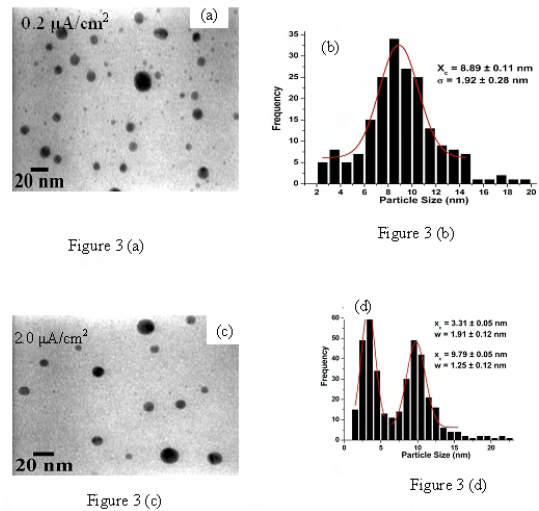
Figure 3 (b)

Figure 3 (c)

Figure 3 (d)

Fig. 3   Schematic representation of ion beam induced nanoscale mixing: (a) As-deposited nanostructures (B) on substrate A. (b) After ion irradiation at appropriate conditions (energy, flux, fluence and impact angle) nanalloy is formed at sub-surface with a composition: A_mB_n. (c) As-deposited two types (B and C) of nanostructures on substrate A (d) After ion irradiation nanoalloy B_mC_n formed on the surface.

substrate (sample A) and (b) as-deposited 4.7 nm thick Au film on silicon substrate (sample B). The effective thickness has been determined using RBS measurements by taking bulk density of Au into consideration. Figures 2(c) and (d) shown sputtered particles collected from sample A and sample B, irradiated with 1.5 MeV Au ions to a fluence of 1×10^{14} ions cm^{-2}, respectively. The average sputtered particle size corresponding to the 1.95 thick film is 12.3 ± 0.1 nm (from Fig. 2(c)) with normalized island coverage on the catcher foil being ≈19%. For a target that was more uniform and continuous (schematic Fig. 1(c) and TEM micrograph Fig. 2(b)), under similar condition as above, the average sputtered [article size corresponding to the 4.5 nm thick film is 2.3 ± 0.1 nm (from Fig. 2(d)) and the normalized island coverage on the catcher foil was ≈ 4%. For much higher thickness of Au (21.4 nm thick), the average sputtered particle size is 2.95 ± 0.1 nm with the normalized island coverage on the catcher foil being 1%. These results show that the average sputtered

particle size obtained from the ion bombardment of isolated – nanoislands if found to be much larger for continuous films. More details can be obtained from the reference [8].

Figures 3(a) and (c) shows the TEM micrograph of sputtered Au particles collected on catcher grid at fluxes of 0.2 and 2.0 μA cm^{-2} at a fluence of 1×10^{15} ions cm^{-2}, respectively. Fig (b) and (d) are the corresponding size distribution of sample (a) and (c) respectively. The average particle size was found to be 8.9 ± 1.9 nm for low flux irradiation conditions (0.02 μA cm^{-2}) and 3.3 ± 1.9 nm and 9.8 ± 1.3 nm under high flux (2.0 μA cm^{-2}) irradiation conditions. Interestingly, a bimodal distribution has been found in case of irradiation with 2.0 $\mu A.cm^{-2}$ (Fig 3(d)). At lower fluences, but with high flux, the sputtered particle size found to be more (data not shown). This is because the sputter particle size
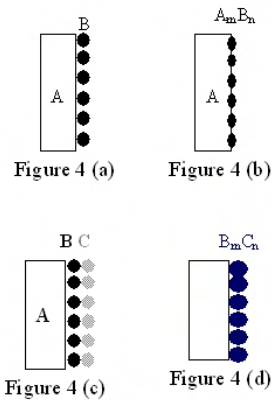
Figure 4 (a)   Figure 4 (b)

Figure 4 (c)   Figure 4 (d)

Figure 5 (a)   Figure 5 (b)

Figure 5 (c)   Figure 5 (d)

Fig. 4 *Schematic representation of ion beam induced nanoscale mixing: (a) As-deposited nanostructures (B) on substrate A. (b) After ion irradiation at appropriate conditions (energy, flux, fluence and impact angle) nanalloy is formed at sub-surface with a composition: A_mB_n. (c) As-deposited two types (B and C) of nanostructures on substrate A (d) After ion irradiation nanoalloy B_mC_n formed on the surface.*

Fig. 5 *The cross-section TEM bright field image of (a) as-deposited Au nanostructures (b) crater in irradiated film at fluence 114 ion cm^{-2} at 60 (c) The planar TEM micrograph of similar system shown in (b) and (d) AFM measurements on the specimen irradiated with 51014 ion cm^{-2} [6,7].*

depends on the substrate conditions. It is to be noted that the width of the distribution is minimum in case of irradiation with 0.2 µA.cm^{-2} [13]. As per the present understanding, for thick films, the sputtering phenomena depends on nuclear energy loss, i.e., at low energies (few tens of keV). Our results show interestingly a reverse effect for the case of sputtering from the nanostructures: the sputtering yield is found to more for 100 MeV Au ions compared to 1.5 MeV and 32 keV Au ions. The sputtering yield (Y) is found to be in the following ratio [15]:

(Y at 32.0 keV): (Y at 1.5 MeV) : (Y at 100 MeV) = 1.0 : 2.1 : 2.4

Energy spike and its distribution in the nanoislands are proposed to be the main reason for the variation in the particle size and the coverage of the sputtered particles on the catcher grid.

Nano-scale Modifications: Crater formation, Embedding and Mixing phenomena:

Energetic ion beam induced modifications in nanostructures is explained by a schematic diagram in Figure 4. The Fig. 4(a) shows a schematic of isolated nanostructures being deposited on substrate A. In our case, silicon substrate was used and Au nanostructures are grown using vacuum deposition method. After irradiating with 1.5 MeV, it is found the sub-surface gold silicide is formed (Fig. 4(b). Figure 4(c) shows presence of two types of nanostructures as -deposited (type B and C). After irradiation, we observed formation of B_mC_n type of nanoalloys on the surface (Fig. 4(d)). To elucidate on these kind of studies, we have observed sub-surface gold silicide (of nano-dimension) in one case [9,10] and AuGe nano-alloy in surface nanomixing cases [14]. For a thin film of thickness ≈ 2 nm thick gold on silicon substrate, isolated nanoisland structures of gold would be formed. Upon irradiation with 1.5 MeV Au^{2+} ions, two types of craters are observed on the Au islands: empty craters and craters with a central hillock (Figure 5(b) – (d)). The contribution of plastic flow, pressure spike, and sputtering to the
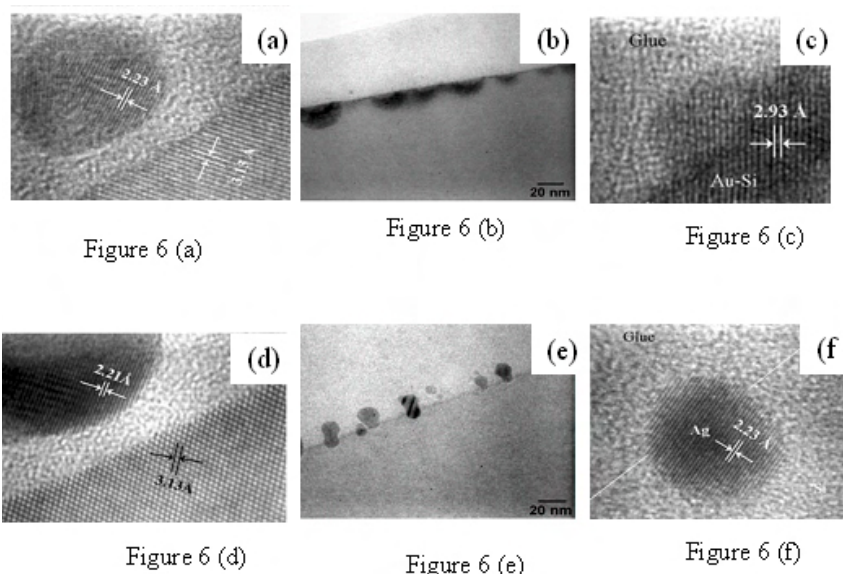
Figure 6 (a)   Figure 6 (b)   Figure 6 (c)

Figure 6 (d)   Figure 6 (e)   Figure 6 (f)

Fig. 6   Cross-section TEM micrographs – nano gold silicide formation due to ion irradiation effects: (a) high resolution TEM image (HRTEM) for as –deposited nanoisland of Au on silicon (b) ion irradiated system (c) HRTEM showing AuSi formation; Cross-section TEM micrographs – nano silver islands embedding due to ion irradiation: (a) high resolution TEM image (HRTEM) for as –deposited nanoisland of Ag on silicon (b) ion irradiated system showing embedding (c) HRTEM showing the embedded part to be of Ag [10].

crater formation during the ion impacts on the gold islands is analyzed. It was also proposed that the energy of the incident ion gets confined in some form due to presence of different surrounding matrix (like for Au on silicon, the surrounding matrix is silicon) [6]. Crater formation has been studied as a function of impact angle at a fluence of 1×10^{14} ions cm^{-2} and found that crater formation is prominent at high impact angles (i.e. at glancing angle geometry) (Figure 5(d)) [8]. At a fluence of 1×10^{14} ions cm^{-2}, a material push-in effect and a metastable Au-Si phase formation have been observed for Au nanoislands, while no push-in effect (similar to burrowing) or mixing has been observed for the case of continuous films (Figures 6(a – f)). The mixed phase of Au-Si system is found to be crystalline in nature (Figure 6(c)). The material push-in and ion beam mixing effects that are observed for the nanoislands, are appeared to be due to combined effect of capillary force, ion-induced viscous flow and ion-induced energy spike effects. MeV Au ion induced mixing at nanoscale regime for Au and Ag nanoislands with

silicon substrate show a metastable mixed phae for Au-Si system at a fluence of 1×10^{14} ions cm^{-2}, while no mixed phase is formed for the Ag-Si system (Figures 6(d – f)), but the Au-Si and Ag-Si systems, a push-in effect was observed (Figure 6b, 6e). The high eutectic temperature, higher heat of mixing and low surface energy of Ag-Si system compared to Au-Si system could be responsible for the lack of mixing in Ag-Si system [9, 10]. In related studies, MeV-ion induced changes in specified Au-nanoislands on silicon substrate are tracked as a function of ion fluence using ex-situ TEM [11]. Strain induced in the bulk silicon substrate surface due to 1.5 MeV Au^{2+} and C^{2+} ion beam irradiation is determined by using HRTEM and asymmetric Bragg x-ray rocking curve methods [12].

The synthesis of nano-dimensional Au-Ge alloy on Si surface by ion beam mixing of nanoisalnds of Au and Ge that are grown by UHV electron beam evaporation technique is carried out. The Au and Ge nanoislands were irradiated by 1.5 MeV Au^{2+} ions over a fluence range of 5×10^{12} –

1×10^{15} ions cm^{-2}. HRTEM has been employed to study the formation of Au-Ge alloy in the form of nanoisalnds. The causes for the formation of such surface alloy have been discussed in the light of ion-matter interaction in nanometer scale regime [14].

Conclusions

Energetic ion beams found to show interesting observations for the case of ion – nanostructure compared to ion – bulk solid systems. A large sputtering, enhanced crater formation, nanoscale embedding and nanoscale mixing are observed for the nanostructured thin films case while this being absent in uniform films at lower flux irradiations. The energy confinement effects are invoked to understand the ion induced effects in nanostructures

Acknowledgements

References

1. M. Nastasi and J. W. Mayer, Ion implantation and synthesis of materials, Springer-Verlag, 2006 and references there in.

2. T. van Dillen, A. Polman, W. Fukarek, and A. van Blaaderen, App. Phys. Lett. **78** (2001) 910.

3. Y. Zhong, Y. Ashkenazy, K. Albe and R. S. Averback, J. Appl. Phys. **94** (2003) 4432.

4. K. –H. Heining, T. Muller, B. Schmidt, M. Strobel amd W. Moller, Appl. Phys. A: Mater. Sci. Process. **A77** (2003) 17.

5. S. Mantl, Mater. Sci. Rep. **8** (1992) 1.

6. P. V. Satyam, J. Kamila, S. Mohapatra, B. Satpati, D. K. Goswami, B. N. Dev, R. E. Cook, L. Assoufid, J. Wang and N. C. Mishra, J. App. Phys., **93** (2003) 6399.

7. B. Satpati, D. K. Goswami, U. D. Vaishnav, T. Som, B. N. Dev, and P. V. Satyam, Nucl. Instr. Meth. Phys. Res. **B212** (2003) 157.

8. B. Satpati, D. K. Goswami, S. Roy, T. Som, B. N. Dev and P. V. Satyam, Nucl. Instr. Meth. Phys. Res. **B212** (2003) 332.

9. B. Satpati, P.V. Satyam, T. Som and B.N. Dev, J. Appl. Phys **96** (2004) 5212.

10. B. Satpati, P.V. Satyam, T. Som, and B.N. Dev, Appl. Phys. **A79** (2004) 447.

11. J. Ghatak, B. Satpati, M. Umananda, D. Kabiraj, T. Som, B. N. Dev, K. Akimoto, K. Ito, T. Emoto, and P.V. Satyam, Nucl. Instr. and Meth. **B244** (2006) 45.

12. J. Ghatak, B. Satpati, M. Umananda, P. V. Satyam, K. Akimoto, K. Ito, T. Emoto, Nucl. Instr. and Meth. **B244** (2006) 64.

13. J. Ghatak, B. Sundaravel, K. G. M. Nair, and P. V. Satyam, J. Nanoscience and Nanotechnology (2007) (submitted).

14. T. Som, B. Satpati, P.V. Satyam, and D. Kabiraj, J. Appl. Phys. **97** (2005) 014305.

15. B. Satpati, J. Ghatak, B. Joseph, T. Som, D. Kabiraj, B. N. Dev and P. V. Satyam, Nucl. Instr. and Meth. **B244** (2006) 278.

Growth of Various Semiconductor Nanostructures by Physical Vapour Deposition and their Application as Gas Sensor

Dr. Manmeet Kaur received her PhD from Devi Ahilya Vishwavidyalaya, Indore in 1998. Her thesis work involved effect of heavy ion irradiation on high temperature superconductors. She joined Bhabha Atomic Research Centre, Mumbai in 1999 as Dr. K.S. Krishnan Research associate and is presently working as Scientific Officer. Her present interests include development of metal oxide thin films and nano-materials for sensing toxic gases.

Dr. Shahswati Sen joined BARC in 1996 through 40th batch of training school. She obtained her PhD degree from Mumbai university in 2003 for her work on "Dissipation mechanism in high temperature superconductors". Currently she is working on gas sensors based on elemental and metal oxide semiconductor thin films and nano structures.

Abstract

We have studied growth and gas sensing properties of nanostructures of various semiconductor material - Nanowires and nanotubes of Tellurium, nanobelts and nanowires of SnO_2, nanowires of CuO, nanowires and nanotetrapods of ZnO, and nanowires and bipyramids of In_2O_3 grown by thermal evaporation in a tubular furnance under a flow of a carrier gas. The starting material heated to a high temperature vaporizes and condenses at lower temperature in form of nanostructure. These structures are characterized by X-ray diffraction, X-ray photoelectron spectroscopy, Scanning electron microscopy, Transmission electron microscopy, Selected area electron diffraction, UV-visible spectroscopy and Photoluminescence. Technological application of these nanostructured materials were investigated by employing them for the detection of different toxic gases and many of these were found to be very effective in detection at low concentrations of toxic gas at room temperatures.

Introduction

The word nano has been assigned to indicate the number 10^{-9} – one billionth of any unit. Widely accepted threshold for a material to be termed as nano is that its dimensions should be less than 100 nm in at least one dimension. Ideally nanostructures are defined as those structures whose size is comparable to the de Broglie wavelength of the carriers. With the reduction in size, the structural features of the matter lies between bulk macroscopic material and that of isolated atoms giving rise to number of interesting properties due to increased surface to volume ratio and resultant discrete electronic states. With reduction in size, novel electrical, mechanical, chemical and optical properties are introduced, which are largely believed to be the result of surface and quantum confinement effects.

With the discovery of carbon nanotubes by Iijima [1] in 1991 tremendous research activities have been directed towards the synthesis,

Dr. Manmeet Kaur and Dr. Shahswati Sen, Technical Physics and Prototype Engineering Division, Bhabha Atomic Research Center, Mumbai 400 085; E-mail: manmeet@barc.gov.in

characterization and application of various one-dimensional (1-D) nanostructures. These have been the focus of extensive studies worldwide since they can be exploited for both - wiring and as nanoscale electronic devices. They have been found to be suitable candidates for future nanoscale, optoelectronics and sensing devices. Metal oxide semiconductors are one of the prominent materials whose nanostructures have been synthesized and investigated for various applications [2]. They have been assembled into nanometer scale light emitting diodes, p-n diodes, FETS, bipolar junction transistors, complementary inverters. Nanowires (1D nanocrystals with large length/diameter ratio) and nanorods of various semiconducting materials including Si, Ge, GaN, ZnO, SnO2 etc. have been synthesized for different potential applications.

ZnO, SnO_2 and In_2O_3 are n-type wide band gap (>3 eV) metal oxide semiconductors with wide applications in optoelectronic devices, transparent conductors and gas sensors. They are widely used for the detection of oxidizing and reducing gases like H_2S, CO and others. CuO is a p-type semiconductor with a narrow band gap that has been a candidate material for photothermal, photoconductive applications, it is used in fabrication of lithium–copper oxide electrochemical cells and widely used in catalysis. Though there are a few reports on gas sensing properties of CuO alone, being a p-type semiconductor it is mainly used as an additive to n-type materials to enhance sensitivity by formation of p-n junctions. Tellurium is an elemental semiconductor with energy gap of 0.34 eV. It shows p-type conduction due to lattice defects acting as acceptors. It exhibits a spectrum of interesting properties such as photoconductivity, thermoelectric effect, catalytic activity and strong peizo-electric effect and has been used in devices such as optical recording medium, thin film transistors, strain sensitive devices, infrared detectors and as gas sensors.

Several synthetic strategies have been developed for 1D nanowires which include (i) use of the anisotropic crystallographic structure of the solid to facilitate 1D growth (ii) introduction of solid-liquid interface (iii) use of templates with 1D morphology to direct the formation of nanostructure (iv) supersaturation control to modify the growth

habit of a seed (v) use of capping agents to kinetically control the growth rates of the various facets of a seed and (vi) self assembly of zero dimensional (0D) nanostructures. These methods can be broadly categorized into two – solution-based growth and vapor phase growth.

Solution-Based Growth

Solution routes include hydrothermal, solvothermal, template based synthesis and sol-gel technique. The hydrothermal route has been used to synthesize nanotubes and related structures of various inorganic materials – e.g. SiO_2, V_2O_5, ZnO. In Solvothermal method a solvent is mixed with certain metal precursors and crystal growth regulating or templating agents such as amines. The solution growth mixture is then placed in an autoclave to carry out crystal growth process. In template based methods, a template is used which serves as a scaffold against which other materials with similar morphologies are synthesized. Sol-gel chemistry is widely used in synthesis of metal oxide nanotubes such as silica and TiO_2. Since we have not used these method to grow nanostructures, we will not discuss these processes in detail.

Vapor Phase Growth

Vapor deposition includes various growth modes such as chemical vapor deposition, precursor decomposition and carbothermal methods.

(i) *Vapor-solid growth:* In this process evaporation, chemical reduction or gaseous reduction generates the vapor. The vapor is subsequently transported and condensed onto substrate. Nanowires of several metal oxides have been grown by this methods.

(ii) *Vapor-liquid-solid growth*: In this process growth of nanowire takes place via a gas phase reaction involving the Vapor-liquid-solid process. Growth of nanowire by this method is assisted by presence of metal clusters (e.g. Gold, Indium, Nickel, Copper etc). The metal clusters form a liquid alloy with the incoming vapors of material to be deposited, when the temperature is higher than the eutectic point. The liquid surface has a large accommodation coefficient and is, therefore a preferred deposition site for the incoming vapor. After

the liquid alloy becomes saturated with the incoming vapor, precipitation of incoming vapor material results in the growth of nanowire. This method provides an efficient means to obtain uniform sized nanowires, since the diameter of nanowires is determined by the diameter of the catalyst particles.

(iii) *Carbothermal method*: In this method mixture of metal oxide and carbon (either activated carbon, graphite or carbon nanotubes) is used. Carbon reacts with the oxide to produce sub-oxide or metal vapors which react with oxygen to produce desired metal oxide nanowires. Carbothermal reaction generally involves following steps.

Metal oxide + C ⇒ metal suboxide + CO

Metal suboxide+O_2⇒ metal oxide nanowires

In this article we discuss synthesis of nanostructures of various metal oxide semiconductors like ZnO [3], CuO [4], In_2O_3 [5] and SnO_2 and an elemental semiconductor Tellurium [6] by vapor phase growth. Nanowires of all these materials grow by vapor-solid route. Nanowires of ZnO and SnO_2 have also been grown by carbothermal method. Further, we have investigated these nanowires/ nanotubes for gas sensor application.

Experimental

Growth of nanostructures of different materials was carried out in a tubular horizontal furnace in presence of a carrier gas. The temperature, rate of flow of gas and the nature of gas was different for different materials.

Growth of nanowires and nanotubes was carried out in a quartz tube at atmospheric pressure under argon gas flow of 50 to 500 cc/min. In case of oxides 50cc/min oxygen was used in addition to Argon gas. High purity (99.99%) metal chunks or metal oxide powders or mixture of metal oxide and grapite powder were loaded in an alumina boat and placed in a 1 m long quartz tube located in a furnace. The source was placed in the hot zone of the furnace and its temperature was measured using a thermocouple kept in the vicinity of the alumina boat. The quartz tube is long enough to produce different temperature zones of reasonable size along

its length. The furnace temperature was increased in the presence of gas flow and maintained at a desired temperature (between 200°C to 1000°C) for 2 hours. After that it was cooled to room temperature.

To grow Te nanorods and nanotubes, we have also carried out thermal deposition of Te on various substrates in a vacuum chamber. For this Te powder was loaded in a molybdenum boat and the deposition chamber was evacuated to $5x\ 10^{-6}$ mbar. During deposition, the substrate temperature was maintained at 100ºC. The deposition was carried at a rate of 1 Å/Second controlled by a quartz crystal thickness monitor. The thickness of these films was 2000 Å.

The nanostructures so obtained were characterized by various techniques. Their morphology was studied using a scanning electron microscope (SEM) VEGA MV2300T/40 (TS 5130 MM TESCAN). The Chemical composition was confirmed by recording Energy Dispersive X-ray analysis (EDX) analysis, while their structural information was obtained using an X-ray diffractometer employing a Cu K$_ά$ radiation source. X-ray photoelectron spectra (XPS) were recorded using Mg-K (1253.6 eV) source in a XPS system (RIBERCX700) comprising of a twin anode X-ray source and a MAC-2 electron analyzer. The binding energy scale was calibrated to C-1s line at 285 eV. The morphology of the nanowires was also observed by transmission electron microscopy (TEM) carried out using a JEOL 2000 FX electron micrscope. The Band gap was calculated from absorption spectra recorded in a UV-Vis spectrophotometer (Chemito model spectroscan UV 2600). Room temperature photoluminescence measurements were carried out with a Hitachi F4010 spectrometer using a xenon arc lamp for excitation. Raman spectra were recorded in a back scattering geometry with a spectral resolution of 2 cm^{-1}. The 514.5 nm line of an Ar$^+$ laser was used for excitation. The Raman scattered light was analyzed using an optically aligned triple monochromator Raman spectrometer (Dilor-XY).

The substrates with pre-deposited contacts were placed at desired locations in the quartz tube during thermal evaporation of some nanostructures. For gas sensitivity measurements, wires were attached to these thick film contact pads.

For investigation of the gas sensitivity of SnO_2 and In_2O_3, the nanostructures were dispersed in methanol to make a thick paste. This paste was applied on a substrate between two gold electrode. The sensitivity measurements were carried out in a system described elsewhere [7].

Results and Discussion

Tellurium

In case of growth of Te nanostructures by furnace route, structures observed at different source and deposition temperatures are summarized in Table 1. These are discussed in the next section followed by discussion of growth mechanism.

Source temp.	Deposition temp.	Microstructure
430°C	430°C	nanowires
550°C	400-350°C	Micro rods
550°C	200°C	Radial nanotubes
550°C	30-50°C	Nanotubes

At furnace temperature between 200 to 400°C no significant change was observed on the Te chunk. At a temperature of 430°C that is slightly below the melting point of Te (~ 452°C), we observed gray colored wool like growth on the surface of the Te chunks (Ar flow of 50 cc/min). SEM micrographs revealed them to be dense growth of nanowires as shown in Fig. 1. Each of the needle like wires is seen to grow on the surface of the Te chunk from a liquid droplet like sphere of Te. The diameter of these wires is maximum at the base and reduces with increase in length. Typical diameter is 150-200 nm at the base and 50-70 nm at tip with length of wires being few tens of micron. The EDX spectra indicate them to be of pure Te phase. The density of these nanowires was found to be larger on the rough surface of the chunk as compared to that on smooth surface.

At source temperature of 550°C, Te was found to evaporate and deposit along the quartz tube with the microstructure of the deposited tellurium dependent on the gas flow rate as well as the local temperature. At temperature (T) of ~200°C, we
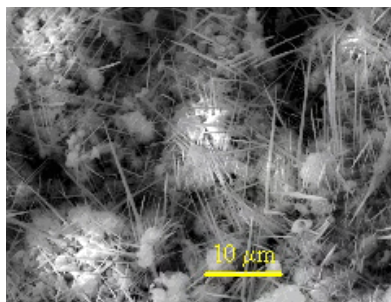
Fig. 1   SEM of Te nanowires grown on source material at 430°C.
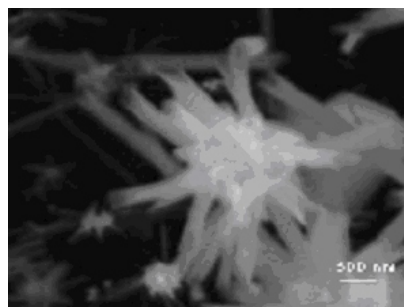
Fig. 2   SEM of Te nanotubes growing radially from Te sphere at T~ 200°C

obtained a black colour deposit on the walls of the quartz tube as well as on different substrates. SEM photograph indicate that the deposited material consists of micon size Te spheres with Te nanotubes growing radially out as shown in Fig. 2. The Te spheres have a diameter between 0.5 to 2 μm while the nanotubes have diameter in the range of 100-200 nm and length upto 1 μm. The Te spheres show small droplet like structure on one end, which seem to be the nucleation site for the growth of the nanotubes. All the tubes show splitting at the ends forming prongs [8]. Xi et al has reported a similar kind of structure as the intermediate product in growth of Te nano-tubes by hydrothermal process. [9].

At the room temperature (30-50°C), black-grey deposit on substrates and walls of the quartz tube consisted of large number of nano tubes dispersed in a matrix of Te spheres shown in Fig 3. These tubes have hexagonal cross section, outer diameter around 150-500 nm and length ~2 μm. TEM picture in Fig. 3 shows tubes with wall
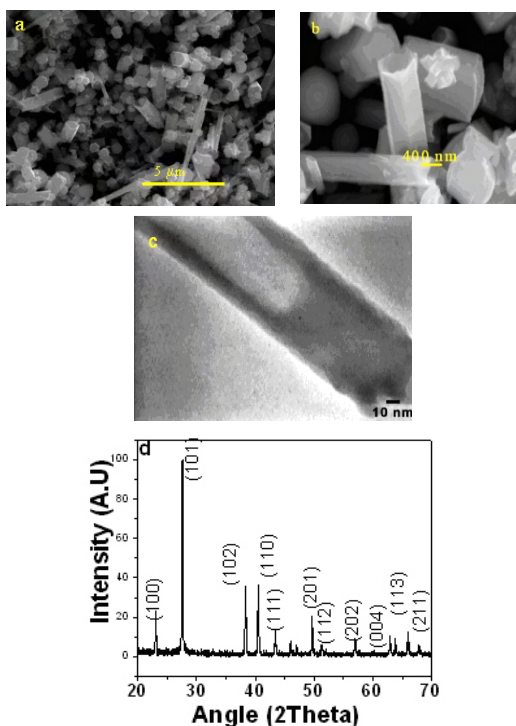
Fig. 3 (a) SEM image (b) SEM at higher magnification, (c) TEM and (d) XRD of nanotubes of Te dispersed in a matrix of Te spheres deposited at T~ 30-50°C

thickness of 10 nm and diameter of 100 nm and that the growth of nanotube originates as Te nanorod. The XRD spectra of these nanotubes in Fig. 3(d) shows trigonal phase of Te. This confirms the crystalline nature of the nano-tubes and that the spherical particles are also nano-crystalline trigonal phase of Te. Although we have not directly identified growth direction for nanotubes, their hexagonal cross section and comparison with earlier studies indicates that these grow along c-axis [10,11].

On further increasing the temperature of the furnace, the size and number of the microrods decreases in the high temperature zone and at lower temperature we get deposition of clusters of Te nanosize particles (spheres). Growth of nanotube is not observed in this case and also in the case of increased gas flow rate to 200 cc/min and above.

The growth of nanowires when the temperature of the furnace is slightly less than melting point (430°C) may be explained by nucleation of Tellurium droplets at the substrate. The droplets form as a result of high vapour pressure of tellurium whereby there is continuous evaporation and condensation of molecules on the surface. Initial formation of these droplets is favored due to low surface area of spherical particle. Due to continuous adsorption and desorption process and because of anisotropic crystal structure of Te, growth along the c-axis is kinetically favored. Growth rate along [001] direction is faster to favor the stronger bond in this direction as compared to that along [010] and [100] directions [10].

Growth at lower temperatures is also initiated by formation of nearly spherical nuclei and growth of nanowires from these nuclei. However due to reduced Te flux and lower vapor pressure, availability of Te atoms for growth reduces. This leads to growth of nanotubes due to gradient of Te flux along the diameter of the tubes [9]. Continuous flux of Te atoms from evaporation source as well as diffusion along the circumference yield lower availability of Te in the central part of tubes. Our studies indicate that the growth of nanotubes occurs in three steps; (a) nucleation of spherical particles from Te vapours, (b) growth of nanorods by condensation of additional Te atoms from source and recrystallization from the spherical nuclei and (c) conversion of nanorods to nanotubes when the flux of atoms from the source is low.

For the fabrication of devices it is required to have nanowires or tubes in the form of film. However it is quite difficult to make a film of the Te nanowires and tubes synthesized in tubular furnace. Also the adherence of material deposited in furnace (on different substrates) was found to be poor. To grow nanorods and nanotubes in the form of thin films we have carried out vacuum deposition of Te on various substrates. For this Te powder was loaded in a molybdenum boat and the deposition chamber was evacuated to 5×10^{-6} mbar. The substrate temperature was maintained at 100ºC using a temperature controller. The depositions were carried at a rate of 1 Å/Second and were controlled by a quartz crystal thickness monitor. The thickness of these films was 2000 Å. Figure 4 shows the
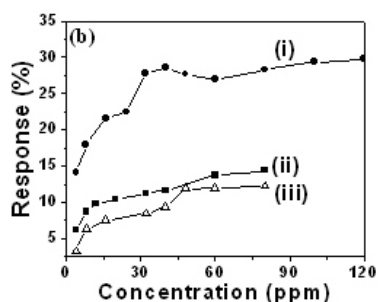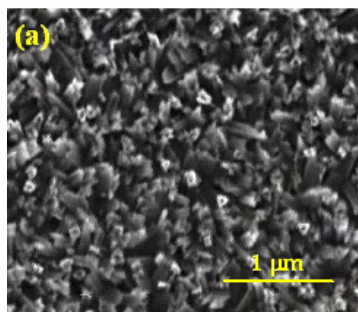
Fig. 4 (a) SEM of Te nanotubes grown on Si (111) and (b) Sensitivity of different Te microstructures for H_2S gas (i) Te nanotubes deposited on Si(111) in vacuum system (ii) Te single micro rod grown in tubular furnace, (iii) thick film consisting of Te nanotubes grown in tubular furnace.

microstructure of Te film deposited on Si(111). We observe the growth of oriented nanotubes with 150 nm dia and c-axis perpendicular to the substrate plane.

In case of Te deposition on alumina substrate in vacuum furnace it has been reported that deposition at high substrate temperature (~100°C) leads to the growth of crystalline thin film with dendrite shape grains. In case of Si (111) substrate it is known that $3a_{surface}Si(111) \sim 2a_{bulk}Te$ (where $a_{surface}$ and a_{bulk} are lattice parameters on surface of silicon and bulk crystalline Te) with a mismatch of only 0.9%. This leads to preferential nucleation of Te (001) parallel to Si(111) [11]. The Te adatoms continue to attach themselves to the energetically favorable edge sites thus leading to the formation of oriented hollow tubes.

These nanostructures of Te were investigated for their sensitivity towards H_2S gas at room temperature. Sensitivity is defined as

$$S(\%) = [|R_g-R_a|/R_a] \times 100$$

Where R_a is the resistance in air and R_g is the resistance in gas. It can be observed that the sensitivity of oriented nanotubes on Si(111) substrate is the largest. This can be attributed to the larger surface area exposed in case of Te nanotubes grown on Si(111) substrate.

SnO_2

The SEM micrograph of white wooly powder of SnO_2 nanostructures grown at 900°C and Ar gas flow of 850 cc/min are shown in figure 5(a). It is observed that it consists of both nanobelts and nanorods with the number of nanobelts higher than the number of nanorods. The nanobelts have a width of around 400 nm, thickness ~ 70-100 nm and length of few μm. The nanorods have with diameter of around 150 nm and length of few μm. With increase in deposition temperature we observe larger number of nanobelts with larger size and the number of nanorods decreases. The XRD spectra of the sample shown in figure 5(b) can be indexed to the tetragonal phase of SnO_2 crystal (normal rutile phase) with a = 4.737 Å and c = 3.188Å [12]. In case when Cu was added to the Sn powder we have not noticed any change in the morphology of the nanowires/nanobelts. The growth of these SnO_2 nanostructures without use of any catalyst can be explained by VS (vapour-solid) mechanism [13]. Under the high temperature of 900°C the source material i.e. Sn powder evaporates. The residual oxygen present in the system oxidize Sn vapours to SnO_2. Since the temperature of the furnace is less than melting point of SnO_2 (1127°C) it condensed and form a seed crystal. This acts as nucleation center and facilitates the growth along specific direction to minimize the surface energy.

The gas sensitivity of the thick film made from the nanobelts and nanowires (for H_2S) was measured at different temperatures and the results are shown in Fig. 6. The sensitivity in this case has been measured as R_g/R_a. In case of thick film from pure SnO_2 we obtain a sensitivity of 1.5 times at ~70 ppm at room temperature and 3.5 times at 145°C. Whereas in case
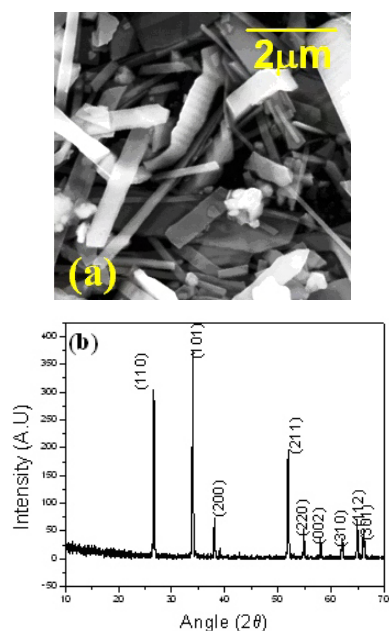
Fig. 5   (a) SEM image and (b) XRD spectra of SnO$_2$ nanowires and nanobelts.

of thick film made from sample made from Sn:Cu mixture we get 10 times more gain than pure Sn powder. Thus doping of Cu is found to enhance the sensitivity and these can be employed for detection of H$_2$S gas at low temperature.

CuO

CuO nanowires have been synthesized by thermal oxidation of copper foils in oxygen atmosphere carried out in a resistively heated furnace at different temperatures (between 400 to 800°C) and times. Nanowires synthesized by this method are always found to grow perpendicular to the surface of copper foil.

Optimum growth of nanowire was observed at 675°C. SEM micrographs of nanowires prepared at 675°C for different times of 15 mins and 22 hrs are shown in Fig. 7. The growth of these nanowires was preceded by the formation of a hill and valley structure (Figure 7a) [14]. SEM of base region of nanowires is shown in Fig. 8a. From these micrographs we observe the following:
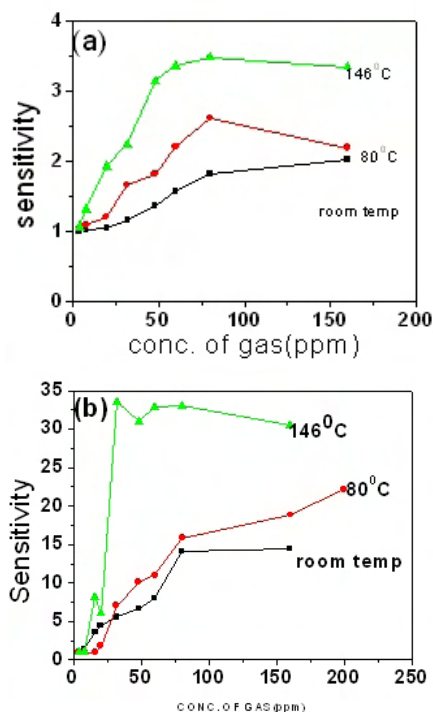
Fig. 6   Sensitivity of thick film of SnO$_2$ nanowires/nanobelts for H$_2$S gas at different temperatures, (a) pure SnO$_2$ and (b) Cu doped SnO$_2$.
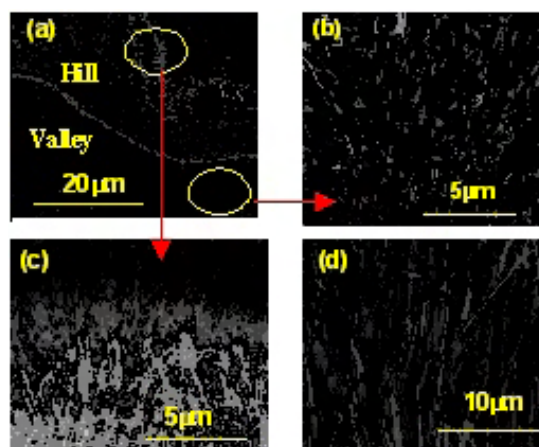
Fig. 7   SEM images of CuO nanowires grown at 675°C for 15 mins (a) hill and valley structure, (b) nanowires in valley and (c) nanowires in hill. Fig (d) shows nanowires after oxidation of copper strip for 22 h.
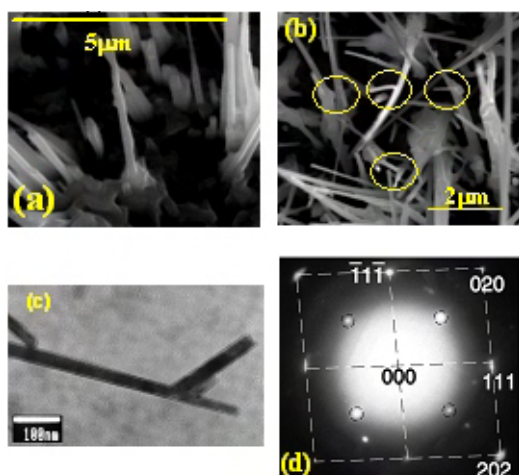
Fig. 8   (a) SEM micrographs of base of nanowires grown at 675°C for 15 mins. Growth of wires from larger crystallites is clearly observed. (b) SEM of branched nanowires. (c) TEM image of branching in a single nanowires and (d) SAD pattern corresponding to the [10$\bar{1}$] zone axis.

1.   Nanowires grow in both hills and valleys formed during initial stage of nanowire growth.

2.   Nanowires in hills are thinner (50–100 nm) and longer (7-15 μm) and those in valleys are thicker (100-200 nm) and shorter (1-4 μm).

3.   The length of nanowires increases with annealing time and for 22 hrs, wires of more than 20 m length were obtained.

4.   In addition to large hill and valley structure as seen in Fig. 7a, copper is structured with crystallites on scale of less than 1 μm (see Fig. 8). Nanowires grow from these small crystallites. The diameter of wires is maximum at the base and reduces as they grow.

Wires grown for times longer than 1.5 hrs at 675°C showed branching as is seen in SEM and TEM micrographs of Fig. 8. Microstructure of nanowires was studied by transmitted selected area electron diffraction (SAD) obtained using TEM system. A SAD pattern corresponding to the [10$\bar{1}$] zone axis is shown in Fig. 8 (d). SAD confirms that the nanowires are of CuO. Some extra reflections,
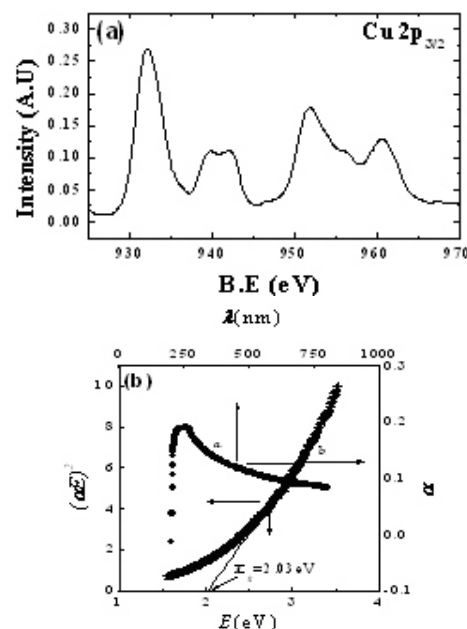

Fig. 9   (a) XPS spectra of nanowires in Cu $_{2p}$ region showing formation of CuO and (b) optical absorption spectra and plot of $(\alpha E)^2$ versus energy for determination of band gap.

encircled by broken circles, at (010) and (101) positions are also observed in this diffraction pattern. These reflections are forbidden as per structure factor calculations. Stereographic analysis of several nanowires and branches showed that the wire always grew along the [010] direction while the branching occurred along the [210] direction. XRD (not shown here) and XPS (Fig. 9 (a)) studies were carried out to determine chemical composition of nanowires.

XRD showed all reflections corresponding to CuO and XPS showed well defined shake up satellite structures on the high binding energy side of the copper $2p_{3/2}$ core line (centered at 932 eV). These satellites are typical of Cu^{2+} species and confirm that the grown nanowires are CuO.

The band gap of CuO nanowires was determined by optical absorption and found to be 2.03 eV (Fig. 9). It is larger than the reported value for bulk CuO (E_g= 1.85 eV [15]).

Various groups have studied growth of nanowires under different conditions of oxygen flow rate, annealing temperature and annealing time [14] but the mechanism of the growth of CuO nanowires is not understood. As discussed earlier the Vapor-liquid-Solid (VLS) catalyst-assisted growth [16] and the vapor-solid (VS) growth [17] are the two well known mechanisms for describing the growth of 1D nanostructures. In the VLS process, growth of the nanowire is initiated by the condensation of the vapor of the material at the tip of the wire. The adoption of such a mechanism is based on the morphology of 1D structure in which a round droplet was usually found near the tip of the wire. Our SEM image of the CuO nanowire indicated that there were no foreign droplets at their tips indicating that VLS mechanism is not applicable here. Regarding possibility of vapor-solid mechanism, it may be noted that CuO is the stable phase upto temperatures of ~1100°C at atmospheric pressure [18]. Vapor pressure of Cu and CuO at temperatures upto 800°C is very small and Cu_2O sublimes with vapor pressure of 10^{-4} Torr at 600°C. Formation of Cu_2O during growth of nanowires has been reported (and was also observed by us at interface of Cu and CuO nanowires) and therefore vapor-solid mechanism of growth could occur by evaporation of Cu_2O. However, if Cu_2O evaporation occurs, we should also get deposit on the walls of quartz tube above the copper disc and at its cold end as well as reduction in mass of Cu disc which were not observed. Further we had carried out oxidation of Cu_2O pellets under similar conditions to oxidation of Cu metal. No nanowire growth was observed indicating that formation of Cu_2O is not related to growth of nanowires. This shows that vapor solid mechanism is not operative in this case. There are some reports of metal oxide nanowire growth from metal by a self-catalytic growth [19]. However this does not seems probable in our case since for this process metals need to be heated slightly above their melting point in appropriate gas mixture. Possible mechanism of nanowire growth in this case is due to relaxation of stress as reported by Kumar et al [14] and indicated by SEM micrographs shown in Fig. 8(a). Copper oxidizes to Cu_2O and then CuO and stress in the foil is generated due to volume and structural changes during oxidation. Sufficiently high rate of oxidation coupled with low mobility of atoms in solid leads to relaxation of stress by formation of small crystallites of CuO from which the nanowires are observed to grow. The growth of nanowires therefore occurs to reduce the stress generated during oxidation of copper. This mechanism explains the observations that the nanowires do not grow (a) during oxidation of Cu_2O pellet, although in case of copper strip, Cu_2O is first formed and (b) at temperatures above 800°C. Cu_2O pellets are sufficiently porous and therefore the stresses due to change in volume are easily accomodated and in case of high temperatures, high mobility of atoms helps in reducing the stress.

ZnO

ZnO micro and nanostructures were prepared by thermal evaporation of Zn and a mixture of ZnO with graphite. On heating Zn powder at temperatures between 600°C to 800°C, radial growth of nanowires was observed on the source (Fig. 10). Nanowires with a diameter of <100 nm grow radially from the grains at 600°C. On increasing the temperature, both the density and diameter of the nanowires was found to increase. The nanowires are found to form a sea-urchin like structure. The nanowires growth in this case has been reported to takes place by a self catalytic growth mechanism [19].
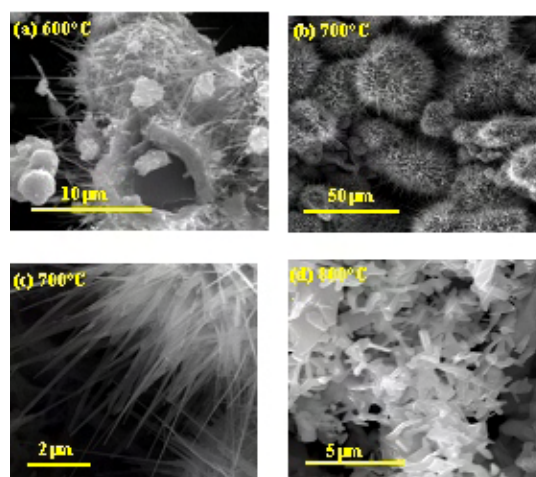

Fig. 10 *ZnO structures grown on Zn powder after heating for five hours at different temperature of (a) 600°C (b) 700°C (c) 700°C at higher magnification (d) 800°C.*
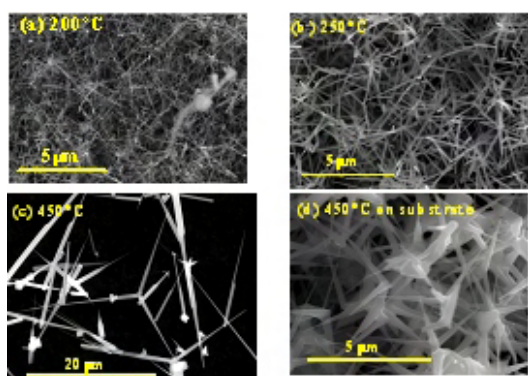
Fig. 11 *Deposition of ZnO nanostructures using ZnO and graphite mixture as source at temperatures of (a) 150°C (b) 250°C (c) 450°C and (d) 450°C on alumina substrate for gas sensing.*

When the Zinc powder is heated to temperatures higher than its melting point (419.53˚C), Zn droplets are formed and when oxygen is introduced in the chamber, it reacts with the outer surface of the previously formed Zn droplets and form nanosized ZnO nuclei on the surface of these droplets. These ZnO nuclei grow outward in the form of ZnO nanowire. On increasing the temperature to 900ºC, various interesting micro and nano structures of Zn and ZnO were observed to have deposited all over the quartz tube.

On the other hand, when ZnO was heated to 1050°C in the presence of graphite, (ratio 3:1), predominant growth of ZnO nanotetrapods was observed. In a tetrapod unit, four rods share a common crystal facet and tetrapod are branched in 3 dimensions. The size of tetrapod as well as diameter of the legs was found to increase with deposition temperature, Fig. 11. Tetrapods with legs of 30-50 nm in diameter and overall size (diameter of tetrapods) of 1.5-2 μm were obtained at ~250ºC (nanotetrapod). At higher temperatures of deposition, tetrapods with around 20 μm size and 400 nm leg diameter (at the base) were obtained. Structure of tetrapods at high resolution is shown by TEM image of Fig.12 a. It is clearly visible from the micrograph that the diameter of the legs reduces with distance from the center of the tetrapod. A selected-area electron diffraction (SAD) pattern
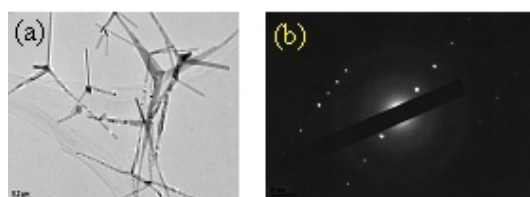

Fig. 12 *(a) Transmission electron micrograph of ZnO nanotetrapod clearly showing four tapering legs. (b) selected-area electron diffraction (SAD) pattern from an individual ZnO tetrapod leg.*

from an individual ZnO tetrapod leg (Fig. 12 b) shows their single crystalline nature.

Optical measurements such as photoluminescence (PL) are useful for the determination of structural defects and impurities in oxide nanostructures. Fig. 13 shows the room-temperature photoluminescence (PL) spectra recorded for ZnO nanorods. For comparison spectra of polycrystalline powder is also shown.

For nano-rods, two peaks are observed in the PL spectra: an UV band at 380 nm and a green band at 475 nm. Since the band gap of ZnO is around 3.37 eV, UV band emission of ZnO is understood to be related to direct recombination of a electron in Zn 4p conduction band with a hole in O 2p valence band, while the green emission has been suggested to be due to the presence of various point defects (oxygen vacancies) which can easily form recombination centers.

From figure, it is clearly visible that the green emission in the case of ZnO nanorods is much more than that observed in bulk sample (inset) indicating increased number of oxygen vacancies. Photoluminescence spectra of tetrapods, Fig. 13 b shows a single absorption band with peak at 475 nm indicating much higher defect density due to oxygen vacancies in this material.

ZnO nanowires and tetrapods were investigated for their use as H_2S gas sensors operating at room temperature. Their sensitivity (defined as $S = (R_a - R_g)/R_a) X100$ where R_a and R_g are resistances in air and gas respectively) to 4 ppm H_2S is shown in Fig. 14. For comparison, response of
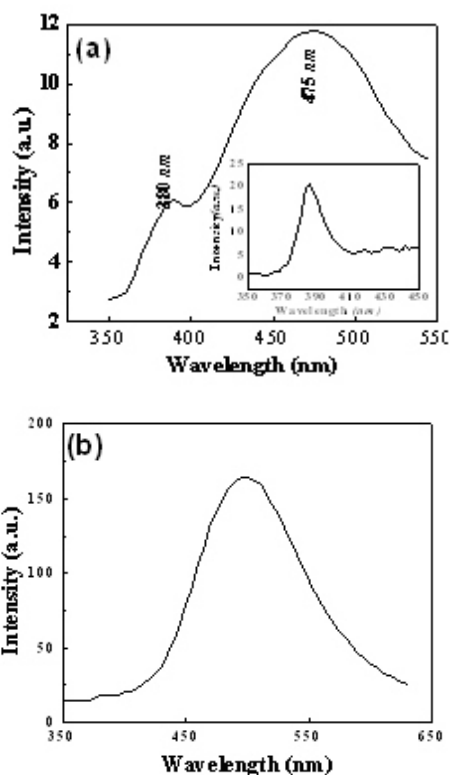
Fig. 13 Photoluminescence spectra of (a) ZnO nanorods prepared using Zn powder, inset shows a PL spectra of a bulk sample and (b) ZnO nanotetrapods obtained at 250ºC.

Fig. 14 (a) Comparision of sensitivity of ZnO bulk, ZnO nanowires and ZnO tetrapod sample towards 4 ppm of H_2S gas and (b) Variation of sensitivity of nanotetrapod film with concentration of H_2S gas.

polycrystalline material to H_2S gas is also shown. It is seen that tetrapods have much higher sensitivity to the gas. The films were found to be sensitive to 1 ppm and still lower concentration of H_2S gas. Fig. 14 also shows the sensitivity of tetrapod film to H_2S gas as function of concentration. Sensitivity is seen to saturate at concentrations higher than 10 ppm.

These sensors showed an improved response time (~ 3.5 min. for 4 ppm of gas) for detection of H_2S at room temperature when compared with earlier studies. Therefore tetrapod thin film may be used as room temperature operating gas sensors at concentration below 10 ppm. Better response of tetrapods to H_2S may be understood with reference to the PL data. The data presented in Figs 13 shows that green emission near 500 nm is minimum for polycrystalline samples and maximum for tetrapods.
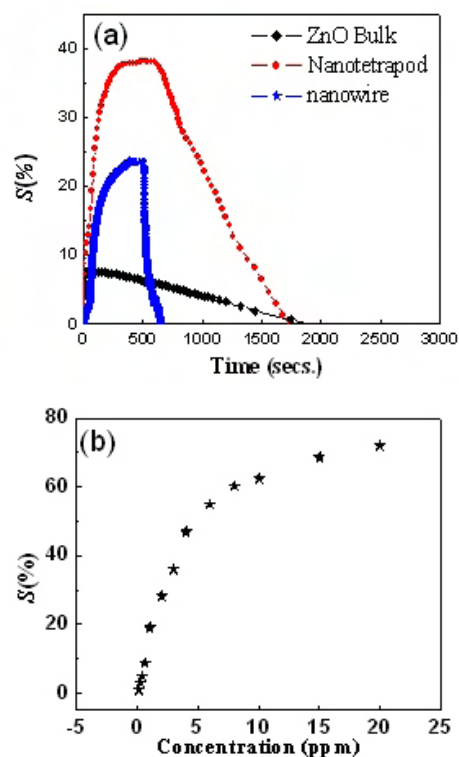
This emission in visible region has been attributed to ionized oxygen vacancies in bulk and at surface [20-22]. These vacancies act as adsorption sites for oxygen from atmosphere. The detection of gases in oxide semiconductors as ZnO originates from interaction of these adsorbed oxygen atoms with reducing gases such as H_2S. As the concentration of defect states and adsorbed atoms is maximum in tetrapods, we observe best response to H_2S in this case.

There are similar studies on H_2S gas sensing by ZnO nanostructure. Wang et al [23] have grown nanorods by hydrothermal method. They find good sensitivity to H_2S at 25°C-200°C and to C_2H_5OH at temperatures of 350°C. They have also investigated response to H_2S at room temperature. While the

sensitivity of the sensors is good, the response time is very long (>25 mins). A steady state is not reached even after 25 mins of exposure and recovery after removal of gas is also not complete. In contrast we observe good response and recovery times and saturation in response at room temperature. Our tetrapod films may therefore be used as sensors working at room temperature. The reason for these sensors showing good response and recovery at room temperature could be the fabrication technique used i.e. in-situ nanowire deposition on the substrates.

In_2O_3

We have studied growth of Indium oxide bipyramidal crystals and nanowires. Irrespective of the source material used – whether we use Indium metal or a mixture of Indium oxide and graphite, In_2O_3 bipyramidal crystals (fig. 15 a) were found to grow at lower temperatures of around 300°C. Every bipyramidal structure consists of four triangular facets on either side of a square facet [24,25]. The growth of pyramid shaped morphology is ascribed to preferential adsorption of In/O species on some special crystallographic planes of In_2O_3, the so called selective epitaxial vapor-solid growth mechanism. The plane with the slowest growth rate tends to appear as the facets over the other plane.

However, on heating mixture of Indium oxide and graphite (in weight ratio 1:1) at temperatures of about 1100°C, the deposits at a temperature of around 450°C show presence of nanowires, Figure 15 (b). Inset of figure 15 (b) shows nanowire originating at octahedrons. Formation of In_2O_3 was confirmed by EDX and XRD. The x-ray diffraction peaks could be indexed to In_2O_3 pattern with cubic structure, lattice constant being a = 10.11 Å.

Recently, Jiaqiang Xu et al. [26] have reported H_2S gas sensing properties of nanocrystalline In_2O_3 at about 250°C. Room temperature H_2S gas sensing properties of thick films made of these bipyramidal crystals was studied. It is observed that the resistance of In_2O_3 films decreases reversibly on exposure to H_2S gas at room temperature. The response and recovery curves of the film on gas exposure were obtained by measuring their resistance as a function of time. The response time was observed to increase marginally with increase in gas concentration from
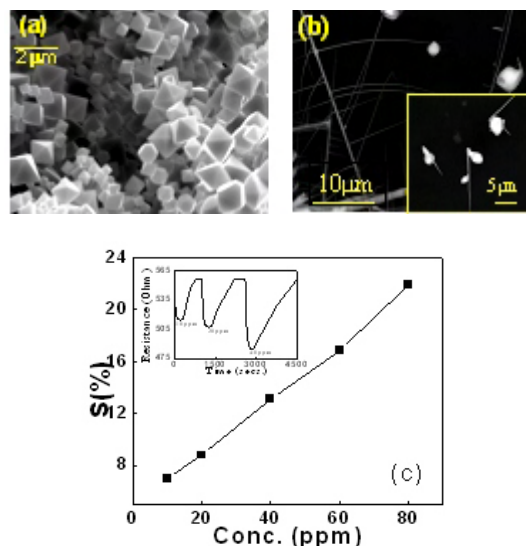

Fig. 15 SEM image of as synthesized (a) In_2O_3 bipyramidsand (b) nanowires. (c) Sensitivity versus concentration for a thick film made of bipyramidal crystals. Inset shows response and recovery curves of a typical film after exposure to 10, 20 and 40 ppm of H_2S gas.

2min. for 20 ppm gas to 2.5 min for 80 ppm of gas. The recovery time was seen to increase appreciably from 20 min. for 20 ppm of gas to 80 min for 80 ppm of gas. Response of the film was measured as a function of H_2S concentration at room temperature, figure 15 c. The response of the film in this figure is defined as $S = [(R_a-R_g)/R_a]*100$, where R_a and R_g are resistances of film in air and gas respectively.

Conclusion

Nanostructures of various semiconductor materials – nanowires and nanotubes of Tellurium, nanobelts and nanowires of SnO_2, nanowires of CuO, nanowires and nanotetrapods of ZnO, and nanowires and bipyramids of In_2O_3 were grown by physical vapour deposition technique and characterized. Most of these materials were employed for the detection of different toxic gases and found to be quite effective in detection of toxic gas at room temperatures.

References

1. S. Iijima, Nature **354** (1991) 56.

2. Wei U, Charles M Lieber, J. Phys. D: Appl. Phys. **39** (2006) R387.

3. M. Kaur, S. Bhattacharya, M. Roy, S. K. Deshpande, P. Sharma, S.K.Gupta, J.V. Yakhmi, Appl. Phys. A **87** (2007) 91.

4. Manmeet Kaur, K.P. Muthe, S.K. Despande, Shipra Choudhury, J.B. Singh, Neetika Verma, S.K. Gupta, J.V. Yakhmi, J. Crys. Growth, **289** (2006) 670.

5. Manmeet kaur, Namrata Jain, Kamalkant Sharma , C. Thinaharan, S.K. Gupta and J.V. Yakhmi, Proc. of DAE-SSPS-2006, 289.

6. Shashwati Sen, K. P. Muthe, Madhvi Sharma, S. K. Gupta, J. V. Yakhmi, Proc. of DAE-SSPS-2006, Pg. 291

7. S. Sen, V. Bhandarkar, K.P.Muthe, M. Roy, S.K Deshpande, R.C. Aiyer, S.K. Gupta, J.V. Yakhmi, V. C. Sahni, Sens. Actuat. B, **115** (2006) 270.

8. I. Nishida, K. Kimoto, Jap. J. Appl. Phys. **14** (1975) 1425.

9. G. Xi, Yankuan Liu, X. Wang, X. Liu, Y. Peng, Y. Qian, Crys. Growth and Design **6** (2006) 2567.

10. P. Mohanty, T. Kang, B. Kim, J. Park, J. Phys. Chem. **110** (2006) 791.

11. C. Métraux, B. Grobéty, J. Mater. Res. **19** (2004) 2159.

12. Y-C Her, J-Y Wu, Y-R Lin, S-Y Tsai, App. Phys Lett. **89** (2006) 043115.

13. X. Kong, Y. Li, Sens. Actuat. **105** (2005) 449.

14. Ashwani Kumar, A.K. Srivastava, Pragya Tiwari and R.V. Nandedkar, J. Phys.: Condens matter **16** (2003) 8531.

15. Hung-Hsiao Lin, Chih-Yuan Wang, Han C. Shih, Jin-Ming Chen and Chien-Te Hsieh, J. Appl. Phys. **95** (2004) 5889.

16. R.S. Wagner and E.C. Ellis, Appl. Phys. Lett. **4** (1964) 89.

17. V.A.L. Roy, A.B. Djurisic, W.K. Chan, J.Gao, H.F. Lui and C. Surya, Appl. Phys. Lett **83** (2003) 141.

18. D. K. Aswal, S. K. Gupta, S. N. Narang, S. C. Sabharwal and M. K. Gupta, Thin Solid Films **292** (1997) 277.

19. H. Y. Dang, J. Wang and S.S Fan, Nanotech. **14** (2003) 738.

20. R. Dingle, Phys. Rev. Lett. **23** (1969) 579.

21. K. Vanheusden, C. H. Seager, W. L. Warren, D. R. Tallant, J. A. Voigt, Appl. Phys. Lett. **68** (1996) 403.

22. Bixia Lin, Zhuxi Fu and Yunbo Jia, Appl. Phys. Lett. **79** (2001) 943.

23. Caihong Wang, Xiangfeng Chu and Mingmei Wu, Sens. Actuat. B **113** (2006) 320.

24. D. Alina Magdas, Ana Cremades and Javier Piqueras Appl. Phys. Lett. **88** (2006) 113107.

25. P.Guha, S. Kar and S.Chaudhuri Appl. Phys. Lett. **85** (2004) 3851.

26. Jiaqiang Xu, Xiaohua Wang, Jianian Shen Sens. Actuat. B **115** (2006) 642.

Carbon Nanotube
A Promising Material for Hydrogen Storage

Dr. D. Sathiyamoorthy joined BARC through 18th Batch of Training School. His areas of expertise are Reaction Engineering, Fluidization, Novel Carbon Materials, Super Critical Fluid processes, CVD for coated particles, Numerical Similation Methods.

Shri K. Dasgupta joined Bhabha Atomic Research Centre (BARC) in 2000 after successful completion of one-year orientation course (OCES 43rd batch) from BARC Training School. He completed his Bachelor in Engineering (Metallurgy) from Jadavpur University, West Bengal with first class honors in 1999. Presently he is working in Powder Metallurgy Division of BARC. He has worked on amorphous carbon, carbon-carbon composite, carbon nanomaterials and silicon carbide coating by CVD method. He has developed flow sheet for making novel amorphous carbon-carbon composites and TRISO coated fuel particles useful for advanced nuclear reactors. He has experience in synthesis and characterization of carbon nanotubes using different techniques like catalytic chemical vapour deposition, spray pyrolysis and fluidized bed method. Presently he is developing carbon nanotube based composites to be used for water purification and hydrogen adsorption. Shri Dasgupta, life members of Indian Institute of Metals and Indian Carbon Society has authored more than 35 scientific articles in refereed journals and conference proceedings.

Abstract

Hydrogen is an ideal fuel, which provides the best route to a sustainable energy with high utilization efficiency. The US Department of Energy (DOE) has set a standard for the amount of reversible hydrogen adsorption as system-weight efficiency (the ratio of stored hydrogen weight to system weight) of 6.5-wt % of hydrogen and a volumetric density of 62 kg H_2/m^3. Nanostructured carbon materials are considered to be the potential material for hydrogen storage. In this article the methods of synthesis of carbon nanotubes and their hydrogen uptake behaviour have been discussed.

Key words: Hydrogen storage, carbon nanotube, chemical vapour deposition, nano agglomerate fluidized bed.

Introduction

The development of social economy and culture brings high standards of living to many of us, while our world is facing a rapid depletion of natural resources and serious global environmental problems. This is connected with the overuse of fossil fuels. There is, therefore, a search for possible alternative sources of energy to replace fossil fuels. There are quite a number of primary energy sources available, such as thermonuclear energy, nuclear reactors, solar energy, wind energy, hydropower, geothermal energy, etc. In contrast to fossil fuels, in most cases, these primary energy sources cannot be used directly (e.g. used as a fuel for transportation), and they must be converted into fuels, that is to say, a new energy carrier is needed. Among the many choices, hydrogen is one of the best candidates.

Dr. D. Sathiyamoorthy and Shri K. Dasgupta, Powder Metallurgy Division, Bhabha Atomic Research Centre, Trombay, Mumbai 400 094; E-mail : dsathiyamoorthy@gmail.com

Hydrogen is an ideal fuel and versatile energy carrier, and its advantages are that it is easy to produce, environmentally compatible, convenient fuel for transportation and has got high utilization efficiency. Hydrogen provides the best route to a sustainable energy for the transportation sector and some other uses, since it can be produced not only from the fossil fuels, but also from non-renewable resources and without pollution of any kind. Putting aside the notion that hydrogen may be directly combusted in a modified engine, the other option for hydrogen power is a fuel cell, where an electrochemical reaction generates the necessary energy. We want an inexpensive, safe, low-weight fuel cell system with a hydrogen storage device capable of quick loading and unloading, comparable in volume to conventional gasoline tanks. The lighter-than-air gas makes the perfect fuel-it contains three times the energy of liquid hydrocarbons and when it reacts with oxygen to produce energy the only byproduct is water-but it isn't easy to contain. One of the biggest challenges of using hydrogen as a fuel is finding a way to store it.

Storage of Hydrogen

Today's hydrogen storage materials hold hydrogen of about 2 to 4 percent of their weight, considerably short of the 6.5 percent. The US Department of Energy (DOE) has set a standard for the amount of reversible hydrogen adsorption. This requires a system-weight efficiency (the ratio of stored hydrogen weight to system weight) of 6.5-wt % of hydrogen and a volumetric density of 62 kg H_2/m^3, since a vehicle powered by a fuel cell would require more than 3.1 kg of hydrogen for a 500 km range [1].

There are three technologies for storing hydrogen fuel as proposed by automobile manufacturers:

1. Compressed gas storage;
2. Metal hydride storage technology.
3. Cryogenic liquid hydrogen;

However these three technologies either cannot reach the standard just mentioned, or have significant disadvantages. Liquefying hydrogen wastes at least $1/3^{rd}$ of the stored energy and the cryogenic storage suffers from potential hydrogen
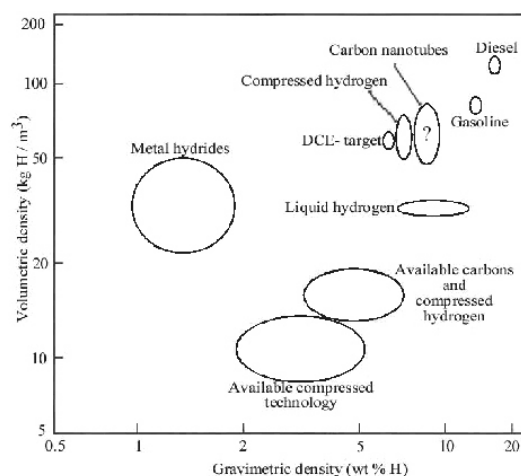

Fig. 1   Summary of how current and future hydrogen storage systems relate with respect to gravimetric and volumetric densities [2].

losses due to evaporation. The hydride-based approach suffers from weight and cost concerns, and the crucial issue connected with the compressed gas storage may be tank volume and safety. Fig.1 provides a summary of the relative volumetric and gravimetric densities of proposed storage media.

More recently, researchers evidenced keen interest in H_2 storage method aroused by the discovery and reproduction of high hydrogen adsorption capacity in carbon nanotubes and other low dimensional carbon materials [3,4]. If encouraging experimental results can be reproduced easily and the large-scale production of carbon nanotubes is made possible in the near future, it will be possible to reach the goals of the DOE hydrogen plan.

Carbon Nanotubes

Among the different forms of carbon, graphite and diamond are well known crystalline polymorphs. While graphite is a hexagonal layered structure with ABAB... stacking (also rhombohedral structure with ABCABC... stacking is possible), diamond is cubic structured with tetragonally bonded carbon atoms. Fullerene, a closed-shell structure, is considered as the third allotrope of the crystalline carbon. Fullerenes are
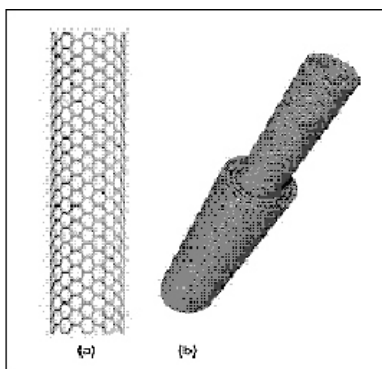
Fig. 2   *Schematic representations of (a) Single walled carbon nanotubes and (b) Multi-walled carbon nanotubes.*

Fig. 3   *Atomic structure of carbon nanotube*

closed-shell structures made up of large numbers of carbon atoms. The archetypical fullerene, C_{60}, consists of twelve pentagons and twenty hexagons with icosahedral symmetry [4,5].

The discovery of the fullerenes opened the door to a new class of carbon materials called carbon nanotubes (CNTs). Sumio Iijima first observed carbon nanotubes in 1991 [6]. Nanotubes are long, slender fullerenes where the walls of the tubes are hexagonal carbon (graphite structure) and often capped at the end. The carbon nanotubes are built up of a finite graphite sheet that is rolled to a tube.

A variety of types exist which is either made of one layer called single-walled nanotube (SWNT) and more than one layer called multi-walled nanotube (MWNT), as illustrated in Fig.2. Typically, the SWNTs have caps at the end which have structures related to the fullerenes.

These cage-like forms of carbon have shown exceptional material properties that are a consequence of their symmetric structure. In terms of mechanical properties carbon nanotubes are among the strongest and resilient materials known to exist in nature in spite of being light-weight and flexible. It possesses a high elastic modulus nearly similar to that of diamond and it has tensile strength 10-100 times than steel. They also possess superior thermal and electric properties – thermal conductivity twice as high as diamond and current-carrying capacity 1000 times higher than
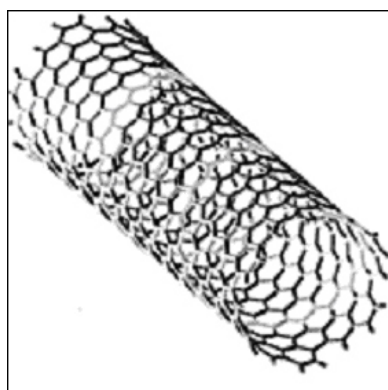
that of copper wires. Its properties are a mix of diamond and graphite; hence it possesses the high strength and thermal conductivity of diamond, and electrical conductivity of graphite. Electrically it behaves both as a metal and a semiconductor.

Atomic Structure of Carbon Nanotubes

In the case of carbon nanotubes each carbon atom is bound to three other carbon atoms. A single-walled nanotube is a graphene sheet rolled up into a cylinder with a typical diameter of 1.4nm. A multi-walled nanotube consists of concentric cylinders with an interlayer spacing of 3.4 A^{o} and a typical diameter of the order of 10-20 nm. The lengths of the two types of tubes can be up to hundreds of microns or even centimeters. The length to diameter ratio of carbon nanotubes are of the order of 10^{2} to 10^{3}, hence CNTs are referred to as 1-Dimensional carbon systems. Fig. 3 gives a representation of the atomic structural arrangement of a carbon nanotube.

The properties of nanotubes depend on the atomic arrangement, diameter and the lengths of the tubes and the morphology of nanostructure. The atomic structure of carbon nanotubes depends upon the chirality or helicity, which is defined by the chiral vector, , and the chiral angle, θ. The chiral vector often known as the roll-up vector can be described by the equation:

$$\vec{C}_h = n\vec{a}_1 + m\vec{a}_2$$

Where $n\vec{a}_1$ & $m\vec{a}_2$ are integers and a_1 and a_2 are unit vectors. The chiral angle determines the amount of
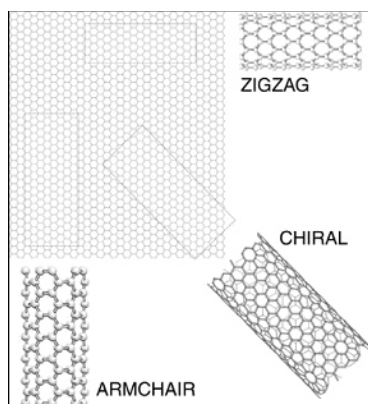
Fig. 4   Illustration representing the various structural arrangements in carbon nanotubes.

Fig. 5   Representation of the working principle of Arc discharge method.

twist of the tube. Based on the chiral angle, the nanotubes are classified as armchair, zigzag and chiral nanotubes as represented in Fig. 4. If the chiral angle is 0°, then the resulting structure is referred to as zigzag. The carbon atoms are bonded here in a zigzag pattern, hence they behave as metals. In the case of armchair, the chiral angle is 30°. So the carbon bonds are perpendicular to the hexagonal structure, it behaves as semiconductor. Another type called chiral nanotubes, in which the chiral angle lies between the above two limiting cases normally between 0° and 30°,and they behave as a semi-metal.

The chirality of the carbon nanotube has significant implications on the material properties. In general chirality is known to have a strong impact on the electronic properties of CNT. Graphite is considered to be a semi metal, but nanotubes can either be metallic or semi conducting depending upon the chirality [7].

Methods of Synthesizing Carbon Nanotubes

Since carbon nanotubes were discovered nearly a decade ago, there have been a variety of techniques developed for producing them. Iijima [6] first observed Multi-walled nanotubes; Iijima et al. and Bethune [8,9] reported the synthesis of Single-walled nanotubes a few years later. Primary synthesis methods for a single and multi-walled carbon nanotubes include:
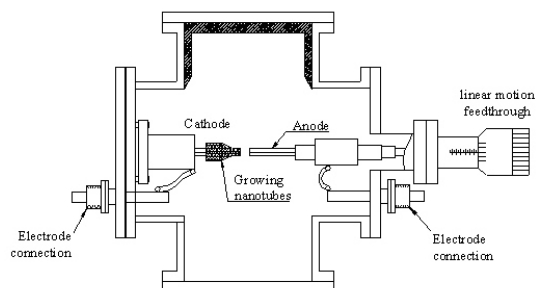
1.   Arc discharge method;

2.   Laser ablation technique;

3.   Chemical vapour deposition method.

Arc-discharge method and laser ablation are the two methods used for growth of nanotubes, which have been actively pursued in the past 10 years. But nowadays chemical vapour deposition (CVD) process is used for producing single-walled and multi-walled carbon nanotubes in bulk amounts.

Arc Discharge Method

Iijima [6] first observed nanotubes synthesized from the electric-arc discharge technique, shown schematically in Fig. 5. The process involves the use of two high-purity graphite rods as the anode and the cathode. The rods are brought together under a helium atmosphere and a voltage is applied until a stable arc is achieved.

As the anode is consumed, a constant gap is maintained by adjusting the position of the anode. The material then deposits on the cathode to form a build-up consisting of an outside shell of fused material and a softer fibrous cone containing nanotubes and other carbon particles. To achieve single-walled nanotubes, the electrodes are doped with a small amount of metallic catalyst particles.

Laser Ablation Method

Laser ablation was initially used for the synthesis of fullerenes. Over the years, the technique has been improved to allow the production of single-walled nanotubes. Smalley and co-workers using laser ablation method achieved the growth of high quality SWNTs at the 1-10g scales [10,11]. The
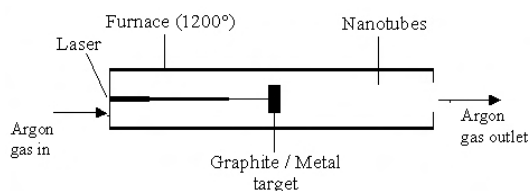
Fig. 6 *Working principle of Laser ablation process*

Fig. 7 *Working principle of Chemical vapour deposition technique.*

condensation of laser-vaporized carbon has 70% more than the production of nanotubes in the yield proportions by catalyst mixture. In this technique laser is used to vaporize a graphite target held in a controlled atmosphere at temperature near 1200°C. To produce SWNTs, graphite target was doped with cobalt and nickel catalyst. This resulting product consists of bundles or ropes of SWNTs arranged in near closest-packed order. The general setup for laser ablation method is shown in Fig. 6.

Both the arc-discharge and laser ablation techniques are limited in the volume of sample they can produce in relation to the size of the carbon source. In addition, subsequent purification steps are necessary to separate the tubes from undesirable by-products. These limitations led to the development of gas-phase techniques, such as chemical vapour deposition (CVD), where nanotubes are formed by the decomposition of a carbon-containing gas. The gas-phase techniques are amenable to continuous processes since the flowing gas continually replaces the carbon source. In addition, the final purity of the produced nanotubes can be quite high, minimizing subsequent purification steps.

Catalytic Chemical Vapour Deposition (CCVD) Method

Gas-phase Catalytic Growth from Carbon Monoxide

Nikolaev and others [12] describes the gas-phase growth of single-walled carbon nanotube with carbon monoxide as the carbon source. They reported the highest yields of single walled nanotubes occurred at the highest accessible temperature and pressure (1200°C, 10 atm.).
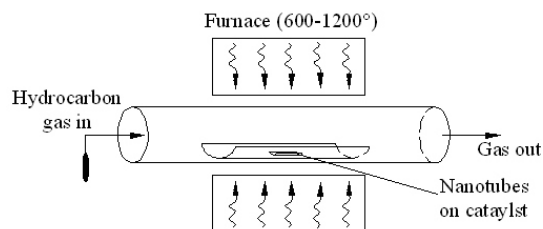
Smalley and his coworkers at Rice University have refined the process to produce large quantities of single walled carbon nanotubes with remarkable purity [13]. The so-called HiPco (high-pressure conversion of carbon monoxide) has received considerable attention as the technology has been commercialized by Carbon Nanotechnologies Inc (Houtson, TX) for large-scale production of high-purity single-walled carbon nanotubes [13].

Chemical vapour Deposition (CVD) in Static Bed

Chemical vapour deposition (CVD) technique in static bed utilizes hydrocarbon gases as the carbon source for production of single-walled and multi-walled carbon nanotubes. The growth process involves heating a catalyst material to high temperature (600-1200°C) in a tube furnace and flowing a hydrocarbon gas through the tube reactor over a period of time. Iron, nickel or cobalt nanoparticles (transition metals) and the combination of these are often used as catalyst. This method can lead to bulk production of carbon nanotube [14-17]. It has also been found that by using methane as carbon feedstock, reaction temperatures in the range of 850-1000°C and with supported catalyst materials one can grow high quality SWNTs by CVD [18]. The schematic illustration of chemical vapour deposition method is provided in Fig. 7.

One unique aspect of CVD techniques is its ability to synthesize aligned arrays of carbon nanotubes with controlled diameter and length. The synthesis of well-aligned, straight carbon nanotubes on a variety of substrates has been accomplished by the use of plasma enhanced chemical vapour

deposition (PECVD) where the plasma is excited by DC source or a microwave source [19,20].

Nano Agglomerate Fluidized-Bed Reactor

Carbon nanotubes produced by catalytic chemical vapour deposition (CCVD) can be formed into loose agglomerates that can be fluidized during the growth process. Fluidization is the operation by which solid particles are transformed into a fluid-like state through suspension in a gas or a liquid. This method of contacting has been used in numerous industrial processes for its unusual characteristics. Large amounts of carbon nanotubes have been successfully produced in a nano agglomerate fluidized-bed reactor (NAFBR) [21,22]. A NAFBR can be simply and inexpensively operated at atmospheric pressure and moderate temperatures. It gives 70-80% multi-walled nanotubes with a high production rate of 50 kg/day.

The success in nanotube growth has led to the wide availability of nanotube materials, which is a main catalyst behind the recent developments in basic physics studies and applications of nanotubes.

Hydrogen Storage in Carbon Nanotubes (CNTs)

Concerning the hydrogen storage in carbon nanotubes [23], the structure has two possible sites: (i) inside the tubes and (ii) in the interstitial sites between the tube array as shown in Fig. 9. In the case of a long SWNT closed with fullerene-like caps at the end, the hydrogen can only get access to the tube interior via the six ring of the graphite-like tube wall. An opened tube with removed caps may give an easier access for the hydrogen molecule into the tube.

Typically, the tubes are very long and therefore a good diffusivity of the hydrogen inside the tube will be required in order to fill the whole tube volume. Furthermore, one can imagine that a structural defect in the tube or a sharp bend of the tube may block the hydrogen diffusion. Therefore, cutting the tubes in shorter pieces may help to improve hydrogen storage and its kinetics to overcome this problem [3]. Concerning the interstitial sites of the rope array similar arguments hold. The access from the side requires diffusion between the closest tube–tube distance whereas the interstitial sites are directly accessible from the rope

ends. To fill the whole volume of these interstitial sites or better cylinders, owing to its extension in one dimension along the whole rope, will require good hydrogen diffusivity inside these cylinders.

Prediction of Hydrogen Uptake in Carbon Nanotubes

Owing to its high surface area and abundant pore volume, porous carbon is considered as good adsorbent. For conventional porous carbon, the hydrogen uptake is proportional to its surface area and pore volume, while, regretfully, a high hydrogen adsorption capacity (4~6 wt%) can be only obtained at very low temperatures such as liquid nitrogen temperature, consistent with theoretical calculations [5].

In contrast, in spite of their relative small surface area and pore volume, carbon nanotubes and carbon nano-fibers show very surprising high hydrogen storage capacity. Scientists employed different theoretical calculations and deductions in search of reasonable interpretation. The intent of this theoretical work is summarized in the following points:

1. How do structural characteristics influence the physical or chemical process?

2. Where does the hydrogen adsorption occur, in inner hollow cavities or other pore space (e.g. inter-tube space)?

3. In the adsorption of hydrogen onto carbon nanotubes, what interaction, chemical or physical occurs between the hydrogen and carbon?

4. What are the adsorption mechanisms and the maximum adsorption capacity?

Simplistic Geometrical Estimate and Qualitative Discussion

Dresselhaus [5] obtained a simple geometric estimate for the close-packing capacity of hydrogen molecules above a plane of graphite using purely geometric arguments, which yields 2.8 wt% or 4.1-wt% of hydrogen adsorbed on a single graphene layer. One important issue currently being debated is whether hydrogen adsorption also occurs in interstitial channels between adjacent nanotubes in a

rope of SWNTs. Dresselhaus presented two geometrical estimates for the filling of ropes (crystalline lattice) of SWNTs. One estimate assumes that hydrogen is a complete deformable fuel that fills the space not occupied by carbon nanotubes and the other is a packing of hydrogen molecules of kinetic diameter 0.29 nm on the inner wall and in the interstitial volume of nanotubes.

Under high-pressure conditions, the compressibility of hydrogen and the attractive intermolecular interactions should lead to closer packing of hydrogen molecules. The amount of hydrogen adsorption under high pressure would be higher than the simplistic geometric estimate. The hydrogen adsorbed in the space would be expected to be denser than on the single graphene surface because the hydrogen molecules adsorbed in the interstitial space undergo much stronger surface attraction than on a single planar graphene surface since it is in close proximity to three graphene surfaces. In short it is concluded that for SWNTs hydrogen is stored in both the pores formed by the inner-tube cavities and the inter-tube space, and the storage density is possibly higher than that on a planar graphene surface. Accordingly the hydrogen adsorption amount may be higher than 4 wt %.

Physisorption and Chemisorption

The adsorption of hydrogen in carbonaceous materials corresponds to the amount of hydrogen adsorption, which takes place near the solid carbon surface due to the physical forces (i.e. Vander Walls interactions) that carbon atoms exert on hydrogen molecules. This phenomenon is called physisorption.

Scientists have reported results of calculation for hydrogen storage behaviour in SWNTs by density functional calculations [24] and proposed that the adsorption of hydrogen in SWNTs is chemisorption process. The calculations predict that the hydrogen storage in nanotubes can exceed 14 wt %($160 kg H_2/m^3$). It is quite difficult to reach the conclusion for maximum adsorption capacity and explain the experimental observations from the results obtained by the different theoretical calculations and predictions. Understanding into pore structure and adsorption process of carbon nanotubes will help us to choose the optimum

intermolecular potential function and modify our calculations to direct the development of carbon nanotube based hydrogen storage systems.

The amount of gas adsorbed is excessive; it represents the additive amount of gas that can be introduced in a given volume with respect to the amount of gas occupying an equivalent volume at the same temperature and pressure in the absence of adsorption. At a given temperature, the amount of gas adsorbed is only a function of the pressure and is released (desorbed) when pressure decreases: the phenomenon is reversible with pressure. So we need, the adsorption measures the additional storage gas capacity compared to the one of compressed gas in the same volume and under identical temperature and pressure conditions.

Experimental Investigation of Hydrogen Uptake In Carbon Nanotubes

In 1997, Dillon first claimed that SWNTs have a high reversible hydrogen storage capacity [1]. Many researchers have been carrying out hydrogen storage experiments and have made noticeable progress. Dillon showed that hydrogen can condense to high density (estimated to 5-10 wt%) inside narrow SWNTs of 12 A^o and predicted that SWNTs with diameters of 16.3 and 20 A^o would come close to the target hydrogen uptake density of 6.5 wt% [1].

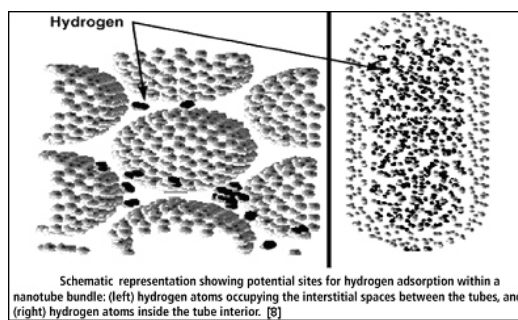The adsorption of hydrogen in SWNT soots was probed with Temperature Program Desorption

Fig. 8   *Schematic representation showing potential sites for hydrogen adsorption within a nanobundle: (left) hydrogen atoms occupying the interstitial spaces between the tubes, and (right) hydrogen atoms inside the tube interior. [23]*

(TPD) spectroscopy and suggested that physi-adsorption of hydrogen mainly occurred within the cavity of SWNTs.

The activation energy for hydrogen desorption was experimentally found to be 19.6 kJ/mol which is much higher than the theoretical predicted value or approximately five times higher than that for a planar graphite surface, thereby promoting hydrogen storage capacity at higher temperature. Scientists have recently developed a method to produce samples with high concentration of short SWNTs with open ends that are accessible to the entry of hydrogen molecules, and these purified cut SWNTs adsorbed 3.4 ~ 4.5 wt% of hydrogen under ambient conditions in several minutes [25].

It has also been reported that the ratio of hydrogen to carbon atoms of about 1.0 was obtained for crystalline ropes of SWNTs at 80 K. At a pressure of 4 MPa a sudden increase in adsorption capacity of SWNT samples was also recorded [3]. High-resolution adsorption measurements showed that the sample has abundant micropores of diameter similar to tube diameters indicating much more open tubes. Dillon [21] and Cheng [26] predicted that this kind of SWNT might be promising as high hydrogen storage carriers. Meanwhile it has been proved that notable changes occur for pore structure in the course of hydrogen uptake in SWNTs. All the above facts indicate that the inner hollow cavity also takes part in hydrogen absorption.

Conclusion

Hydrogen storage in carbon nanostructures is a very attractive topic owing to the small mass of carbon and its newly found nanostructures have high potential storage capacities. More and more experimental and theoretical results continue to appear and more and more reproducible evidence proves that carbon nanotubes are a potential hydrogen storage carries although there are a few negative results reported as well.

In order to use carbon nanotubes as a practical hydrogen storage medium, the mass production and utilisation of carbon nanotube still have a long way to go, considering the following points:

1. The mass production of carbon nanotubes at a reasonable cost.

(Researchers in US have reported that the production of 1 gm of gold would cost $10 while that for Multi-walled carbon nanotubes would cost about $100 and that for Single-walled carbon nanotubes it would cost about $200).

2. Purification and surface functionisation of carbon nanotubes.
(It has been suggested that opening the caps at the tube ends improve the hydrogen storage capacity).

3. Understanding the adsorption/desorption mechanisms and the volumetric capacity of carbon nanostructures.

In all, hydrogen is a clean, versatile, efficient and safe fuel, and is also the best fuel for transportation. Hydrogen energy will play an important role in the future demand of energy. Preliminary experimental results and theoretical predictions indicate that carbon nanotubes to be a promising candidate for hydrogen storage, which may accelerate the development of hydrogen fuel cell-driven vehicles.

Many efforts have to be made to reproduce and verify the hydrogen storage capacity of carbon nanotubes both theoretically and experimentally, to investigate their volumetric capacity and release behaviour, to clarify their adsorption/desorption mechanism, and finally to clarify the feasibility of carbon nanotubes as a practical onboard hydrogen-storage material.

References

1. Dillon AC, Jones KM, Bekkedahl TA, Kiang CH, Bethune DS, Heben MJ. *Nature* 1997; 386:377

2. Schmid M. (2001), Diplomarbeiten thesis, Universität Stuttgart, Germany.

3. Ye Y, Ahn CC, Witham C, Fultz B, Liu j, Rinzler AG, Colbert D, Smith KA, Smalley RE. *Appl Phys Lett* 1999; 74(16): 2307

4. Kroto HW, Heath JR, O'Brien SC, Curl RF, Smalley RE. *Nature* 1985; 318:162

5. Dresselhaus MS, Dresselhaus G, Eklund PC. *Science of Fullerenes and Carbon Nanotubes.* San Diego: Academic Press, 1996.

6. Iijima S. *Nature* 1991; 354:56

7. Dresselhaus MS, Dresselhaus G and Saito R. *Phys. Rev. B* 1992; 45:6234

8. Iijima S and Ichihashi T. *Nature* 1993; 363:603

9. Bethune DS, Kiang CH, Vries de MS, Gorman G, Savoy R, Vazquez J and Bayers R., *Nature* 1993; 363:605

10. Guo T, Jin CM and Smalley RE. *Chem. Phys. Lett* 1995; 243:49

11. Thess A, Lee R, Nikolev P, Dai H, Petit P, Robert J, Xu C, Lee YH, Kim SG, Rinzler AG, Colbert DT, Scuseria GE, Tomanek D, Fischer JE and Smalley RE., *Science* 1996; 273:483

12. Nikolaev P, Bronikowski MJ, Bradley RK, Fohmund F, Colbert DT and Smith KA, *Chem. Phys. Lett.* 1999; 313:91

13. Thostenson ET, Ren ZF, Chou TW. *Composites Science and Technology* 2001; 61:1899

14. Colomer JF, Stephan C, Lefrant S, Van Tendeloo G, Willems I, Konya Z, et al. *Chem. Phys. Lett.* 2000; 317; 83

15. Andrews R, Jacques D, Rao AM. *Chem. Phys. Lett.* 1999; 303; 467

16. Dasgupta K, Venugopalan R, Sathiyamoorthy D. *Mater. Lett.* (2007) Doi: 10.1016/j.matlet.2007.02.042

17. Dasgupta K, Venugopalan R, Dey GK, Sathiyamoorthy D. *J. Nanopart. Res.* (2007). Doi: 10.1007/s11051-007-9219-5

18. Yan H, Li Q, Zhang J and Liu Z. *Carbon* 2002; 40:2693

19. Bower C, Zhu W, Jin S and Zhou O. *Appl. Phys. Lett.* 2000; 77(6):830

20. Ren ZF, Huang ZP, Xu JW, Wang DJ, Wen JG and Wang JH. *Appl. Phys. Lett.* 1999; 75(8):1086

21. Wang Y, Wei F, Luo G, Yu H, Gu G. *Chem. Phys. Lett.* 2002; 364:568.

22. Luo G, Li Z, Wei F, Xiang L, Deng X, Jin Y. *Physica B* 2002; 323:314

23. NASA Ames research center. (http://atrs.arc.nasa.gov/r_t/1997/aero/revol9.html)

24. Lee SM, Lee YH. *Appl. Phys. Lett.* 2000; 76(20): 2877

25. Dillon AC, Gennett T, Alleman JL, Jones KM, Parilla PA and Heben MJ. Carbon nanotube materials for hydrogen storage. *Proceedings of the 1999 US DOE Hydrogen Program Review Vol.II* (http://www.er_Hlt43642950_Hlt43642951e BM_1_BM_2_n.doe.gov/hydrogen/pdfs/269 38jjj.pdf)

26. Hui-Ming Cheng, Quan-Hong Yang, Chang Liu. *Carbon* 2001; 39:1447

Molecule/Silicon Hybrid Nanoelectronics

Dr. D.K. Aswal *joined Technical Physics and Prototype Engineering Division through 30th Batch of Training School. He has made several contributions in the field of thin/thick films and single crystals of various high temperature superconductors and colossal magnetoresistive materials. He has investigated various properties of magnesium-di-boride superconductor, metallic multilayer grown by molecular beam epitaxy and thermoelectric materials. Currently is is working on organic/molecular electronics. He is a recipient of several international fellowships including, JSPS, Japan (1997-99), IFCPAR, France (2004-05) and BMBF, Germany (2006). He is reviewer for 11 international journals. He has coedited one book entitled "Science and Technology of Chemiresistive Gas Sensors" and authored more than 120 scientific publications.*

Dr. J.V. Yakhmi, *Associate Director (S), Physics Group and Head, Technical Physics and Prototype Engineering Division of BARC, has worked for the past 40 years on diverse areas of research in materials science, such as, high Tc systems, magnetic alloys, molecular materials etc. He is reciepent of several nantional and international awards/fellowships, including Fellow, National Academy of Sciences, India; Maharashtra Academy of Sciences; Elected Member, Asia Pacific Academy of Materials; MRSI-ICSC Superconductivity and Materials Science Prize 1995 by Materials Res. Soc. of India; Distinguished Alumni Award from Kurukshetra University (India) 1996; IIS Gold Medal by Institute of Industrial Science, University of Tokyo, 1996; "UDCT Golden Jubilee Visiting Fellow", University of Bombay, 1997; Award of 'Excellence' by the CEFIPRA Scientific Council to the Indo-French Project 1308-4 "Chemistry and Physics of Molecular-based Materials" carried out during 1996-99. He has coedited a book entitled "Thallium-Based High Temperature Superconductors", and authored more than 300 scientific publications.*

Introduction

One of the ultimate goals in nanotechnology is to build electronic devices using individual molecules and, this branch of research is popularly termed as molecular electronics. Molecular electronics is being proposed as an alternative to the silicon based microelectronics [1]. It is anticipated that the Si technology is likely to face the scaling limits in a very near future. This is because as the projected size of the transistors goes down to 20 nm or below it, the physics of the transistors lead to unacceptable power dissipation. An intense research carried worldwide during last couple of years has demonstrated that molecules exhibit unique electronic functions and, the chemists around the world are synthesizing many more new molecules with desired properties. Physicist and engineering, on the other hand, devised several new methods to measure the electronic transport of a single molecule. These include, break-junction, cross wire, metal nano-particle, conductive probe atomic force microscope (CP-AFM), scanning tunneling microscope (STM), nano-pore and planar sandwich geometry. Despite of these developments, building electronics solely using molecules might take a much longer time (may be several decades!). Thus, a medium term solution, say for next 5-10 years, is to make molecules compatible to the silicon, so that the nanoscale electronic functnality of molecules can be utilized in silicon based microelectronics, and this

Dr. D.K. Aswal and Dr. J.V. Yakhmi, Technical Physics and Prototypr Engineering Division, Bhabha Atomic Research Center. Mumbai 400085; E-mail: dkaswal@barc.gov.in

research field is termed as hybrid nanoelectronics. The advantage of molecule/Si hybrid concept is that the inputs available from an already existing powerful silicon-based integrated circuit industry can be used effectively for the development of integrated hybrid devices. For last two years, our group is actively engaged in the development of hybrid nanoelectronics and in this brief review we present some of our ideas and their realization. To begin with we describe how one can graft organic molecules on silicon to form a monolayer. The techniques used for characterization of the organic monolayers are summarized. We then demonstrate functionality of various molecular electronic components i.e. dielectric, rectifier, resonant tunnel diode, transistor and memory.

Monolayer on Silicon

The monolayers of organic molecules on silicon, as schematically shown in Fig. 1, can be grafted by two different methods: self-assembly and cathodic electrografting method.

The self-assembled monolayer (SAMs) are formed spontaneously by immersing the Si substrates into an active solution e.g. surfactant molecules $R(CH_2)_nSiX_3$ (X = Cl, OCH_3 or OC_2H_5) dissolved in alkane/carbon tetrachloride [1,2]. The self-assembling molecule can be divided into three parts: (i) Head group i.e. $-SiX_3$: forms the chemical bond with surface atoms of the substrate (exothermic: ~40-45 kcal/mol or ~1.7 eV) causing the pinning of surfactant molecule to the substrate, (ii) Alkyl chain i.e. $-(CH_2)_n-$: the inter-chain van der Waals interactions (exothermic <10 kcal/mol or <0.4 eV) could assist in formation of ordered molecular structure which, of course, depends on the pinning density of the head groups, and (iii) Surface group i.e. $-R$: this is the terminal group which is replaced with different functional groups to obtain molecular electronics devices. For a high density of head groups chemisorbed at the surface of the substrate – implying a good surface coverage – the alkyl chains become closer. Therefore, the inter-chain van der Waals interactions become effective, which leads to formation of a close-packed "ordered" monolayer (as schematically shown in Fig. 1). The alkyl chains, depending upon the surface coverage, have a tilt (Φ) from the surface normal.
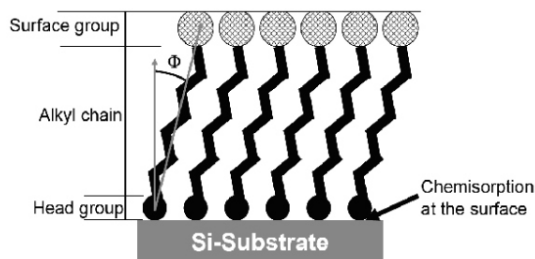

Fig. 1   A cartoon showing different parts of a self-assembled monolayer deposited on a Si-substrate suitable for molecular electronics. Φ is the tilt of the chain axis from the surface normal.

Usually higher the packing density, lower is the Φ. On the other hand, if the surface coverage is poor, the alkyl chains form a "disordered" monolayer, and the Φ could be very large.

The deposition of organic SAMs on Si can be carried out using following two approaches. (i) Deposition of SAMs on native silicon oxide of Si (SiO_x/Si) by "silanization": SiO_x/Si substrates are first cleaned in piranha solution (H_2SO_4/H_2O_2: 2:1 v/v) to obtain OH-terminated SiO_x/Si, which are then immersed into a solution of surfactant molecules $R(CH_2)_nSiX_3$ (X = Cl, OCH_3 or OC_2H_5) prepared using aliphatic or aromatic hydrocarbons. The chemical reaction between the hydroxylated SiX_3 and OH results in the formation of the chemical bonds. (ii) Direct deposition of SAMs on silicon: In this case the SiO_x layer is first etched out using 1-2% HF (aqueous) or 40% NH_4F (aqueous) to obtain an H-terminated Si surface. The SAM can be deposited by dipping the H-terminated Si substrate into a solution of 1-alkenes at 100ºC, which results in formation of Si–C bonds. The disadvantage of self-assembly process is that, apart from the natural chemisorption of organic molecules on Si—H or Si—OH surfaces and van der Waals interactions among alkyl-chains, there is no external controlling parameter that can force deposition of organic molecules and prevent adsorption of impurities on the Si surface.

Cathodic electrografting is an emerging method for the deposition of monolayers on Si substrates [3,4]. Electrografting essentially is an

electro-initiated process and it requires a charged electrode (e.g. doped Si) for the grafting of organic molecules, which takes place by formation of covalent bonds between the substrate atoms and the molecules. Cathodic electrografting method has a distinct advantage: since a negative potential is applied to the Si substrate, the oxidation and/or hydrolysis of Si surface is out of question during the grafting of organic molecules. In fact, even if some oxide/hydroxide is present at the Si surface, it gets destroyed by a reduction process and therefore yields a clean Si surface. Moreover, the applied negative potential becomes a controlling parameter for driving the molecules to the Si surface, which yields a highly dense monolayer.

Monolayer Characterization

The quality of deposited SAMs is assessed by characterizing them for the following parameters [1].

(i) Thickness of the monolayer: Optical ellipsometry is the most routinely used technique to determine the thickness of the SAMs, though other techniques, such as, plasmon surface polarization, X-ray reflectivity, X-ray standing waves etc.

(ii) Molecular orientation and ordering: Fourier transform infrared (FTIR) spectroscopy is the most powerful tool for studying the molecular orientation and ordering in a self-assembled monolayer. FTIR is usually done in two different spectroscopy modes (i) attenuated total reflection (ATR) and (ii) reflection-absorption (RA). In the ATR mode, individual s- and p-polarized (the parallel and perpendicular components of a plane polarized light, respectively) attenuated total internal reflection spectra are recorded. The dichroic ratio (D), defined as, $D = A^{s-pol}/A^{p-pol}$ (where A^{s-pol} and A^{p-pol} are s- and p- polarized absorbance, respectively) gives the information on the molecular orientation. The peak positions of symmetric (ν_s) and asymmetric (ν_a) stretching modes of CH_2 group give the required information about the molecular order in the monolayers. For a well ordered (i.e. crystalline) monolayers the peak positions of ν_s and ν_a are at 2851 ± 1 and 2918 ± 1 cm^{-1}, respectively; while for a highly disordered (i.e. liquid) monolayers these peak positions shift to 2855 ± 1 and 2924 ± 1 cm^{-1}, respectively. The information about the structure of SAMs can also be obtained by a variety of techniques, such as, X-ray, electron and neutron diffraction, high-resolution electron loss spectroscopy, Raman spectroscopy, Near-edge X-ray absorption fine structure spectroscopy (NEXRAF) etc.

(iii) Uniformity and coverage: The quality and uniformity of a monolayer at various lengths (from macro to nano) can be assessed by wetting measurements and/or by directly imaging the surface topography by atomic force microscope, scanning electron microscopy and tunneling electron microscopy. The wetting measurement is simple and effective technique because the "shape" of a liquid drop (de-ionized water or hexadecane, for instance) on a uniform surface depends on the free energies of the liquid and surface. The "advancing" and "receding" contact angles give information about the surface group of the monolayer and its uniformity.

(iv) Chemical composition: The chemical composition of monolayers can be determined by Auger electron spectroscopy (AES), X-ray photoelectron spectroscopy (XPS) and secondary ion mass spectrometry. Among these XPS is a unique technique as it not only determines the chemical composition of the monolayers but also gives information on the oxidation state of its elements. The biggest advantage of XPS is that it provides the information of the surface-group of the monolayer, if spectra are recorded as a function of takeoff-angles (α: angle between the sample surface and the analyzer acceptance plane). If 95% of the signal arises from a depth into the solid of 3λ (λ is the inelastic mean free path of the emitted photoelectrons) then the depth sampled, d, is given by the equation; $d = 3\lambda \sin \alpha$. Thus, as the α tends to 0° the outermost surface species account for a larger proportion of the signal detected.

Metal counterelectrodes on SAMs

In order to measure the electronic transport properties of SAMs, they are grown on highly doped Si substrates and the metal counterelectrodes are prepared on top of the SAMs [1,5]. An essential criterion for the fabrication of metal counterelectrodes is that during the process it should not damage or short-circuit the monolayer. The various types of counterelectrodes and their fabrication processes are as follows.

(a) Liquid Hg contacts: In this case a small drop of the mercury is kept on top of the SAM. Mercury, being liquid at room temperature, moulds into the surface topology of the monolayer and does not damage the monolayer. While soft contacts based on liquid mercury are useful for generating experimental data, which in turn, improve our understanding of the interfaces and molecular properties, they are unsuitable for practical fabrication in the electronics industry.

(b) Vacuum deposition: In order to have compatibility with photolithography and electron beam lithography processes to fabricate well defines structures, metal contacts are directly deposited onto the monolayer surface. The conventional deposition methods viz. thermal evaporation, electron-beam evaporation or sputtering, can be used for the deposition of metal counterelectrodes. However, these techniques – owing to the impingement of high energetic metal flux – can damage the monolayer by altering their structure significantly and/or metal atoms can diffuse through the monolayers causing short-circuits.

(c) Soft lithography: "Soft lithography" is a new high resolution patterning technique, which is also known as nano-transfer printing (nTP). In this process, a desired pattern of gold layer is thermally deposited on a stamp made using polydimethylsiloxane (PDMS), which is subsequently transferred on to SAM by a simple stamping.

Molecular Dielectric

The monolayer of the alkanes consisting of saturated C–C bonds has been found a good molecular dielectric. These molecules have large gaps (~9 eV) between their highest occupied molecular orbitals (HOMO) and lowest unoccupied molecular orbitals (LUMO). Typical current-voltage (J-V) data for CH_3-terminated n-alkanes (n = 3, 8, 11, 14 and 18 carbon atoms) SAMs with Al as counterelectrode are presented in Fig. 2(a). The solid lines are fit of experimental data using theoretical relationship between direct tunneling current density (J) and V for a metal-dielectric-metal like structure [6]:

$$J = \frac{\alpha}{d^2}\left[\phi e^{-Ad\sqrt{\phi}} - (\phi+eV)e^{-Ad\sqrt{\phi+eV}} \right] \qquad (1)$$

where $\alpha = \dfrac{e}{4\pi^2\beta^2\hbar}$ and $A = 2\beta'\sqrt{\dfrac{2m^*}{\hbar^2}}$ (e is the electron charge, m^* is the effective mass of electron in the insulator, β' is a constant and has value ~1, $\hbar$ is the reduced Planck's constant), ϕ is average barrier height, d is the barrier width or molecule length and V voltage between the electrodes. It is seen that the ϕ value reduces with increasing chain length and becomes as low as 1.5 eV for n = 18 SAM. As shown in Fig. 2(b) that the J through alkanes decreases exponentially with d, and can be described by J = Aexp(–βd), where A is a constant and β is a decay constant varying between 0.4 Å^{-1} (Fig. 1b). However, theoretical calculations predict the β value of ~0.8 Å^{-1}, and experimental values range over 0.4–0.9 Å^{-1}. The exponential decay, together with characteristic current–voltage (I–V) curves, which are temperature independent, suggests electron tunneling as the conduction mechanism for these SAMs.

From Fig. 2 it is evident that the leakage current though the alkane SAMs is quite low. However, for using them as a dielectric in electronic devices, low leakage current is not the only concern. Under high field stress, dielectric films will eventually reach breakdown, which causes an irreversible damage leading to increased leakage current and eventually fatal device failure. The simplest way of investigating the electric breakdown in a dielectric is to record J–V data to very high voltages till one
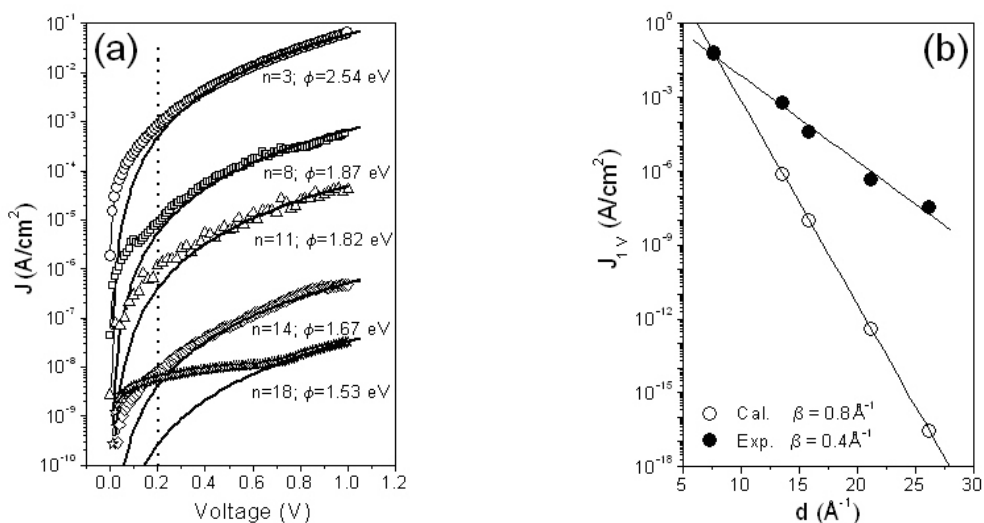
Fig. 2   (a) The J-V data for n-alkanes (n = 3, 8, 11, 14 and 18 carbon atoms) SAMs on Si. The full curves are data fit using equation 1. (b) The plot of J (at 1V) as a function of molecule length. Filled circles correspond to experimentally measured; while open circles are the calculated values using equation 1 and assuming ϕ = 2.54 eV, and m* = 0.16m$_e$.

observes a breakdown. For a 3 carbon atom alkane SAMs the breakdown field was found to be ~50 MV/cm [7]. This value is much larger than the 12-20 MV/cm reported for longer alkane chains (no. of carbon atoms > 10), suggesting that the shorter chains have higher breakdown fields. This is believed to be due to a reduction in impact ionization at reduced thickness. These breakdown fields are much larger than the breakdown field of ~2 MV/cm observed for SiO$_2$ of a thickness of ~2 nm, suggesting suitability of these monolayers for hybrid electronics.

Molecular Diodes

Device applications demand SAMs to work not only like a passive element (e.g. dielectric) but also an active element that can perform one or a set of controllable functions. A diode or rectifier is an important component in electronics that allows an electric current to flow in one direction, but blocks it in the opposite direction. Inspired by the visionary work by Aviram and Ratner [8], building diodes using single molecules has been pursued by many groups. The basic structure of early molecular diodes consisted of a donor and an acceptor separated by a σ bridge, with σ being some saturated

covalent bond linking the donor and acceptor and providing a tunnelling barrier between them. In this donor–σ–acceptor structure, the diode behaviour was expected to occur as a consequence of different thresholds at positive and negative bias voltages. Up to now, the most interesting results to date were obtained with the hexadecylquinolinium tricyanoquinodimethanide molecule (C$_{16}$H$_{33}$-Q-3CNQ) [9]. However, the donor and acceptor groups in this molecule are not sufficiently isolated by the π-bridge, and the molecular orbitals are too delocalized over the entire Q-3CNQ unit to allow a correct implementation of the AR paradigm. Thus, the rectification effect can be attributed to the geometrical asymmetry induced by the long alkyl chain, which places the Q-3CNQ unit close to one of the electrodes (inducing an asymmetric electrostatic profile across the molecule). These results thus indicate that rectifier effect should be expected from the molecules having only one donor group (π moiety) and an alkyl spacer chain (σ), and the concept of such a molecular rectifier is demonstrated in Fig. 3. The J-V curves of such a diode indicate rectification behaviour. The rectification ratio (RR) is defined as a ratio of current density at -1V (in absolute value) and the current density at +1V (RR =
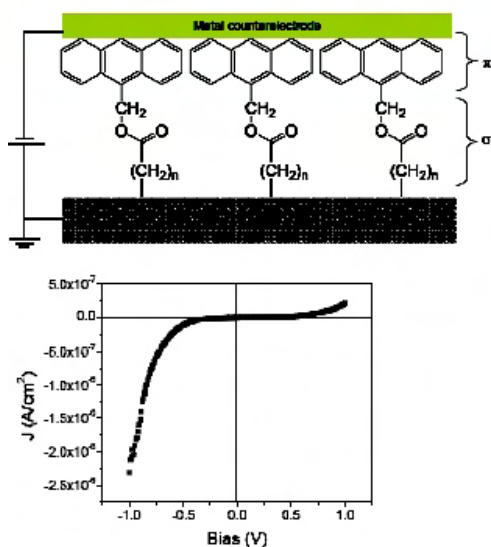
Fig. 3   A σ-π molecular diode prepared using 9-anthracenemethanol as π group. Right: J-V characteristics showing the rectification vehavior.

$|J_{-1V}|/J_{+1V}$). The value of RR found in this case 23. The rectification behavior in these σ-π SAMs arise due to the resonant tunneling through the HOMO of the π group. The rectification effect arises for a negative bias applied on the metallic counterelectrode (e.g. Al or Au) because the energy difference between the Si Fermi energy (pinned at the conduction band - CB - in the degenerated Si) and the HOMO (π orbital) is lower than that with the LUMO (π* orbital). If we assume that the π-end group is almost at the Al electrode potential (since this group is at a close contact with the electrode) and that a large part of the potential is dropped in the alkyl chains, a lower threshold (in absolute value) is required to have a resonance between the Si CB and the HOMO when applying a negative bias on the metal electrode than between the Si CB and the LUMO for a positive bias

Resonant Tunnel Diodes

The resonant tunnele diodes are based on negative differential resistance (NDR) effect. A region of decreasing current with increasing voltage in the J–V curve characteristic of a device is referred to as NDR. The NDR effect was first discovered in the Esaki diode, which opened a new avenue in many niche applications such as low-power memory. In an Esaki diode the current initially increases with the bias as electrons tunnel through the p–n junction barrier because the conduction band on the n-side is aligned with the valence band on the p-side. As voltage increases further the conduction and valence bands become misaligned and the current drops, resulting in NDR. Conceptually the resonant tunnel diode consists of a double barrier heterostructure with barrier thickness of only few monolayers. Based on this concept a design of molecular resonant tunnel diode (MRTD) is presented in Fig. 4(a). It essentially consists of a σ-π-σ self assembled monolayer on Si substrate. The two σ chains act as two tunnel barriers. The J-V behavior for such a σ-π-σ SAM, shown schematically in Fig. 4(b), is expected to exhibit a NDR, which arises due to a resonant tunneling mechanism. The schematic illustrations of simplified energy band diagrams that explain the charge transport mechanism in MRTD are shown in Fig. 3(c). In equilibrium i.e. for V=0, the Fermi level, E_F, of Al lies with respect to the conduction band (CB) of the silicon. For simplicity, the band bending of Si at the interface is not shown. Also the HOMO and LUMO of σ molecules are not shown as the HOMO-LUMO gap for these molecules is much larger than that of π molecule. Under an increasing applied bias i.e. V>0, the current, largely due to the non-resonant tunneling mechanism, increases. At a critical applied bias, V_R, the potential of the sample aligns with the LUMO, leading to resonant tunneling and a peak in the conduction. At a bias slightly higher than this critical value i.e. $V>V_R$, conduction electrons move off resonance and the current reduces, which leads to a NDR.

According to the mechanism of NDR described in Fig. 4 (c), in principle a single π-molecule chemisorbed on Si should be sufficient to act as MRTD. The most outstanding results on NDR have been observed through individual organic molecules, namely, styrene and 2,2,6,6-tetramethyl-1-piperidinyloxy (TEMPO), deposited on degenerately doped Si(100) 2×1 reconstructed surfaces using ultrahigh vacuum STM. For styrene molecules on n-type Si(100), NDR is observed only for negative sample bias,
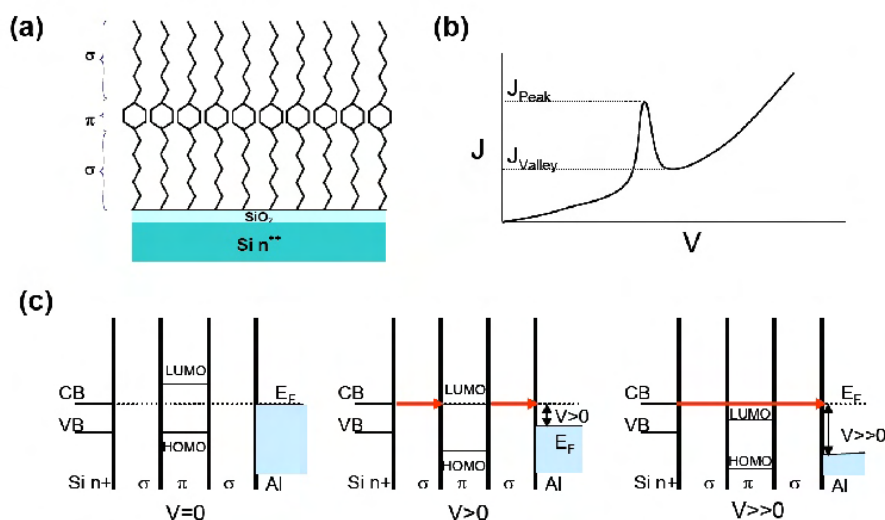
Fig. 4   Schematic diagram showing (a) concept, (b) characteristic J-V and (c) the mechanism of the occurrence of a negative differential resistance in a σ-π-σ SAM based MRTD.

while positive sample bias leads to electron stimulated desorption. For 2,2,6,6-tetramethyl-1-piperidinyloxy molecules, electron stimulated desorption was not observed at either bias polarity. In this case, NDR has been observed only for negative sample bias on n-type Si(100) and for positive sample bias on p-type Si(100). This unique behavior is consistent with a resonant tunneling mechanism between the bulk silicon band structure and the discrete orbitals of the adsorbed molecule, and opens new possibilities for silicon-based molecular electronic devices.

Molecular Transistors

The concept of molecular field effect transistor (MFET) is analogous to its inorganic counterpart in basic design and function. It is a three-terminal device, in which a voltage applied to a gate electrode (G) controls current flow between a source (S) and drain (D) electrode under an imposed bias. A basic schematic is shown in Fig. 5, where V_g and V_{ds} are the applied gate and source-drain voltages, respectively. The control of source-drain current in FETs via a third terminal has resulted in their widespread use as switches. In order to fabricate MFET, one grafts a σ-π monolayer on highly doped Si substrates. The π moiety acts as a semiconducting
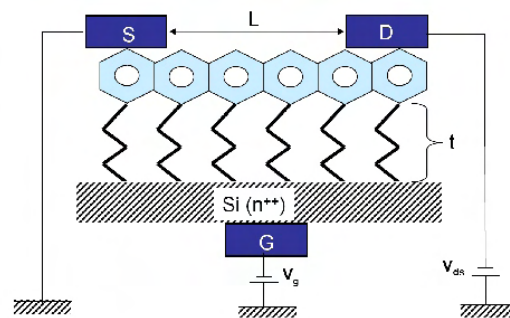
Fig. 5   Schematic diagram showing the concept of a molecular field affect transistor (MFET) based on a σ-π molecule. No experimental demonstration of such a MFET has been made so far.

channel, and therefore the selected π moiety should have a very good mobility for charge carriers. The alkyl-chains (σ) act as a dielectric. Theoretical analyses using electron tunneling and device electrostatics have shown that in order to achieve MFET characteristics, the distance (L) between the source and drain should be 2.5-3 nm and a minimum dielectric thickness (t) of L/1.5. Attempts are being
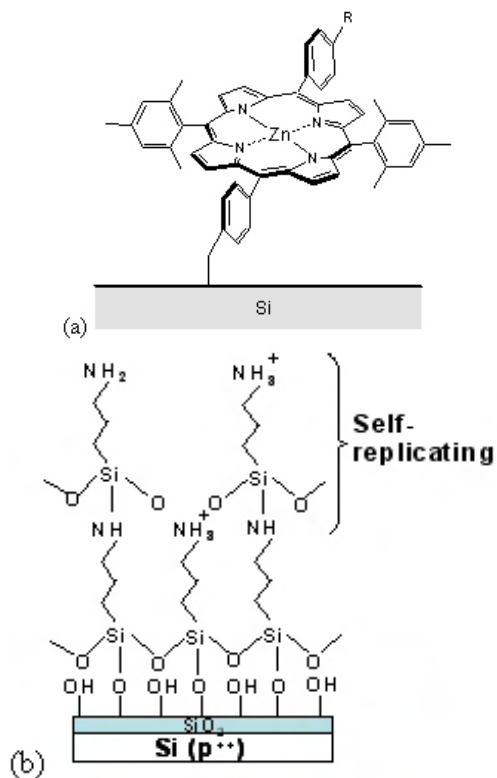
Fig. 6 Molecular memories compitable to the Si technology: (a) redox-active molecules i.e. porphyrin and (b) multilayers of APTMS molecules.

made to fabricate such MFET devices, however no success has been reported so far.

Molecular Memories

Two types of molecular memories, as shown in Fig. 6, compitable to the Si technology have been reported. These are: (a) redox-active molecules and (b) multilayers of APTMS molecules.

The redox-active molecules, such as, metallocene, porphyrin, and triple-decker sandwich coordination compounds have been found to act as charge storage elements. These molecules can be attached to device grade Si by self-assembly process. The molecular memory effect in these molecules works on the principle of charging or discharging of the molecules into different chemically reduced or oxidized (redox) states. Oxidation is equivalent to
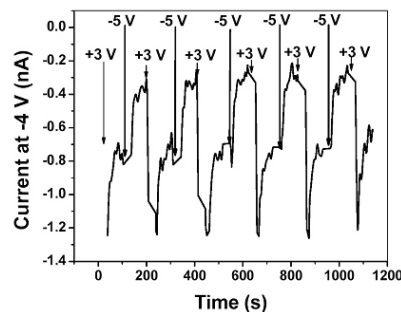
Fig. 7 The memory effect in Hg/APTMS-multilayer/ Si(p^{++}) device. The "write-read-erase-read" operations were performed by 10 s pulsing of +3V and -5V, consecutively. The device was read 50 times at -4V after each write (+3V) and erase (-5V) pulse.

writing a bit of information, while reduction equates to erasing or destructively reading out that bit. It has been demonstrated that porphyrins molecules (i) offer the possibility of multibit storage at relatively low potentials (below about 1.6 V), (ii) can undergo trillions of write/read cycles, (iii) exhibit charge-retention times that are long (minutes) compared with those of the semiconductor elements in dynamic random access devices (tens of milliseconds) and, (iv) are extremely stable under harsh conditions (e.g. monolayer of porphyrin molecules covalently attached to a silicon substrate are stable when subjected to temperatures of 400°C for half an hour) and, therefore meet the processing and operating challenges required for use in semiconducting devices.

The multilayers of 3-aminopropyltri methoxysilane [APTMS: $NH_2(CH_2)_3Si(OCH_3)_3$)] trapped with NH_3^+–ions grafted on $SiO_2/Si(p^{++})$ substrates by a self-assembly process exhibit pronounced hysteresis effect in J-V characteristics, which can be effectively used for memory applications. The memory phenomenon in electrically bistable devices is best demonstrated under "write-read-erase-read" operations. In such a sequence of cycles, the high-conducting ("write") and low-conducting ("erase") states are induced repeatedly and the states are monitored ("read") in between. In the present case, +3 V and −5 V pulses

for 10 s were applied, respectively, to "write" the high-conducting state and "erase" to a low-conducting one. These states were monitored ("read") by measuring the device current at -4 V. It is evident from the Fig. 7 that the magnitude of the device current under the "read" voltage pulse is much higher for high-conducting state as compared to that for low-conducting state. These results indicate that one can flip the two states of the electronically addressable devices and probe them successfully for rewritable or random access memory devices. The observed on/off ratio for our device is ~2, which is good enough for memory applications.

Summary

At present molecular electronics is one of the fastest growing fields and has brought together scientists and engineers from different disciplines. Much has been learned about the fundamental electron transport in molecules, and niche applications in selected areas are emerging, but many of the remaining challenges are still formidable. It is anticipated that the first generation of molecular devices will be hybrid designs where molecules are integrated with Si- based microelectronics. Some of passive and active molecular devices (dielectric, diodes, resonant tunnel diodes and memory) compiatble to Si-microelectronics has been demonstrated. However, functional molecular transistors have not been demonstrated so far, and a breakthrough in this direction is expected in a very near future.

Acknowledgement

References

1. D.K. Aswal, S. Lenfant, D. Guerin, J.V. Yakhmi and D. Vuillaume, Anal. Chimi. Acta, 568 (2006) 84.

2. A. Ulman, An Introduction to Ultrathin Organic Films From Langmuir-Blogett to Self-Assembly, Academic Press, 1991.

3. D. K. Aswal, S.P. Koiry, V. Saxena, N. Padma, S.K. Gupta, J.V. Yakhmi, S. Nayak A. Singh, and C. Suergers, in "Physics, Chemistry and Applications of Nanostructures: Reviews and Short Notes to Nanomeeting 2007", eds. V. E. Borisenko, S. V. Gaponenko V. S. Gurin, World Scientific, Sinagpore.

4. S.P. Koiry, D.K. Aswal, Vibha Saxena, N. Joshi, S.K. Gupta J.V. Yakhmi and D. Vuillaume, Appl. Phys. Lett. 90 (2007) 113118.

5. D. K. Aswal, C. Petit, G. Salace, S. Lenfant, D. Guerin, J.V. Yakhmi and D. Vuillaume, Phys. Stat. Sol. 203 (2006) 1464.

6. D.K. Aswal, S. Lenfant, D. Guerin, J.V. Yakhmi and D. Vuillaume, Small 1 (2005) 725

7. D.K. Aswal, S. Lenfant, D. Guerin, D. Vuillaume and J.V. Yakhmi, Nanotechnology 16 (2005) 3064

8. A. Aviram and M.A. Ratner, Chem. Phys. Lett. 29 (1974) 277.

9. R.M. Metzger, Chem. Rev. 103 (2003) 3803.

# Advances in MENS Technology

Ms Monika Chaudhary *did her MSc. Physics from IIT Roorkee in 2004 .The specialization was Solid-State Physics. She was JRF at IIT Rookee from july-2005 to April –2006. Ms Chaudhary joined DRDO as a scientist 'B' in april-2006. Now working in Adaptive Mirror Group of Solid State Physics Laboratory, Delhi. Her research areas of interest are Simulation, Fabrication and testing of the different MEMS, MOEMS and Microfludics devices.*

Dr. Amita Gupta *did her Ph.D from B.I.T.S., Pilani in 1979-80. She worked there as assistant lecturer and at I.I.T Delhi as research associate before joining DRDO as Scientist 'C' in 1982. Her research areas include solar cells, photodetectors, porous silicon, semiconductor fuse, silicon sensors, deformable mirror and MEMS. She has visited Moscow under a joint program with General Physics Institute & Moscow state University. She has published more than 48 papers in various journals and conference proceedings. She is a life member of semiconductor society of India and Material Research Society of India. Currently, she is Scientist 'F' at Solid State Physics Laboratory, Delhi where she is heading the silicon devices &MEMS Group.*

Introduction

Micro-Electro-Mechanical Systems, or MEMS, are integrated micro devices or systems combining electrical and mechanical components. They are fabricated using integrated circuit (IC) batch processing techniques and can range in size from micrometers to millimeters. These systems can sense, control and actuate on the micro scale, and function individually or in arrays to generate effects on the macro scale. With the help of MEMS technology it is possible to realize the complete systems-on-a-chip.


Sense   Think
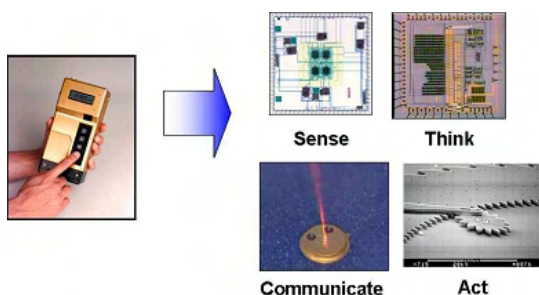
Communicate   Act

Applications of MEMS devices vary in many fields from automotive transducers, biomedical technologies, communication systems, robotics, aerospace, micro-optics, industrial sensors and actuators. Various disciplines associated with MEMS are as shown in the diagram:
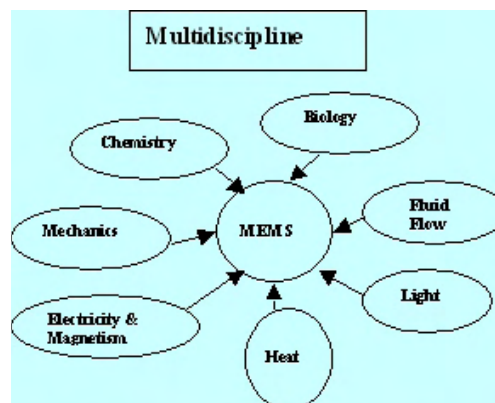
Why MEMS?

Need of MEMS technology can be classified broadly in three classes:

Ms. Monika Chaudhary and Dr. Amita Gupta, Solid State Physics Laboratory, Delhi 110 054;
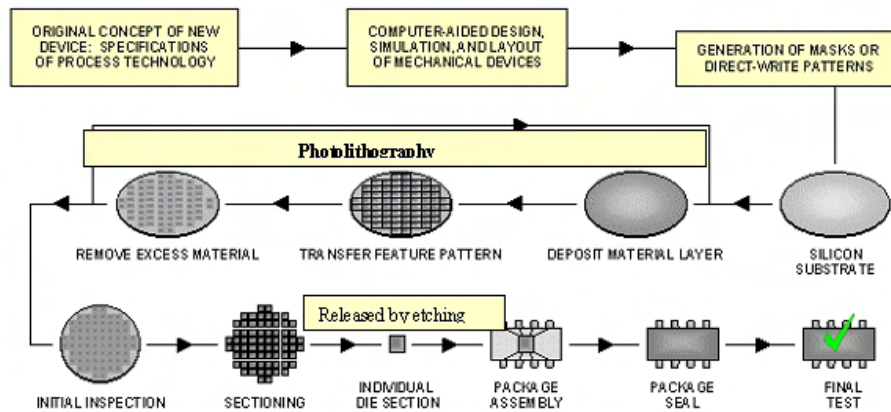
1. Miniaturization of existing devices,

2. Development of new devices based on principles that do not work at larger scale.

3. Development of new tools to interact with the micro-world. The development of a new class of microscopes (atomic force microscope, scanning near-field optical microscope) that shares the presence of micromachined sharp micro-tips with radius below 50 nm.

The common perception is that miniaturization reduces cost, by decreasing material consumption and allowing batch fabrication, but an important benefit is also in the increase of applicability. Actually, reduced mass and size allow placing the MEMS in places where a traditional system won't have been able to fit. A typical example is brought by the accelerometer developed as a replacement for traditional airbag triggering sensor, which is now used in many appliances, such as in digital cameras to help stabilize the image.

Another advantage that MEMS can bring relates with the system integration. Instead of having a series of external components (sensor, inductor…) connected by wire or soldered to a printed circuit board, the MEMS on silicon can be integrated directly with the electronics. Whether it is on the same chip or in the same package it results in increased reliability and decreased assembly cost, opening new application opportunities. So, we can say that development of MEMS leads toward the smaller, cheaper, faster and better devices.

Whole process of MEMS devices (Design, fabrication, bonding, packaging, and testing, optimization) is shown in the flow Diagram

MEMS Design

MEMS Design Tools

The Design process is not an exact analytical science, but rather involves developing engineering models, many for the purpose of obtaining basics physical insight. Various Software packages are available to design & simulate different MEMS structures. These Software tools are useful for improving device's performance with fewer fabrication trials, reduce development time, manufacturing costs and develop manufacturable devices with higher yields. As we know that MEMS are associated not only with one field interaction, it is multidisciplinary. So we need software having Multiphysics environment for the simulation of MEMS structures and devices or in other words we can say that software should have mechanical, electrostatic, electromagnetic, fluidics, thermal, structural etc. domain for the simulation. Some simulation tools like Intellisuite by Intellisense or Coventorware by Coventor have been specifically devised for MEMS. They allow accurate modeling using meshing method Finite Element Model (FEM) to solve the partial differential equation that describes a device in different physical domains. Moreover, they try to give a complete view of the MEMS design. In this way, it is possible to build quickly 3D model of MEMS from the mask layout using simulated process. ANSYS is also powerful
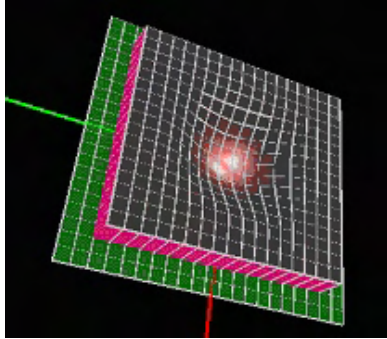
Simulation of Membrane under pressure with MEMS design software

software for MEMS structure & device simulation; however it is not having the fabrication module like in Intellisuite & coventorware. ANSYS is used to generate the reduced model, which then is run in circuit-analysis software like Spice.

MEMS Materials

The choice of a good material for MEMS application is not based on carrier mobility, like in microelectronics but on mechanical aspects such as small or controllable internal stress, low processing temperature, compatibility with other materials, possibility to obtain thick layer, patterning possibilities. In addition, depending on the field of application, the material often needs to have extra properties. RF MEMS will be based on material with small loss tangent (for example high resistivity silicon), optical MEMS may need a transparent substrate, BioMEMS will need biocompatibility, sensor application will need a material showing piezoresistance or piezoelectricity, etc.

MEMS have retained the predominant use of silicon and its compounds, silicon dioxide (SiO_2) and silicon nitride (SixNy). Actually, silicon is almost as strong but lighter than steel, has large critical stress and no elasticity limit at room temperature, as it is a perfect crystal. Silicon is the most abundant element on earth and due to its good mechanical and electrical properties is widely used as a substrate material in MEMS technology. Silicon as an element exists in any of three forms: Crystalline, Polycrystalline and amorphous. But MEMS materials are not confined up to silicon only.

Different kinds of polymers, Quartz, Shape memory alloys (Cu-Ni-Al alloy, Fe-Ni, Fe-Pt alloy etc.) are also used for making the MEMS structures and devices. Shape memory effect is a unique property of special class of alloys that return to a predetermined shape when heated above a critical transition temperature. The material remembers its original shape after being strained and deformed.

MEMS Fabrication Process

MEMS devices have features below 100 ìm that are not machined using standard machining (such as milling, drilling, turning, forging and casting because of the scale) but using other techniques globally called micro-fabrication technology. Techniques like photolithography, thin film deposition by chemical vapor deposition (CVD) or physical vapor deposition (PVD), thin film growth by oxidation and epitaxy, doping by ion implantation or diffusion, wet etching, dry etching, etc have all been adopted by the MEMS technologists.

In general, MEMS fabrication tries to be a batch process to benefit from the same economy of scale that is so successful in reducing cost of ICs. As such, the fabrication process often starts with a wafer (silicon, polymer, glass...) that may play an active role in the final device or may only be a substrate on which the MEMS are built. This wafer is processed with a succession of processes that add, modify or remove selectively materials.

Important techniques developed for fabricating MEMS structures are:

Bulk Micromachining

Bulk micromachining refers to the formation of microstructures by removal of materials from bulk substrates. The bulk substrate in wafer form can be silicon, glass, and quartz, crystalline Ge, SiC, GaAs, GaP or InP. The methods commonly used to remove excess material are wet and dry etching, allowing varying degree of control on the profile of the final structure.

*Isotropic and Anisotropic Wet Etching*

Wet etching is obtained by immersing the material in a chemical bath that dissolves the

surfaces not covered by a protective layer. The main advantages of the technique are that it can be quick, uniform, very selective and cheap. The etching rate and the resulting profile depend on the material, the chemical, the temperature of the bath, the presence of agitation, and the etch stop technique used if any. Wet etching is usually divided between isotropic and anisotropic etching. Isotropic etching happens when the chemical etches the bulk material at the same rate in all directions, while anisotropic etching happens when different etching rate exists along different directions. Some Anisotropic etchants for silicon are KOH, Ethylene Diamine Pyrocatechol (EDP), Tetra Methyl Ammonium Hydroxide (TMAH) etc.

Dry Etching

Dry etching is a series of methods where the solid substrate surface is etched by gaseous species. Plasma is usually involved in the process to increase etching rate and supply reacting ions and radicals. The etching can be conducted physically by ion bombardment (ion etching or sputtering and ion-beam milling), chemically through a chemical reaction occurring at the solid surface (plasma etching or radical etching), or by mechanisms combining both physical and chemical effects (reactive ion etching or RIE). These methods have various etching selectivity and achieve different etching profiles and usually the etching is more anisotropic and vertical when the etching is more physical, while it is more selective and isotropic when it is more chemical. With the help of Deep Reactive Ion Etching (DRIE) one can make the high Aspect Ratio structures (particular to obtain vertical sidewall).

Effect of different types of etching on silicon wafer is shown below:

(A) wet isotropic   (B) anisotropic in (100) silicon   (C) reactive-ion (RIE)
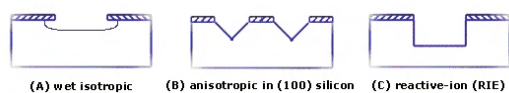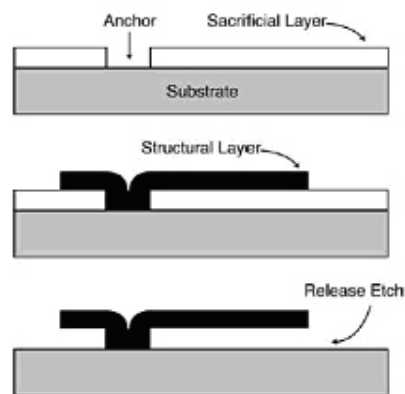
Surface Micromachining

Unlike bulk micromachining in which microstructures are formed by etching into the bulk substrate, surface micromachining builds up structures by adding materials, layer by layer, on the surface of the substrate. The thin film layers deposited are typically 1μm thick, some acting as structural layer and others as sacrificial layer. Dry etching is usually used to define the shape of the structure layers, and a final wet etching step releases them from the substrate by removing the supporting sacrificial layer. Some structural materials are polysilicon, silicon nitride, silicon oxide, Al, polyimide etc. Whereas oxide (PSG,etc.), poly-Si, poly-Si photoresist, Cu, can be used as sacrificial material respectively.
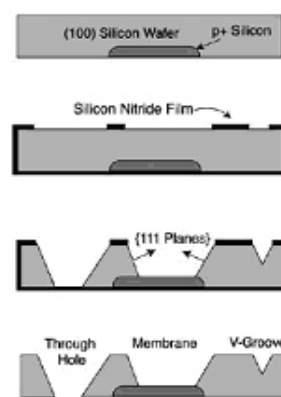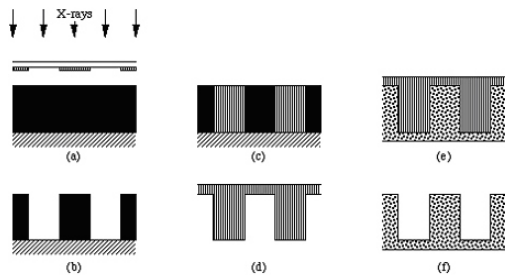

Bulk micromachining

Surface micromachining

LIGA Process

The acronym LIGA comes from the German name for the process (Lithographie, Galvanoformung, Abformung). LIGA uses

Flow diagram of LIGA process

lithography, electroplating, and moulding processes to produce microstructures. It is capable of creating very finely defined microstructures of up to 1000 μm high. In the process as originally developed, a special kind of photolithography using X-rays (X-ray lithography) is used to produce patterns in very thick layers of photoresist.

In flow diagram of LIGA process (as shown below) The X-rays from a synchrotron source are shone through a special mask onto a thick photoresist layer (sensitive to X-rays), which covers a conductive substrate (a). This resist is then developed (b). The pattern formed is then electroplated with metal (c). The metal structures produced can be the final product; however it is common to produce a metal mould (d). This mould can then be filled with a suitable material, such as a plastic (e), to produce the finished product in that material (f).

Wafer Bonding

Wafer bonding is an assembly technique where two or more precisely aligned wafers are bonded together. Some techniques used are anodic, adhesive, eutectic bonding etc. Wafer bonding method is at the frontier between a fabrication method and a packaging method and belong both to front-end and back-end process. The most commonly used MEMS bonding method is probably anodic bonding which is mainly used to bond silicon wafers with glass wafers. The technique work by applying a high voltage to the stacked wafers that induce migration of ion from glass to silicon, allowing a strong field assisted bond to form. Another type of bonding is Direct (silicon-fusion) bonding which requires two flat, clean surfaces in intimate contact. Direct bonding of a silicon/glass

stack can be achieved by applying pressure. Adhesion bonding& Eutectic bonding are also used. For all kinds of bonding techniques following two basic conditions are required: 1) Bonding surfaces must be flattened to have intimate contact for bonding and 2) Proper processing temperature, pressure and voltage should be provided to get the bonding energy.

Packaging and Assembly of Microelectromechanical Systems

No MEMS product is complete unless it is fully packaged. Packaging of a MEMS device provides a protective housing to prevent mechanical damage, minimize stresses and vibrations, guard against contamination, protect from harsh environmental conditions, dissipate heat, and shield from electromagnetic interference. At present, packaging is one of the major technical barriers that has caused long development times and high-costs of MEMS products. Since MEMS device structures are typically very small, stresses and thermal effects, induced in the substrates during the packaging and interconnection steps, can adversely affect their mechanical performance. Thus package strongly affects a MEMS device performance and reliability.

Application of MEMS

As MEMS Technology is the revolution toward miniaturization, it is having tremendous potential in different fields. Some common commercial applications of MEMS technology in different industries are as follows:

MEMS based Read/Write Heads, inkjet nozzle are important applications in field of Information Technology. Whereas for consumer services MEMS based projectors and Scanners are available. Optical Switch, RF tunable components and switches are important for the communication. Different types of MEMS based sensors are available which can be used in many places, like Blood pressure sensor, Gas Sensor, chemical sensor, Humidity Sensors and many more. Air bag sensor, temperature sensors, accelerometers etc. are important for Automobile Industry. MEMS technology is not confined up to only mechanical and electric field rather it is merging with different fields like Optics (MOEMS), Bio (Bio-MEMS) to create new emerging

technologies. The applications of MEMS in optics include display systems, optical switching, optical communication, optical data storage, optical processing and interconnection, and adaptive optics.

In medical science MEMS having vast applications like in drug delivery systems, blood Pressure sensor, blood parameters monitoring etc. With the help of different MEMS devices like microchannels, microneedle, micromixture, microheater, it is possible to make "LAB-ON-CHIP" for medical applications.

MEMS technology is not only useful for commercial purposes, but also have great potential in military like; Inertial systems for munitions guidance & navigation, embedded sensor and Actuators, Integrated fluidics systems for the miniature propellant and combustion control, miniaturize fluidic systems for early detection of biochemical warfare etc. Some MEMS based system and devices are shown below:
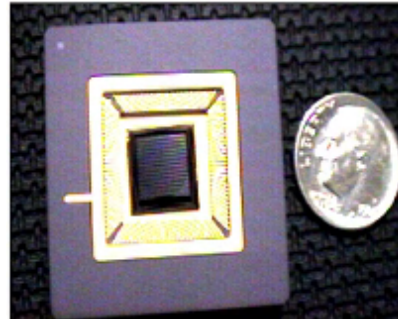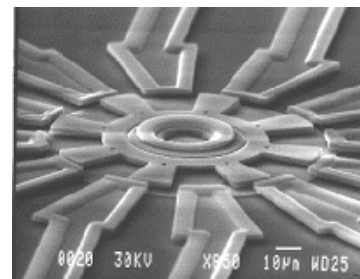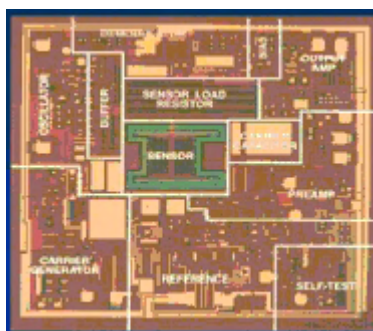

Deformable Mirror
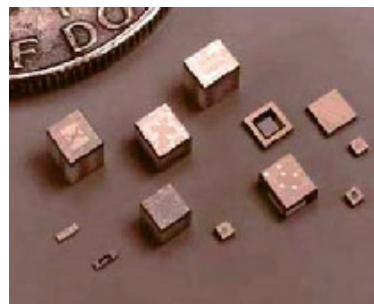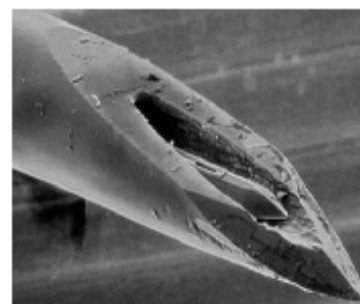

MEMS technology based Pressure sensor
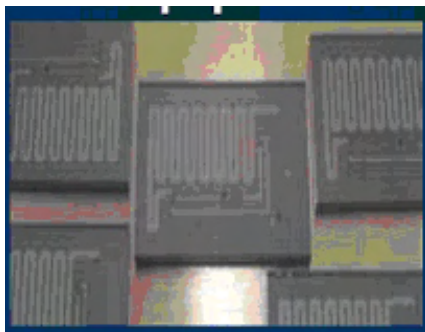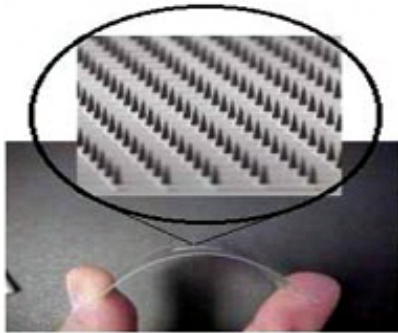

Micro fluidic chip

Electrostatic motor

Accelerometer

Plastic microneedle array

Conclusion

Current trends in MEMS indicate a bright future leading to better, cheaper and smaller devices and systems. Increasing demand for miniaturization to get the system with more functionality, more efficiency/sensitivity, and reduced cost is pushing the present Microsystems to nano level. In the new era of advanced technology development, novel MEMS devices with the nanometric features including quantum structures called NEMS (Nano Electro mechanical Systems) are emerging. NEMS are nanoscopic devices that have the characteristics length of less than 100nm & combine electrical and mechanical components. Presently, researchers are predicting NEMS as the future of MEMS.

At Solid State physics Laboratory,Delhi, scientists are working hard to develop various micro& nano devices.

Acknowledgements

Bibliography

1. Marc Madou, *Fundamentals of Microfabrication*, CRC Press 1997, ISBN 0-8493-9451-1

2. Julian W. Gardner, *Microsensors: Principles and Applications*, Wiley 1994, ISBN 0-4719-4135-2

3. Gregory Kovacs, *Micromachined Transducers Sourcebook*, McGraw-Hill 1998, ISBN 0-0729-0722-3

4. Héctor J. De Los Santos, *Introduction to Microelectromechanical (MEM) Microwave Systems*, Artech House 1999, ISBN 0-8900-6282-x

5. Sergey Edward Lyshevski, *Nano- and Microelectromechanical Systems*, CRC Press 2000, ISBN 0-8493-0916-6

6. P. Rai-Choudhury, ed., *Handbook of Microlithography, Micromachining, and Microfabrication*, Vol 1 and Vol 2, SPIE Press and IEE Press 1997, ISBN 0-8529-6906-6 (Vol 1) and 0-8529-6911-2 (Vol 2)

7. Mohamed Gad-el-Hak, ed., *The MEMS Handbook*, CRC Press 2001, ISBN 0-8493-0077-0

8. P. Rai-Choudhury, ed., *MEMS and MOEMS: Technology and Applications*, SPIE Press Monograph 2000, ISBN 0-8194-3716-6

9. Julian W. Gardner, and Vijay K. Varadan, and Osama O. Awadelkarim, *Microsensors, MEMS and Smart Devices*, Wiley 2001, ISBN 0-4718-6109-X

10. Nadim Maluf, *An Introduction to Microelectromechanical Systems Engineering*, Artech House 1999, ISBN 0-8900-6581-0

11. Randy Frank, *Understanding Smart Sensors, 2nd ed.*, Artech House 2000, ISBN 0-8900-6311-7

12. Ljubisa Ristic, ed., *Sensor Technology and Devices*, Artech House 1994, ISBN 0-8900-6532-2

13. Vijay Varadan, Xiaoning Jiang, and Vasundara Varadan, *Microstereolithography and other Fabrication Techniques for 3D MEMS*, Wiley 2001, ISBN 0-4715-2185-X

14. Tai-Ran Hsu, *MEMS and Microsystems: Design and Manufacture*, McGraw-Hill 2001, ISBN 0-0723-9391-2

15. Remco J. Wiegerink, Miko Elwenspoek, *Mechanical Microsensors (Microtechnology*

and MEMS), Springer Verlag 2001, ISBN 3-5406-7582-5.

16. Amita Gupta, Ranvir Singh, Amir Ahmad, "A capacitive pressure sensor for MEMS" proceedings of SPIE Volume 5062, Smart Materials, Structures, and Systems, October 2003,

17. Amita Gupta, Ranvir Singh, Amir Ahmad, Mahesh Kumar, "Silicon based Vibration sensors", Proceedings of SPIE Volume 5062, Smart Materials, Structures, and Systems, October 2003, pp. 462-467.

18. http://www.ansys.com

19. http://intellisensesoftware.com

20. http://www.algor.com

21. Parameswaran, M., Bates H. P., Ristic J.,Dhanded A.C., Robinson A. M., A new approach for the fabrication of micromechanical structures, Sensor and Actuators, 19, 289,1989.

22. Vijay K. Vardhan, K.J. Vinoy, K.A.Jose, RF MEMS and Their Application,, John Wiley & Sons Ltd, 2003.

23. Vision Statement, MEMS future-http://www.darpa.mil/mto/mems/vision/.

IANCAS Roundup

64TH BRNS IANCAS National Workshop Report

IANCAS organized the 64th BRNS-IANCAS National Workshop on Radiochemistry and Applications of Radioisotopes at the Department of Chemistry, Rastrasant Tukadoji Maharaj Nagpur (RTMN) University, Nagpur during 2nd to 10th July, 2007. Forty-eight persons from different disciplines such as chemistry, zoology etc and were affiliated to IIT Roorki, NEERI, CISF and various colleges and Departments affiliated to Nagpur University, M. S.University (Baroda) and Sant Gadgebaba Amaravati University participated in the workshop.

Dr. V. C. Sahni, Director, RRCAT and Director, Physics Group, B.A.R.C. in his inaugural address, briefly mentioned the challenges in the nuclear field and stated that the activities of IANCAS by way of conducting such workshops and dissemination of information through bulletins and web-site would help in enhancing the professional competence providing impetus to increasing use of nuclear energy and radioisotopes in the welfare of mankind. In a function presided over by Dr. S. N. Pathan, Vice-Chancellor, RTMN University, Dr. V. K. Manchanda, Head, Radiochemistry Division, B.A.R.C. and President, IANCAS provided detailed information about activities of IANCAS and said that in emerging world scenario nuclear energy and related activities are going to play an important role and will require the personnel having specialization in nuclear chemistry and radiochemistry. Dr. H. D. Juneja, Head, Department of Chemistry, RTMNU delivered the welcome address. Dr. S. V. Godbole, Coordinator of Workshop, emphasized the importance of the workshop and briefed the participants about its theme and scope. Dr. D. V. Parwate, Host Coordinator of the Workshop proposed a vote of thanks.

In the span of 8 days, 16 lectures were delivered and 6 experiments were conducted. The lectures were highly interactive and led to useful discussions between the participants and the team of resource persons. In the laboratory work, the participants got hands-on experience in dealing with radioisotopes and Radiation Instruments. Dr. Aparna Banerji, the practical coordinator gave the details about the experiments and the procedure to be followed in safe handling radioactivity in the university laboratories.

Special lectures were delivered by Dr. Manchanda, Shri S.G. Markandeya, Dr.S.P.Kale, Prof. A.N.Garg, Shri B.K.Sen and Sri M.K.Roy from AMD.

Shri B. K. Sen, Head, Product Development Section, B.A.R.C., delivered the valedictory address and donated a set of G.M. Counter & NaI (Tl) detector along with standard radioisotope sources to the host institute on behalf of IANCAS. The participants in the workshop were awarded certificates of participation. Dr. Parashar, Pro-Vice Chancellor, RTMNU was the Chief Guest. He promised that funds would be made available to Department of Chemistry, RTMNU for setting up of facilities for Nuclear Chemistry and for the promotion of the subject.

Three workshops were organized at local school and colleges and more than 600 students got benefit of this hands-on experience. Lectures on Introduction to Radioactivity, Nuclear power and safety aspects of handling radioactivity were delivered along with the demonstration of experiments on radioactivity counting to the students at schools and college. Dr. S.V Godbole, Dr. Sarbjeet Singh, Dr. Aparna Banerji, Mr. T. V. Vittal Rao, Mr. Rahul Tripathi, Shri. A. Sarkar from BARC and Dr. Yojana Singh, BRIT served as resource persons during these workshops.